

DTIC FILE COPY

UNCLASSIFIED

SECURITY CLASSIFICATION OF THIS PAGE (When Data Entered)

4

AD-A199 252

REPORT DOCUMENTATION PAGE		READ INSTRUCTIONS BEFORE COMPLETING FORM
1. REPORT NUMBER	2. GOVT ACCESSION NO. N/A	3. RECIPIENT'S CATALOG NUMBER N/A
4. TITLE (and Subtitle) Beam Line and Associated Work: Operational Phase 1985 - 1987		5. TYPE OF REPORT & PERIOD COVERED Final Report 10/1/85 - 1/31/88
7. AUTHOR(s) I. Lindau W. E. Spicer		6. PERFORMING ORG. REPORT NUMBER
8. CONTRACT OR GRANT NUMBER(s) N00014-85-K-0388		9. PERFORMING ORGANIZATION NAME AND ADDRESS Stanford University Stanford, California 94305
10. PROGRAM ELEMENT, PROJECT, TASK AREA & WORK UNIT NUMBERS		11. CONTROLLING OFFICE NAME AND ADDRESS U. S. Army Research Office Post Office Box 12211 Research Triangle Park, NC 27709
12. REPORT DATE August 26, 1988		13. NUMBER OF PAGES 6 plus appendices
14. MONITORING AGENCY NAME & ADDRESS (if different from Controlling Office) Office of Naval Research 800 N. Quincy Street Arlington, VA 22217-5000		15. SECURITY CLASS. (of this report) Unclassified
15a. DECLASSIFICATION/DOWNGRADING SCHEDULE		16. DISTRIBUTION STATEMENT (of this Report) Approved for public release; distribution unlimited.
17. DISTRIBUTION STATEMENT (of the abstract entered in Block 20, if different from Report) NA		
18. SUPPLEMENTARY NOTES The view, opinions, and/or findings contained in this report are those of the author(s) and should not be construed as an official Department of the Army position, policy, or decision, unless so designated by other documentation.		
19. KEY WORDS (Continue on reverse side if necessary and identify by block number) Synchrotron radiation; multi-undulator beam line		
20. ABSTRACT (Continue on reverse side if necessary and identify by block number) This is the final report of the operational phase 1985-88 of the DOD supported beam line at the Stanford Synchrotron Radiation Laboratory. During this first phase of operation, the multi-undulator insertion device has been operated successfully and applied to a number of research projects. The experimental end station, equipped with a number of modern surface analytical capabilities to be used in conjunction with the synchrotron radiation, was put into full operation. Finally, the construction and installation of the high-resolution monochromator were completed.		

FINAL REPORT

covering the period

October 1, 1985 - January 31, 1988

Sponsored by

DARPA AND ONR

CONTRACTOR: The Board of Trustees of the Leland Stanford Junior University

CONTRACT: N00014-85-K-0388

PRINCIPAL INVESTIGATORS: Prof. I. Lindau
Prof. W. E. Spicer

TITLE OF WORK: Beam Line and Associated Work: Operational Phase
1985-1987

August 1988

ABSTRACT

This is the final report of the operational phase 1985-88 of the DOD supported beam line at the Stanford Synchrotron Radiation Laboratory. During this first phase of operation, the multi-undulator insertion device has been operated successfully and applied to a number of research projects. The experimental end station, equipped with a number of modern surface analytical capabilities to be used in conjunction with the synchrotron radiation, was put into full operation. Finally, the construction and installation of the high-resolution monochromator were completed.



Accession For	
NTIS SPA&I	<input checked="" type="checkbox"/>
DTIC TAB	<input type="checkbox"/>
Unannounced	<input type="checkbox"/>
Justification	
By _____	
Distribution/	
Availability Codes	
Avail and/or	
Dist	Special
A-1	

TABLE OF CONTENTS

I.	INTRODUCTION	1
II.	STATUS OF BEAM-LINE OPERATION	2
III.	DOD USER COMMUNITY	5
IV.	PAPERS PUBLISHED IN REFEREED JOURNALS	6
	APPENDICES	7

I. INTRODUCTION

This is the final report on the first three years of operation of the DOD funded undulator beam line at the Stanford Synchrotron Radiation Laboratory, Beam Line V.

As a matter of introduction, we are summarizing some of the milestones from the first three years of operation (FY 85-87) of Beam Line V. The first synchrotron radiation beam was extracted from the beam line on October 25, 1984, and the beam line was commissioned with one undulator in Jan/Febr 1985. The first scientific programs started in June 1985 using the quasi-monochromatic undulator radiation. The multi-undulator stand (designed to hold 4 undulators) was installed with two undulators in September 1985 and used for scientific programs the following month (October 1985). The multi-undulator was completed with the four-undulator configuration in March 1986 and was immediately commissioned successfully for scientific programs. The utilization of the beam line for research programs was put on hold for most of 1987 while the high-resolution monochromator was assembled and installed. The monochromator is now fully completed and will be ready for full use in the research programs as soon as the synchrotron radiation beam becomes available in 1988.

It should also be pointed out that the first meeting for beam-time allocation of the DOD users took place in October 24, 1986. At that time, procedures were discussed and established for assigning beam time. A copy of the Minutes and Policy Statement is enclosed in Appendix 1.

II. STATUS OF BEAM-LINE OPERATION

Technical descriptions of the beam line have been published in the open literature. The project has also been presented at several scientific meetings to give as broad a scientific community as possible the opportunity to become familiar with the capabilities of the beam line. The two most recent technical papers describing the beam line are attached as Appendices II and III. In total, eight articles describing the technical capabilities of the beam line have been published. A comprehensive paper treating all the technical aspects of the beam, in particular the operation of the high-resolution monochromator, is presently being prepared.

The DOD funded beam line is located at SSRL in a straight section of the storage ring SPEAR at the Stanford Linear Accelerator Center. The synchrotron radiation is created by magnetic insertion devices, so-called undulators, located in the 2m long straight section. The undulators are made of permanent magnetics, SmCo₅, which are positioned outside the vacuum tank of the storage ring. When the relativistic electron beam undulates in the periodic magnetic structure, a characteristic radiation peak with extreme intensity is produced. Its peak energy can conveniently be tuned by changing the magnet gap. By constructing four undulators, easily interchangeable, with different magnetic periodicity, the DOD beam line will provide photon beams with unmatched intensity and brightness in the entire spectral region from 10 to 1200 eV (1200 to 10 Å). Specifically, it provides 100-1000 times larger photon flux in this spectral region than any of the existing beam lines at SSRL. One novel and unique feature of the DOD funded beam line is thus the superior intensity over a large spectral region. The undulators deliver quasimonochromatic radiation which can be used directly for certain research projects (e.g., within topography, microscopy, lithography, and Auger electron spectroscopy) or be further monochromatized for high-resolution spectroscopies (e.g., photoemission, surface EXAFS, etc.). The high resolution monochromator is based on four different gratings, easily interchangeable and optimized for different parts of the spectral region. A resolution of 0.1-0.3 eV is readily

achievable for the entire spectral region, 10-1200 eV. The end station equipment can be configured either to accept the quasimonochromatic undulator radiation or the highly monochromatic radiation. The main experimental chamber is equipped with an angle-resolved photoemission spectrometer, an Auger electron spectrometer, LEED, ion sputtering gun, sample manipulator for heating (2000 K) and cooling (100 K), cleaver and various metal evaporation sources. Preparation chambers can be attached to the main chamber, and samples can be transferred via vacuum interlocks from chemical hood or MBE growth environments into the main chamber (ultra-high vacuum, $\lesssim 1 \cdot 10^{-10}$ torr) in a matter of minutes. A PDP 11/73 computer is presently used for both the beam line operation and the data acquisition.

Since April 1986, we have accumulated several months of operational experience with the multi-undulator device for experimental research programs. No major problems have been encountered and all the minor ones have been overcome. The operation of the multi-undulator device is now considered to be well established and routinely done. A number of research programs have been pursued using the quasi-monochromatic radiation from the undulators.

The mechanical assembly and installation of the high-resolution monochromator took considerably longer than originally anticipated, mainly due to the requirements of exceedingly high tolerances and severe heat levels, but these problems were finally overcome in late 1987. The monochromator is now fully completed and will be used for experimentation as soon as beam becomes available in 1988. This is a very important development, since many of the proposed research programs are critically dependent on a high spectral resolution over the entire photon energy range, 10-1200 eV. However, for a number of experiments, the quasimonochromatic radiation is preferable. Therefore, we have made provisions so that we can switch between the two modes of operation and optimize the photon source conditions.

It should be recognized that Beam Line V is indeed a very complex experimental setup with several technologically advanced components. An international symposium held at Stanford in October 1985 (organized by Dr. Tatchyn and Prof. Lindau) was of critical importance to form the basis for a successful operation of the beam line. The proceedings (368 pages) were published by the International Society for Optical Engineering. The table of contents is attached as Appendix IV. It has been clearly demonstrated that the undulators produce radiation with the spectral characteristics very close to the calculated ones, see for instance the work described in Appendices V and VI. Appendix VI also reports on a scheme for focusing the undulator light, an approach which will be very important for many applications.

III. DOD USER COMMUNITY

SSRL is operating about 800 eight hour shifts per year in a dedicated mode (i.e., 2400 hours) and an equal amount of time in a parasitic mode on the high-energy physics program. According to the agreement of assigning beam time on the undulator beam line, the DOD user community has the exclusive priority to one-third of the available time, i.e., nominally about 100 shifts (800 hours) of dedicated time and an equal amount, 100 shifts (800 hours), of parasitic time. During dedicated mode of operation, the storage ring is typically run at 3 GeV (and 100 mA), and the four-undulator configuration is optimized to cover the spectral region 10-1200 eV under these conditions. During parasitic operation, the storage ring is usually run at lower energies, which will limit the spectral region covered by the undulators. But, even under the most unfavorable conditions, 1.5 GeV, the spectral region up to 300 eV will be covered. The undulator beam line will thus provide very powerful radiation for the DOD user community also under parasitic conditions.

The procedures and policies for assigning beam time were discussed briefly in the Introduction, and more details can be found in Appendix I. At the present time, there are six DOD supported research groups actively doing or planning research in connection with Beam Line V: Profs. Lindau/Spicer, Stanford (interfacial chemistry and metallurgy of metal/semiconductor systems, DARPA/ONR); Dr. Pate, Stanford (synthetically fabricated diamond films, SDIO/ONR); Prof. Csonka, Oregon (Li-based x-ray laser, AFOSR); Dr. V. Rehn (MBE grown superlattices, ONR, planned); and Prof. Schwuttky, Arizona (GaAs surface topography, DARPA). With the completion of the high-resolution monochromator, it is anticipated that both the number of user groups and demand for beam time will increase dramatically during the next phase of operation. As pointed out earlier, we have a mechanism in place to handle the beam time assignments (see Appendix I).

IV. PAPERS PUBLISHED IN REFEREED JOURNALS

1. R. Z. Bachrach, R. D. Bringans, B. B. Pate, and R. G. Carr, "International Conference on Insertion Devices for Synchrotron Sources," (R. Tatchyn and I. Lindau, eds.), Proc. SPIE 582, 251 (1986), enclosed as an Appendix.
2. W. Eberhardt, E. W. Plummer, C. T. Chem, R. Carr, and W. KJ. Ford, "New Experiments Using a Soft X-Ray Undulator," in "Proceedings of the International Conference on X-Ray and VUV Synchrotron Radiation Instrumentation," (G. S. Brown and I. Lindau, eds.), Nucl. Instrum. Meth. 246, 825 (1986).
3. R. Tatchyn, P. L. Csonka, E. Källne, A. Toor, C. Gillespie, I. Lindau, and A. Fuller, "Surface Heating in a Lacquer-Coated Mirror Irradiated with Undulator Light," in "International Conference on Insertion Devices for Synchrotron Sources," (R. Tatchyn and I. Lindau, eds.), Proc. SPIE 582, 291 (1986).
4. W. Eberhardt, E. W. Plummer, I.-W. Lyo, R. Carr, and KJ. Ford, "Auger-Electron-Ion Coincidence Studies of Soft X-Ray Induced Fragmentation of N₂," Phys. Rev. Lett. 58, 207 (1987).
5. R. Tatchyn and I. Lindau, "Off-Axis Radial Properties of Undulator Light," in Soft X-Ray Optics and Technology (E. E. Koch and G. Schmahl, eds.), Proc. SPIE 733, 115-123 (1987).
6. R. Tatchyn, P. Csonjka, H. Kilic, H. Watanabe, A. Fuller, M. Beck, A. Toor, J. Underwood, and R. Catura, "Focusing of Undulator Light at SPEAR with a Lacquer-Coated Mirror to Power Densities of 10⁹ watts/cm²," in Soft X-Ray Optics and Technology, (E. E. Koch and G. Schmahl, eds.), Proc. SPIE 733, 368-378 (1987).
7. R. Tatchyn, A. Toor, H. Kilic, J. Hares, J. Kilkenney, P. Csonka, H. Watanabe, and A. Fuller, "On-Axis Streak Camera Measurements of Undulator Light on BL V at SSRL," in Soft X-Ray Optics and Technology, (E. E. Koch and G. Schmahl, eds.), Proc. SPIE 733, 101-105 (1987).
8. R. Z. Bachrach, R. D. Bringans, L. E. Swartz, I. Lindau, B. B. Pate, R. G. Carr, N. Hower, B. Youngman, H. Morales, and P. Pianetta, "Multi-Undulator Beam Line V at SSRL: A Progress Report," in Proceedings of the 5th National Conference on Synchrotron Radiation Instrumentation, University of Wisconsin, Madison, 21-25 June 1987; Nucl. Instrum. Meth. A 266, 83-90 (1988).

APPENDICES

"Minutes from the First Beam-Time Assignment Meeting" and Procedure for Assigning Beam Time on the DOD Funded Beam Line at SSRL"

I. Lindau, November 1986

Minutes from the First Beam-time Assignments Meeting at Stanford, October 24, 1986

The first meeting to discuss procedures for assigning beam-time on the DOD funded beam-line at SSRL was held at Stanford October 24, 1986, in conjunction with the Annual SSRL Users' Meeting.

Present: Prof. P. Pianetta, SSRL
Prof. I. Lindau, Stanford
Prof. W. E. Spicer, Stanford
Dr. M. A. Stroschio, AFOSR
Dr. M. A. Stroschio for
Dr. L. Cooper, ONR

Since this was Dr. Stroschio's first visit to the Stanford Synchrotron Radiation Laboratory, a visit was arranged to the facilities of the DOD funded multi-undulator beam-line. After the Laboratory tour a discussion followed regarding beam-time allocations. The general policy for these allocations is described in the document "Procedure for Assigning Beam Time on the DOD Funded Beam Line at SSRL." A copy of this document is enclosed. The following guidelines were proposed for assignment of beam-time for the period 1/1/87-12/31/87:

1. The priority time assigned to the DOD user community (one third of the total beam-time) should be shared equally for research work supported by DARPA, AFOSR, ARO and ONR, respectively.

2. The beam-time assignment described under point 1) can be subject to adjustments as found appropriate when the real beam-time requests are available. In this case the Beam Line Committee will be polled by phone.

3. Due to the technical complexity of the multi-undulator beam-line it is highly recommended that new users seek advice and/or form collaborative programs with more experienced users. (Prof. Pianetta or Prof. Lindau should be contacted).

A discussion followed about the best means to provide the DOD supported user community with information about the multi-undulator beam-line and its unique capabilities. General information about the new beam-line is provided to the existing user community of the Stanford Synchrotron Radiation Laboratory through its users' meeting and annual activity report (about 900 persons on the mailing list). The great success of the multi-undulator operation has also given the project high visibility and publicity in the synchrotron radiation user community. To further broaden the user community it was felt important that the scientific program officers at the respective funding agencies inform principal investigators who may benefit from the new capabilities. The final DARPA/ONR report for the beam-line construction (authored by Prof. I. Lindau and W. E. Spicer) is a useful document for technical information. But all prospective users are encouraged to contact Prof. Lindau or Prof. Pianetta for the detailed planning of their experiment.

PROCEDURE FOR ASSIGNING BEAM TIME ON THE
DOD FUNDED BEAM LINE AT SSRL

Introduction

The DOD funded beam line at the Stanford Synchrotron Radiation Laboratory (SSRL) became operational in October 1984 and has been accessible for the general DOD user community since May 1985. According to an agreement, as described in the original proposal submitted to DARPA in December 1981, the DOD user community will have priority access to one third of the total beam time for a period of three years. The priority time is renewable for additional periods of three years, based on the recommendation of a review committee appointed by the Stanford Vice Provost for Research. The following criteria will be used in the evaluation of renewal: (1) quality of research; (2) significant contributions to the general education and research missions of Stanford University; and (3) effective support and responsibility for the beam line operation. The research work done under the priority time should be specified in proposals admitted to SSRL, following guidelines as defined by SSRL. DOD funded users will have access to beam time on beam lines accessible to the general SSRL user community on a competitive basis and independent of priority time allocation. In accordance with Stanford University policy, only unclassified research can be carried out at SSRL.

Beam Time Allocation Committee

The assignment of beam time on the DOD funded beam line at SSRL will be done by a committee, hereafter referred to as the Beam Line Committee. The Beam Line Committee will be composed of the following eight members, one of which has nonvoting status:

- one representative each from AFOSR, ARO, and ONR or their designates;
- two representatives from DARPA or their designates;
- the two principal investigators from Stanford University, Professors I. Lindau and W. E. Spicer or their designates;
- one SSRL representative, Professor Pianetta or his designate with non-voting status and acting as liaison person to SSRL.

Meeting Schedule of the Beam Line Committee

The Beam Line Committee will meet annually in conjunction with the SSRL User's Meeting, presently held at the end of October. At this meeting, the Committee will make beam time allocation for the entire following year, starting January 1. Under compelling circumstances, a majority vote of the Beam Line Committee can decide to hold a meeting at any other time during the year to resolve an urgent problem on beam time allocation. Whenever necessary for timely decisions, the Beam Line Committee can be polled by mail and/or phone.

Guidelines for Beam Time Allocation

The Beam Line Committee will allocate beam time according to the following guidelines: (1) Any individual researcher(s) and research group(s) receiving DOD support are invited to request priority time on the DOD funded beam line. (2) The prime considerations in allocating beam time will be the scientific quality of the proposed work and its relevance to DOD needs and objectives. (3) A minimum amount of beam time will be guaranteed each year to each of AFOSR, ARO, ONR, and DARPA to insure that the particular needs and objectives of each research office will be taken into consideration. This minimum amount of beam time will be decided at the first Beam Line Committee Meeting. (4) A minimum amount of beam time will be guaranteed to each of the principal investigators in recognition of their contributions to the beam line project.

This minimum amount of beam time will be decided at the first Beam Line Committee meeting.

Logistics of Beam Time Assignment

Consideration of beam time allocation will be based on proposals submitted in time for the annual Beam Line Committee Meeting. The proposals should give a short description of the scientific and/or technological motivation of the proposed work and be as broad and generic as possible. The format of the proposals should be consistent with the SSRL Proposal Guidelines. In addition to the information requested in the SSRL Proposal Guidelines, it is important to emphasize how the proposed work can benefit from the unique characteristics of the beam line. The required set-up time and the required assistance from the beam line support organization should also be spelled out. The Beam Line Committee will submit its decision about the beam line allocation to the SSRL proposal coordinator, who will then apply the existing SSRL policy (e.g., regarding beam time request forms, safety information, etc.) to the actual scheduling of the experiments. All proposals will also be forwarded to the Proposal Review Panel (after the Beam Line Committee has made its decision) in order to obtain an independent evaluation of the scientific quality. This process is particularly important in terms of the renewal of the priority time agreement which takes place every third year.

Summary

The procedures of assigning beam time, as discussed above, will be reviewed at each of the annual Beam Line Committee Meetings and appropriate changes made by majority vote.

Technical Paper: "Multi-Undulator Beam Line V at SSRL:
A Progress Report" by R.Z. Bachrach et al, Nucl. Inst.
Meth (to be published 1988).

Synchrotron Radiation Instrumentation, 5th National Conference
University of Wisconsin - Madison
21-25 June 1987

Multi-Undulator Beam Line V at SSRL: A Progress Report

R.Z. Bachrach, R.D. Bringans, L.E. Swartz
Xerox Palo Alto Research Center
3333 Coyote Hill Road, Palo Alto, Ca 94304

I. Lindau, B.B. Pate, R.G. Carr, N. Hower, B. Youngman, H. Morales, and P. Pianetta
Stanford Synchrotron Radiation Laboratory
Stanford University
Stanford, Ca. 94305

Abstract

A progress report is given on the implementation of Multi-Undulator Beam Line V at SSRL, also known as Beam Line Wunder. The beam line has been designed to exploit insertion device technology in the spectral range from 10-1000 eV. Aspects of the multi-undulator, the monochromator, and the experimental areas are described

1. Introduction

This report provides an overview of the progress on the implementation of Multi-undulator Beam Line V at SSRL. The beam line is also known as beam line wunder, because of its use of wiggler-undulator insertion source technology. The last phase of the construction is due for completion in the fall of 1987. This paper highlights the operational success of the new multi-undulator concept and the status of the Locust monochromator. We have previously given a complete review of the design of the beam line in reference 1 and the technical details presented here are a summary of that more complete report. Reference 1 cites the other pertinent papers.

The specific focus for Beam Line V is the spectral range from 10-1000 eV and the design goal is to deliver the highest possible power density to the sample in the smallest feasible bandwidth. We have previously summarized the status of the main beam line elements: the Xerox/Stanford SSRL BLV Multi-undulator; the Locus Monochromator; and the experimental area.

The design of the beam line is dominated by the increased beam power density from an undulator source which necessitated active cooling of most elements likely to be hit by the beam. In the case of optical elements, this requirement arises not only because of possible damage, but also because distortions of the optics must be minimized to maintain ultimate performance. As a result of our studies, presented in reference 1, we have shown a new way for configuring undulators as sources, we have shown the expected improvements to be gained from silicon carbide optics, we have formulated a state of the art second generation soft X-ray monochromator which can handle the high power and deliver high resolution, and we have resolved issues on the best experimental configurations for the use of undulator beams.

2. SSRL BLV Multi-undulator

2.1 Multi-Undulator Design

Early in the design studies of the beam line, we specified that several undulator periods would be required to span fully the design range of 10-1000 eV. The result of the considerations is the discovery that specific insertions could be sized so that they could be placed close together. Previous to this, considerations for New Rings such as ALS or the 6 GeV ring had been predicated upon having beam lines with narrow undulator ranges and narrowly defined function. The multi-undulator concept is therefore important for broadly expanding the utility of insertion devices.

The SSRL BLV Multi-undulator, shown in figure 1 with five possible insertion devices, was installed into SPEAR on September 10, 1985. Table 1 lists many of the relevant parameters. Figure 1 depicts the five possible insertion devices mounted on individual stainless steel I beams set in the mover structure surrounding the SPEAR beam pipe. The inset shows how the SmCo₅ magnet bars are held. Scanning the undulators can be accomplished in a straightforward

manner by varying the magnet jaw gaps of all the undulators simultaneously with the active one positioned over the SPEAR beam pipe. Interchange between the different periods can then be carried out by opening the jaws and sliding the undulators across the beam pipe within the confines of the SPEAR tunnel. An important part of the design is the end coil corrections which were implemented with a single stationary set of electromagnets.

The Multi-undulator innovation represents a major advance in the art of permanent magnet undulator devices and solves the problem of achieving a wide range while remaining in the undulator regime. We have chosen to implement devices with $N = 10, 15, 24$ and 30 periods in the available 183cm SPEAR straight section corresponding to $18.3, 12.2, 7.6,$ and 6.1 cm period lengths. This selection of periods allows the whole tuning range to be covered with the undulator fundamental.

The parameters in Table 1 characterize the Multi-undulator for SPEAR operating at 3GeV , a typical dedicated operating condition. For each device the range of the fundamental will have a low energy cutoff set by the requirement that the magnets have a remanent field of 0.93 Tesla and a minimum gap of 3.0cm , and an absolute high energy cutoff set by $K = 0$. Table one shows the tuning ranges achievable with the Multi-undulator based upon power criteria and also characterizes the photon energy and radiated power at K values of $3.5, 1.4,$ and 0.5 corresponding to the half power and maximum of the fundamental.

2.2 Multi-undulator Construction

The multi-undulator consists of the individual period insertions, the mover frame, and the control electronics. The periods are built up from SmCo_5 blocks mounted into keepers which are then attached to the I beams mounted in the mover frame. The mover is constructed to be able to separate the magnet jaws while keeping them parallel to within 1 mil over the two meter length. The drive system allows for a vertical scanning resolution of 1 mil. In the original design, everything above the horizontal slide except the magnets was made of stainless or aluminum to minimize the possibility of field distortions. Due to delivery problems, magnetic steel lead screws were substituted in order to achieve the completion schedule. As described below, this substitution does not seem to have led to operational problems.

In the Original SSRL-LBL permanent magnet undulator, the magnets were epoxied to the keepers. We have developed a scheme for mechanically clamping the magnets which eliminates the gluing shown in figure 1. The square cross section magnet bars are beveled on the ends such that the bars can be clamped into the keeper with a flush mounting design so that the minimum achievable gap is not compromised. Thus we can still use the minimum 3cm gap available with the SPEAR Vacuum Chamber. The substitution of mechanical clamping for gluing results in substantial reduction of assembly labor and in addition permits for correction of problems should they develop. After the assembly procedure was established with the first device, the remaining devices were assembled with just a few days each.

The first phase in the assembly of the insertions upon receipt of the magnets is inspection of the magnets. Examination of the measurements provided by the manufacturer relative to tests made at SSRL on one set showed that remeasuring was not needed. Thus the remaining magnets were checked for uniformity and for mislabeling with a visualization card and then set on rubber cushioned steel plates for storage. Once a pool of acceptable magnets was designated, the sorting was performed by computer. A previous hand sort had taken three weeks, and the computer sort required only several hours of computer time. The physical magnets were then arranged according to the sort and inserted into the keepers using some specially prepared fixturing. The individual keepers were then mounted onto the I beams, putting the upper ones in first and then covering them with a protective spacer. We have found it possible to install the individual sections onto the I beams with the mover in the SPEAR tunnel. Originally we thought we might have to move the I beams as a unit.

Once the I beams were set, the phase was checked with the visualization card and measurements taken using a coil and integrating voltmeter of SB-dI. The measurements were taken as a function of gap and determined the corrector coil settings required for the integral to be zero.

2.3 Multi-Undulator Operational Testing

The testing of the multi-undulator commenced with the 10 and 15 period devices inserted. The presence of these two devices allowed us to explore all aspects of the device. The testing started from the table of compensation measurements

developed during the construction. This was tested against operational criteria for beam stability in SPEAR. Because very limited machine physics time has been available to date, this description is preliminary, but indicative of the compatibility of the multi-undulator concept with stable operation of the storage ring. The 24 and 30 period devices were then installed with the mover in the SPEAR tunnel and also successfully operated.

The testing had several objectives. The first was to refine the trim coil compensation requirements; the second was to characterize any possible tune resonances which might disrupt the operation of the storage ring; the third was to examine any injection problems the presence of the multi-undulator might create; and the fourth was to explore the limits on horizontal exchange with beam in the machine.

An SSRL position monitor was used to determine orbital motion of the beam as the multi-undulator gap is changed. Starting from an extreme open position, the trim coil current required to maintain the beam position as the gap was closed was determined. These measurements essentially reproduced the previously established table.

The horizontal motion of the beam was found to be 3mm per ampere, so that close control of the trim is required to maintain the orbital tolerances required by many of the beam line experiments.

To date, no significant tune resonances have been found, injection is not disturbed by the presence of the multi-undulator, horizontal interchange can be accomplished without dumping the beam and it seems feasible to track the trim as the horizontal motion is performed so that the beam position will not be significantly disturbed. The multi-undulator design has therefore met its objectives.

A number of experiments were performed using the unmonochromatized beam from the multi-undulator, but these were interrupted in June, 1986, in order to begin installation of the Locust Monochromator which has been assembled in place. The measurements included calorimetric determination of the beam power. These measurements confirmed our modeling results of the beam power. A more complete technical description of the multi-undulator will be given at a later date.

3. The Locust Monochromator

3.1 Overview

In specifying a monochromator for this beam line, we sought an instrument which would match well to the multi-undulator and SPEAR characteristics and which would advance the state of the art. The resulting Locust monochromator implements a constant deviation Vodar geometry Rowland Circle mounting and is descended from the Grasshopper Monochromator. By using closed loop computer control and configurational changes, the design incorporates a number of features that would not be achievable with either the Grasshopper or the Extended Range Grasshopper, ERG, configuration for these optics. As with the Grasshopper, the Locust uses principally spherical or conic section optics. The Grasshopper was the first fully UHV monochromator. The Locust achieves both variable angle of incidence optics and is the first to be fully water cooled to enable it to maintain performance with the powers delivered by an undulator. The incorporation of water cooling consistent with accepted vacuum practice while maintaining the required mechanical and optical tolerances proved to be a major design problem and added immensely to the scope of design work required. The Locust uses an elliptically figured SiC entrance mirror fabricated by TRW2, SiC entrance codling slit, and both spherical and cylindrical gratings.

3.2 Ranges and expected performance

Achieving the desired ranges shown in Table 2 was a process of considerable trade off. We describe these ranges as optimized predicated by the choice of grating blaze which is within the accessible range. This categorization is useful because all the gratings can go to zero order. Figure 2 shows the resolution versus photon energy over the ranges for each of the gratings. These are accompanied with some flux numbers based upon a theoretical estimate of the monochromator throughput with 100ma in the ring. Note the high resolution over the wide operating range if realized will be significantly greater than that available with most currently operating instruments and competitive with the best ever achieved. The beam spot size on the sample with the optics described below should be about 0.6mm half width at focus.

3.3 Configurational Description

Figure 3 shows the primary configurational elements in the monochromator: the entrance separation chamber; the entrance bellows; the moving chamber; the exit chamber; the air bearing system; the laser interferometer; and the granite reference surface. Figure 4 shows the same elements in the actual assembly drawing. Figures 5 through 8 show perspective views of the monochromator. Figure 5 shows the vacuum chamber and Fig 6 shows the optical mechanism, and the lower half of the vacuum chamber mounted on the granite base. Figure 7 shows the air bearing system and we have used both straight air bearings as well as combination air-vacuum pads. The air-vacuum pads maintain the horizontal position of the instrument on the granite. Figure 8 shows the laser interferometer path. The three axis interferometer allows the motions to be tracked to the necessary precision. The Interferometer is backed up by some conventional encoders so the instrument can be used even if the interferometer is not working. Several of the other extensive alignment and positioning aids can be seen in figure 6. These include mirrors on the main shaft for auto-collimating the angular position during setup.

The optical platform is mounted to the granite separately from the vacuum chamber to eliminate inducing distortions in the optics. The optical base and the chamber are coupled at the drive nut on the lead screw. All the connections to the optical mechanism are made through the bottom of the chamber, so the top can be readily removed, thus exposing the instrument as depicted in figure 6. The chamber was fabricated by Thermionics and is closed with a Helicoflex seal. As of this writing, the chamber has performed to mechanical and vacuum specifications and has been installed on the granite base. A detailed paper on the monochromator will be presented once operational data have been obtained.

The moving component of the instrument weighs approximately 1300 Kg, but the drive shaft and stepping motor seen in the lower right of figure 6 and 7 is capable of driving the the mechanism through a single resolution step in less than 50 msec and attain a maximum velocity of about 10 mm/sec. Thus the system can scan its full range in about 1.5 minutes.

4. Experimental Area and Refocusing

The refocusing system is built into the monochromator. The refocusing system creates three work areas by providing two beams deflected horizontally at 14 degrees from mirrors 0.5 meters from the exit slit and one vertically at four degrees with a mirror 1.0 meter from the exit slit. The side stations are at 2.25 meters and the end station 3.5 meters from their respective mirrors. Although we would have liked to have moved experimental stations further back, the focusing aberrations substantially increased the size of the beam so that the apertures of typical electron spectrometers would have been overfilled. Fully optimized optics can only be accomplished with a single end station because of the space requirements.

The current design plan is based on toroidal optics with evolution to conically formed optics planned in the future. The two side stations have a more limited energy range than the end station, but this is offset by the participating research groups being able to maintain experimental chambers in place permanently. The end station port is for general use and has no permanently installed chamber. Provision has been developed, however, for rapidly changing and positioning chambers including the SSRL facility chambers available for general users.

ACKNOWLEDGEMENT: We are indebted to Art Bienenstock for his continuing support of the Beam Line V project. We thank Herman Winick for his interest and for discussion of the Multi-undulator. We thank all of the SSRL staff who have also made important contributions to the beam line.

This work was supported by NSF/UIC Grant DMR 81-08343, DARPA, the DOE, and Xerox and was performed at the Stanford Synchrotron Radiation Laboratory and SLAC which are supported by the DOE.

References

1. R.Z. Bachrach, R.D. Bringans, B.B. Pate, and R.G. Carr, in "Proceedings of the International Conference on Insertion Devices for Synchrotron Sources", edited by R. Tatchyn and I. Lindau, 1986.
2. For information contact: H.Y. Chmait, TRW Space and technology Group, Optics Dept 01/1141, One Space Park, Redondo Beach, Ca 90278. (213) 536-4278

Tables:

1. Xerox/Stanford SSRL BLV Multi-Undulator Parameters
2. Locust Monochromator Parameters

FIGURES

Fig. 1 Pictorial of the Xerox/Stanford SSRL BLV Multi-undulator. The five possible insertions mounted on stainless steel I beams are shown installed in the mover assembly surrounding the SPEAR beam pipe. The inset shows how the SmCo₅ magnet bars are mounted.

Fig. 2 Estimated energy resolution versus photon energy for each of the gratings. The inset numbers give estimated fluxes at the sample for SPEAR running 100 ma at 3 GeV.

Fig. 3 Schematic side view of the Locust Monochromator showing the major assemblies. The details are given in the text. A perspective view of the Moving Chamber is shown in figure 5. The exit chamber contains the exit slit and the refocusing mirrors.

Fig. 4 Assembly side view of the Locust Monochromator. A perspective view of the monochromator is shown in figures 5-8.

Fig. 5 Perspective view of the monochromator moving vacuum chamber assembly depicted in figures 2 and 3. The chamber was fabricated by Thermionics and the upper and lower pieces are closed with a Helicoflex seal.

Fig. 6 Perspective view of the main optical mechanism with the vacuum envelope removed. All the connections are introduced through the bottom plate to allow opening without disassembly of the optical mechanism. Note the water cooling, the laser interferometer cubes, and the other alignment aids.

Fig. 7 Perspective view of the lower chamber assembly and the air bearing system.

Fig. 8 Perspective view of the laser interferometer system, showing the optical paths for the three axes.

TABLE 1

Xerox/Stanford SSRL BLV Multi-Undulator Parameters

Length: 183 cm Minimum Gap: 3cm
SPEAR: 3.0 GeV 100ma

Number of periods	10	15	24	30
Period Length- λ (cm)	18.3	12.2	7.6	6.1
Magnet Block Size (cm)	$1/8 \times 1/8 \times 8$	$1/8 \times 1/8 \times 7$	$1/4 \times 1/4 \times 6$	$1/4 \times 1/4 \times 7$
Tuning Range* (eV)	16-417	84-622	360-1020	800-1260
K maximum (3 cm gap)	9.0	4.6	2.6	1.6
	<u>eV, watts</u>	<u>eV, watts</u>	<u>eV, watts</u>	<u>eV, watts</u>
E ₁ , P _{tot} (max K)	11.3, 289.4	59.8, 173.2	260.7, 136.3	616.5, 82.3
E ₁ , P _{tot} (K=3.5)	65.8, 56.6	99.0, 98.5	--	--
E ₁ , P _{tot} (K=1.4)	237.5, 7.3	356.3, 16.4	570.0, 42.0	--
E ₁ , P _{tot} (K=0.5)	417.0, 0.9	621.6, 2.0	993.4, 5.0	1245.0, 8.0
E ₁ , P _{tot} (K=0.0)	467	700.8	1120.6	1401.6

* The lower limit of this tuning range is set by the power limit. With suitable power filtering the maximum K range can be reached. Note that if the storage ring energy is reduced these numbers scale by the square of the energy.

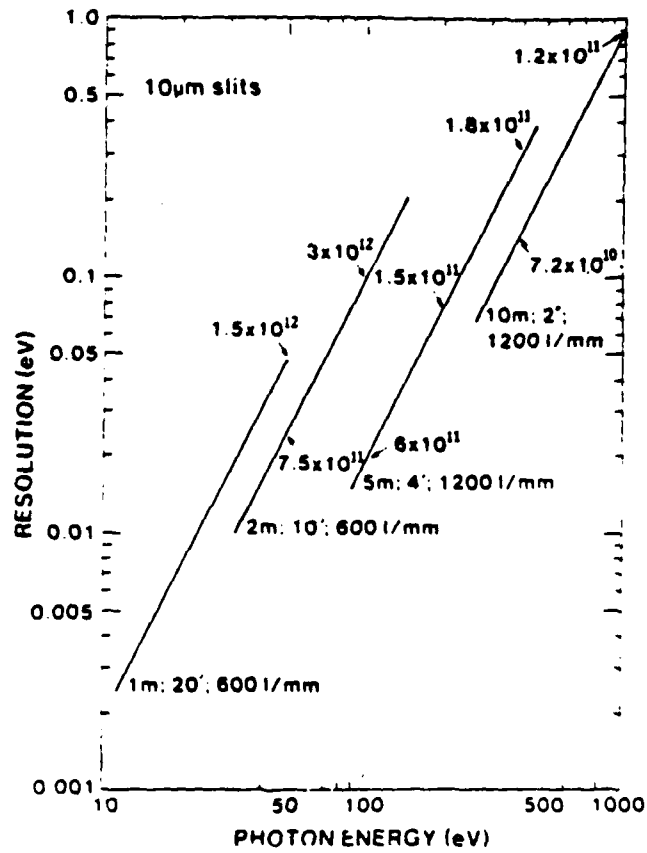
TABLE 2

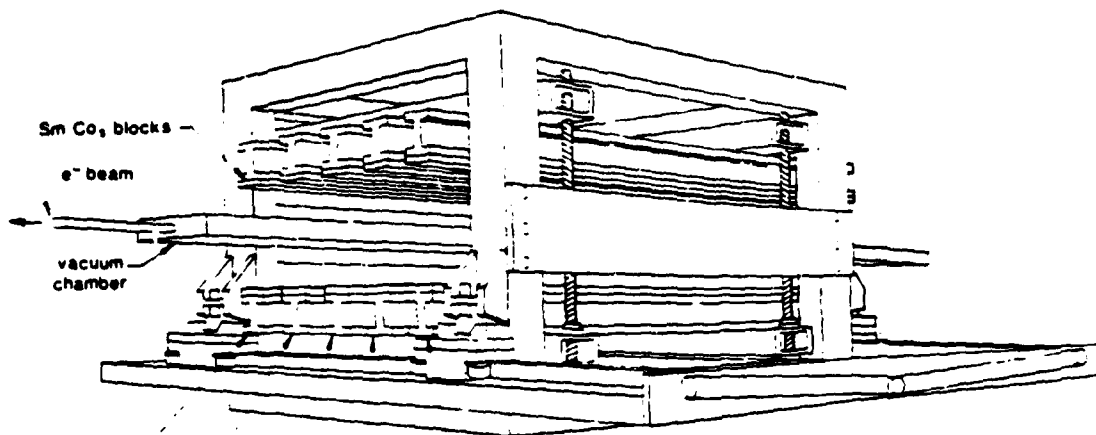
Locust Monochromator Parameters

**Operating Range: 10-1000 eV
 100 Watts Input Power
 Silicon Carbide Optics
 Water Cooled Optics
 Laser Interferometer Encoding
 Fully Computer Controlled**

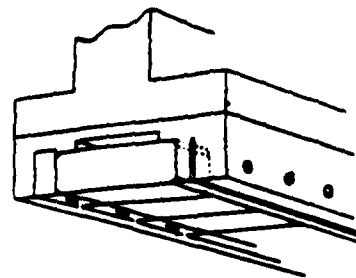
	20	40	100	200
Grating Angle	20	40	100	200
Grating Radius (mm)	9355	4817	1986	1037
Grating Blank (l.w.d-mm)	100x40x30	80x40x30	60x40x30	60x40x30
grooves/mm	1200	1200	600	600
Resolution (A)	0.0126	0.0242	0.0593	0.1136
S1G (mm)	3265	3360	3448	3547
Linear Travel (mm)	820	800	400	150
Angular Travel	50	120	180	130
Blaze angle	1.30	2.00	--*	--*
Blaze Energy (eV)	600	210	70*	20*
Resolution at Blaze (eV)	0.37	0.086	0.023	0.0036
Optimized Range (eV)	1500 - 250	450 - 90	150 - 30	50 - 10
Mechanical Range (eV)	zero order - 220	zero order - 60	zero order - 27	zero order - 10

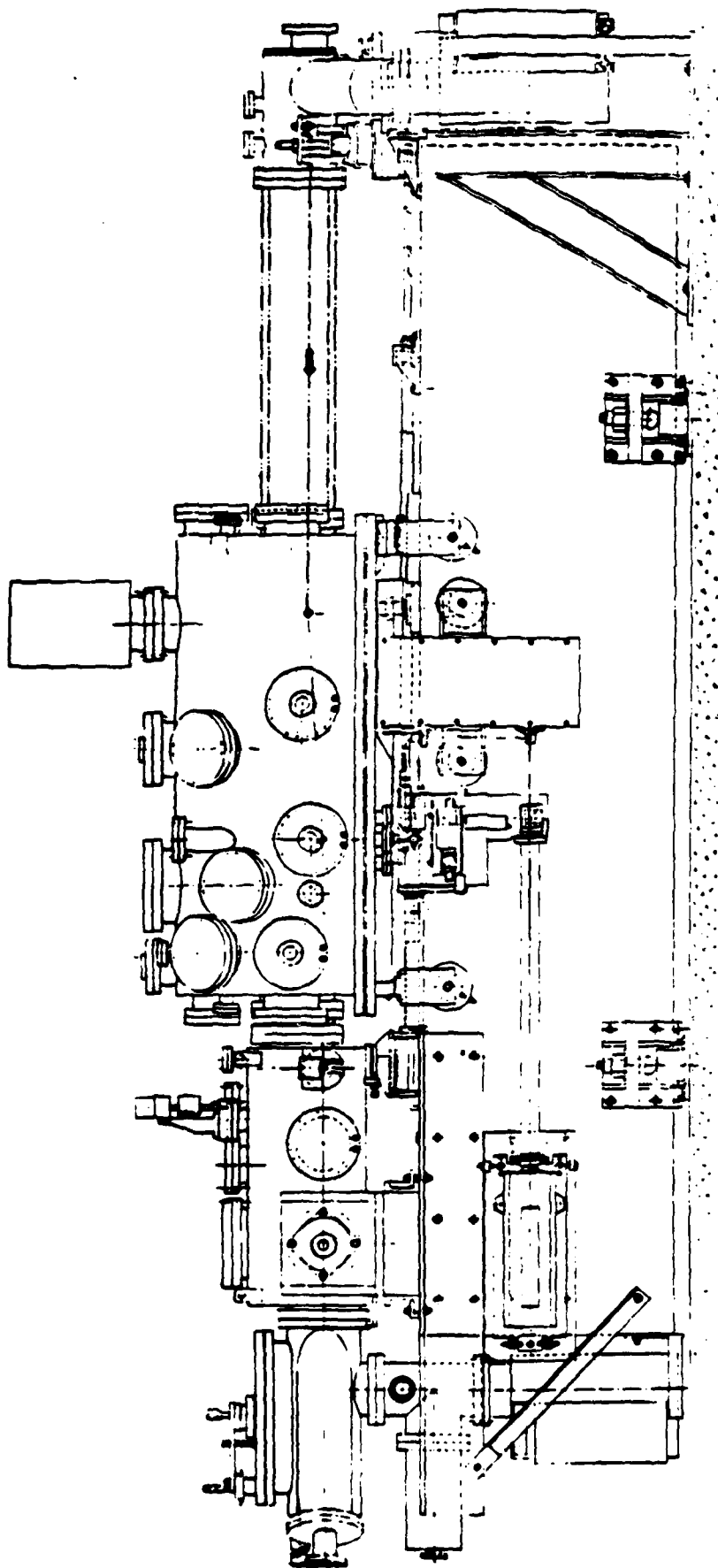
* These are laminar cylindrical gratings which are not blazed



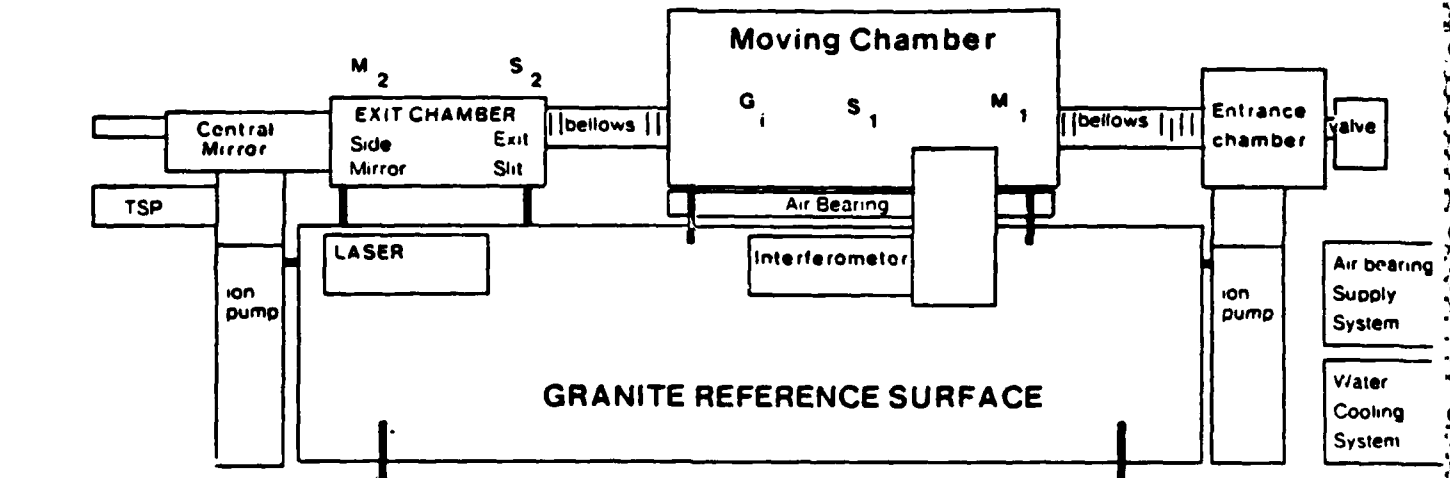


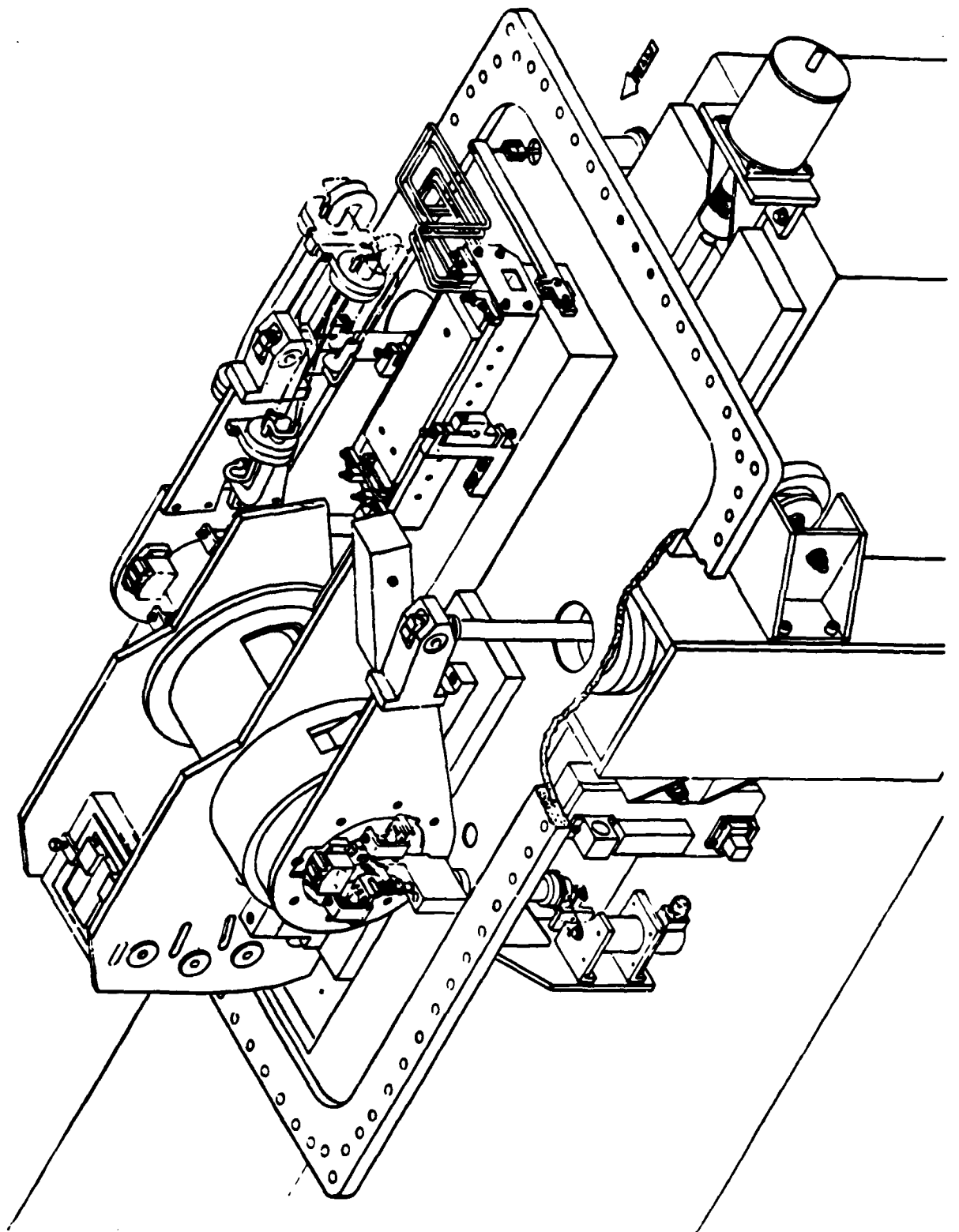
Future —
30 Periods —
24 Periods — — 10 Periods
15 Periods —

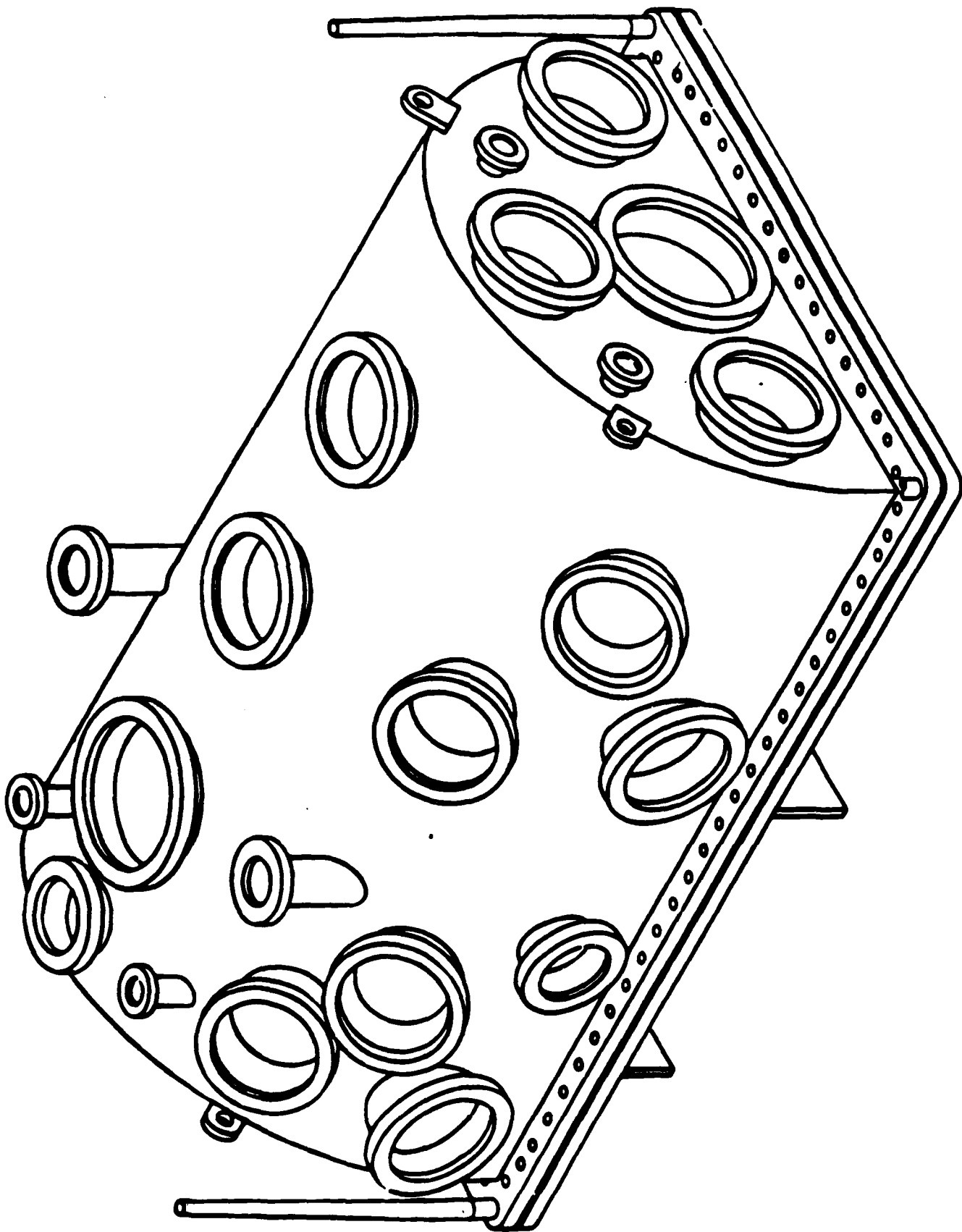


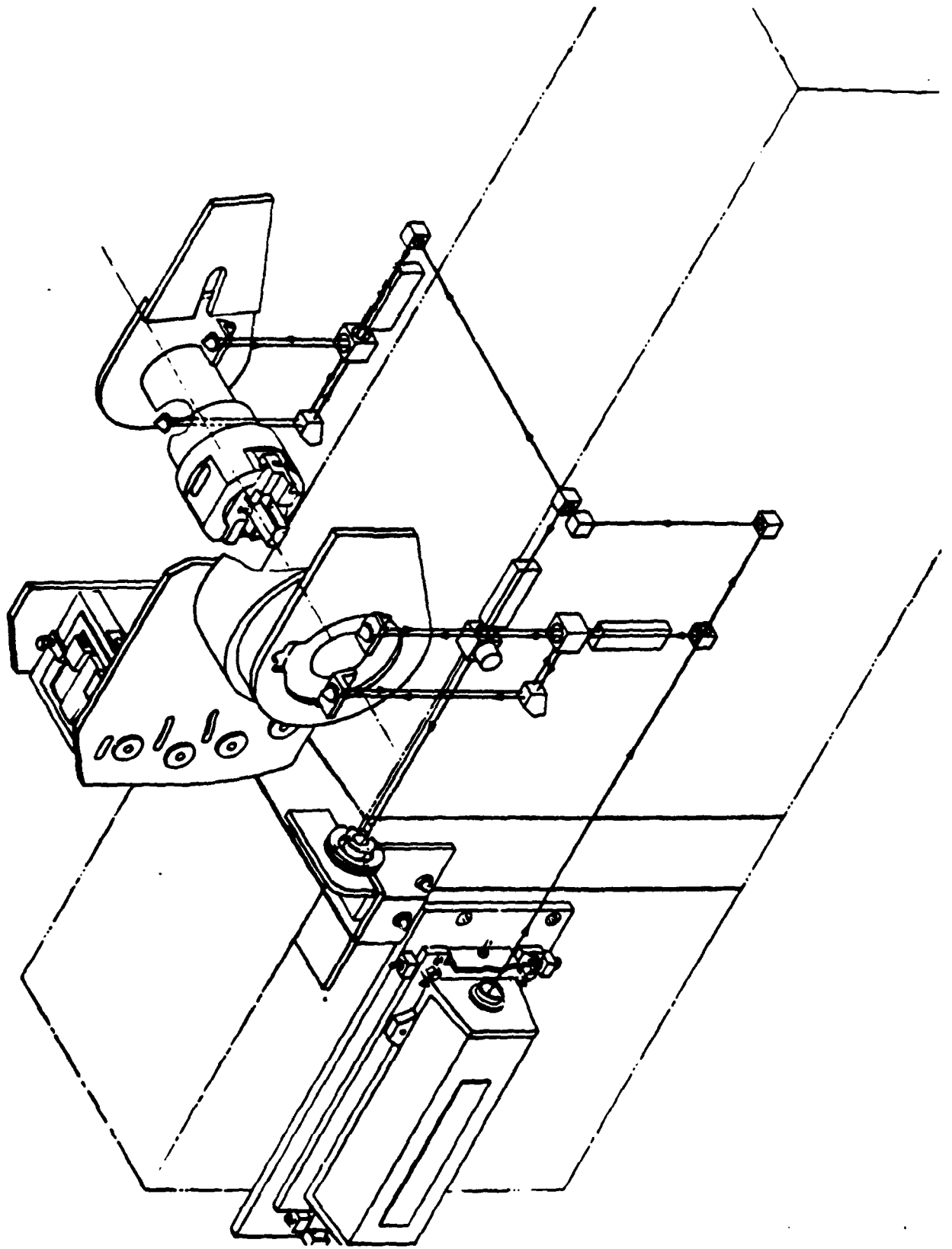


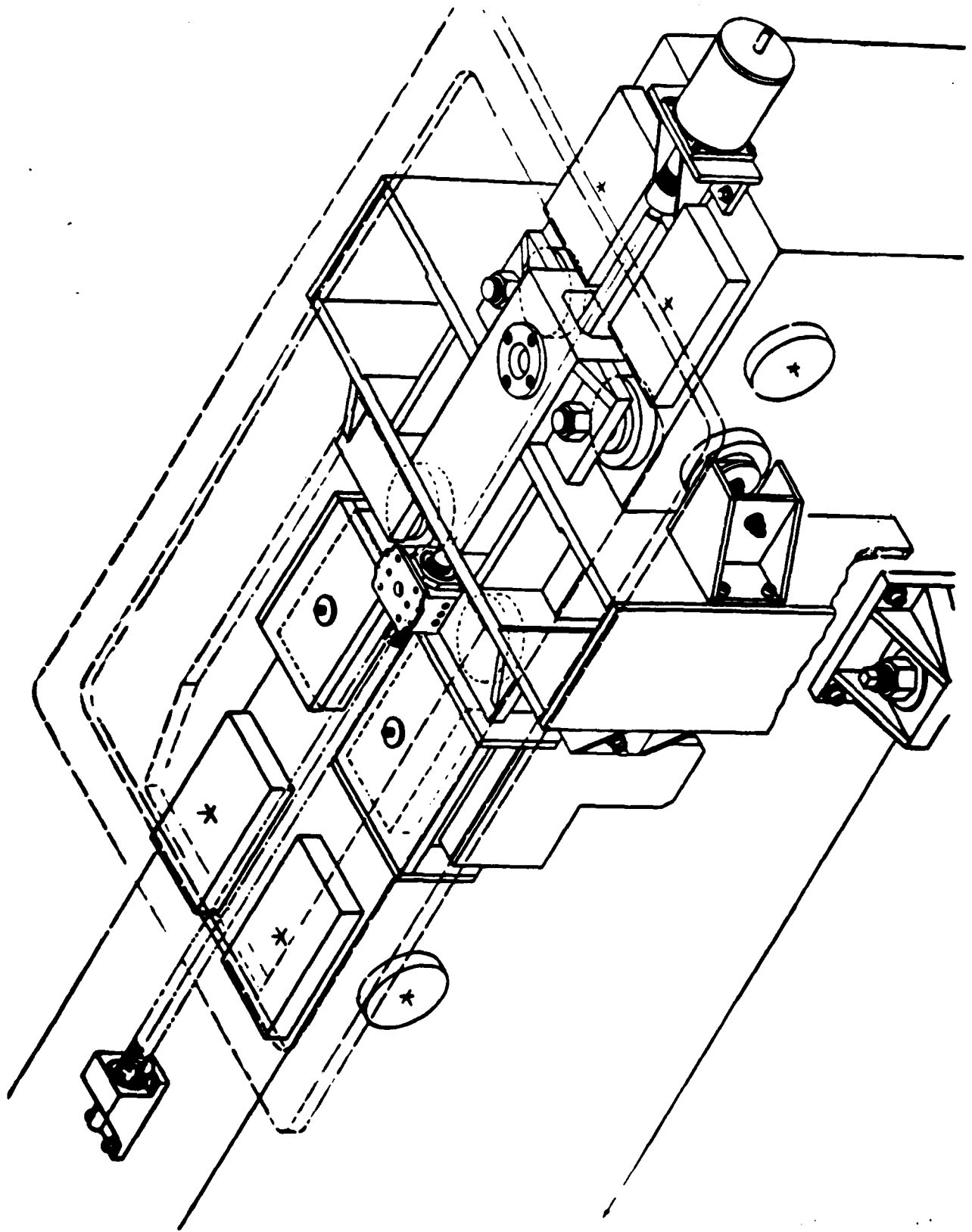
LOCUST MONOCHROMATOR











Technical Paper: "The SSRL Insertion Device Beam Line Wunder", by R.Z. Bachrach et al in SPIE 582, pp. 257-267 (1986); R. Tatchyn and I. Lindau eds.

The SSRL Insertion Device Beam Line 'Wunder'

R.Z. Bachrach and R.D. Bringans

Xerox Palo Alto Research Center
3333 Coyote Hill Road, Palo Alto, Ca 94304, (415)494-4157

B.B. Pate and R.G. Carr

Stanford Synchrotron Radiation Laboratory
SLAC Bin 69, PO Box 4349, Stanford University, Stanford, Ca 94305

Abstract

Insertion devices as radiation sources on storage rings offer potential for substantial gains in beam brightness and flux delivered to a sample. Achieving these gains, however, requires several new aspects of beam line design. New aspects of beam line design arise from the high beam power, the complex spectral and geometrical characteristics, and the need for a wide spectral range. We discuss these aspects of insertion device soft X-ray synchrotron radiation beam lines with examples drawn from our project creating Beam Line Wunder at the Stanford Synchrotron Radiation Laboratory. The major research use envisioned for this beam line is for spectroscopic experiments which require the highest possible intensity and resolution for a tunable constant deviation source. We summarize the current status of each of the beam line major components: the Multi-undulator, the transport system, the Locust Monochromator, the computer control system, and the experimental area.

I. Introduction

Several new aspects of synchrotron radiation beam line design become important when bending magnet sources are replaced by an undulator. Our project creating Beam Line Wunder at the Stanford Synchrotron Radiation Laboratory^{1,2}, SSRL, has elucidated and evaluated these aspects for their impact on all the beam line system elements. In this paper, we describe the requirements for an undulator based beam line in the context of the formulation of SSRL Beam Line Wunder. We review specific detail on the designs and implementations aimed at a beam line for the spectral range from 10-1000 eV which will deliver the highest possible power density to the sample in the smallest feasible bandwidth.

The primary system concerns can be partitioned into beam collimation, spectral range, spatial characteristics, and power. In particular, the increased beam power density from an undulator source necessitates active cooling of most elements likely to be hit by the beam. In the case of optical elements, this requirement arises not only because of possible damage, but also because distortions of the optics must be minimized to maintain ultimate performance. As a result of our studies, we have shown a new way for configuring undulators as sources, we have shown the expected improvements to be gained from silicon carbide optics, we have formulated a state of the art second generation soft X-ray monochromator which can handle the high power and deliver high resolution, and we have resolved issues on the best experimental configurations for the use of undulator beams.

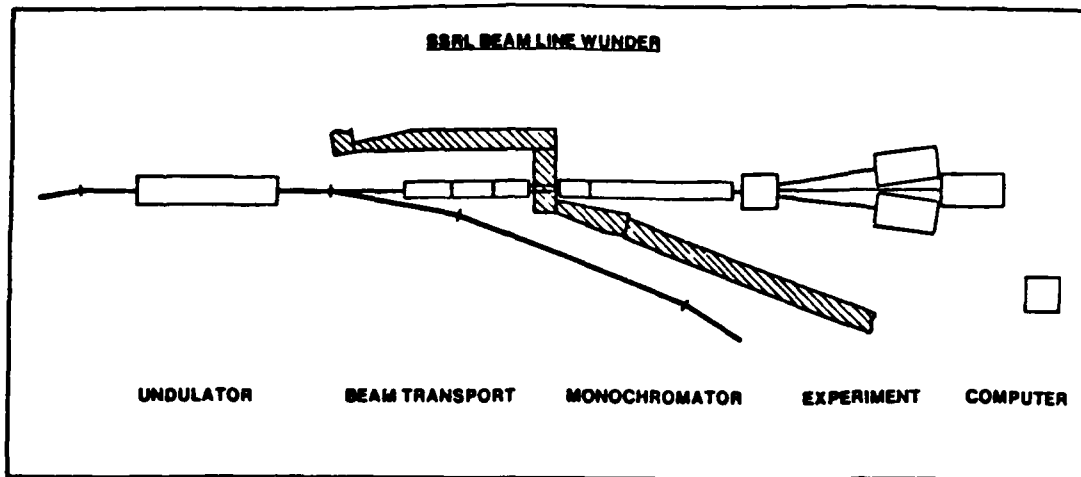


Fig. 1 Beam line description consisting of the elements: Source, transport, monochromator, experiment, computer.

The project began in 1979 as a bending magnet beam line but shifted to wiggler-undulator technology after the successful operation of a permanent magnet device in SPEAR.^{3,4} The collaborative project¹ between Xerox and Stanford motivated the funding from NSF/UIC, DARPA, DOE, and Xerox and then first needed to modify the SPEAR storage ring to free up the physical space for the required straight section by replacing the previous four SPEAR design RF cavities with two of the PEP design. The funding required for the construction and installation of these two RF cavities was substantial and therefore our beam line development work was delayed several years as the initial funding was used to modify the storage ring. In the mean time, we pursued detailed studies both of undulators as sources and of the impact of achieving the desired performance with the high powers anticipated before embarking on specific designs.² These studies led us to the beam line system implementation described here.

Figure 1 summarizes the main beam line elements that are discussed in this paper. The Xerox/Stanford SSRL BLV Multi-undulator; the beam transport system; the Locust Monochromator; the experimental area; and the beam line computer. We will discuss aspects of each of these elements in that order, but these descriptions should be considered previews until operational data is available in the next year to two.

II. The Xerox/Stanford SSRL BLV Multi-undulator

Early in the design studies of the beam line,^{1,2} we specified that several undulator periods would be required to span fully the design range of 10-1000 eV. The result of the considerations is the discovery that specific insertions could be sized so that they could be placed close together. Scanning the undulators can be accomplished in a straightforward manner by varying the magnet jaw gaps of all the undulators simultaneously with the active one positioned over the SPEAR beam pipe. Interchange between the different periods can then be carried out by opening the jaws to full gap and sliding the undulators across the beam pipe within the confines of the SPEAR tunnel. The resultant Xerox/Stanford SSRL BLV Multi-undulator, shown in figure 2 with five possible insertion devices, was installed into SPEAR on September 10, 1985, and its construction and operation will be detailed in a subsequent paper. Table 1 lists many of the relevant parameters. Figure 2 depicts the five possible insertion devices mounted on individual stainless steel I beams mounted in the mover structure surrounding the SPEAR beam pipe. The inset shows how the SmCo₅ magnet bars are held.

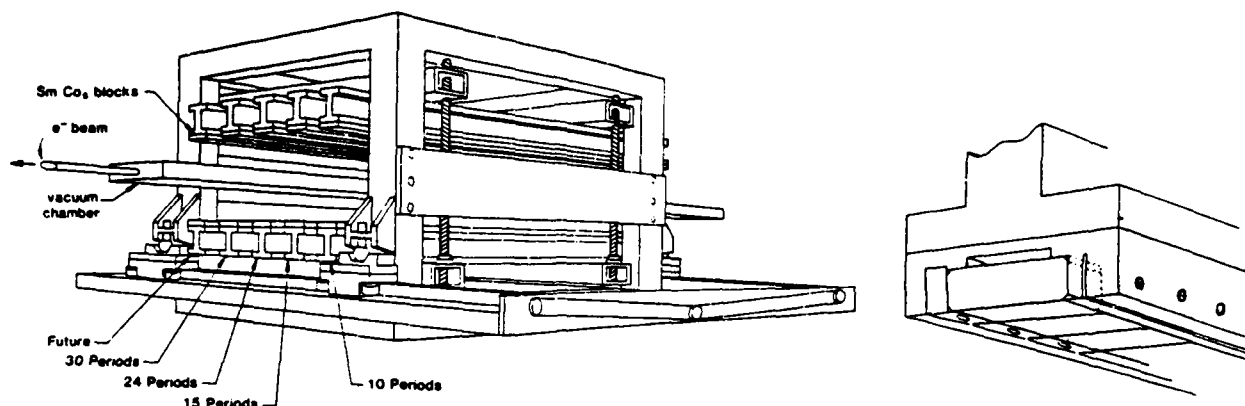


Fig. 2. Pictorial of the Xerox/Stanford SSRL BLV Multi-undulator. The five possible insertions mounted on stainless steel I beams are shown installed in the mover assembly surrounding the SPEAR beam pipe. The inset shows how the SmCo₅ magnet bars are mounted.

TABLE I
Xerox/Stanford SSRL BLV Multi-Undulator Parameters

	Length: 183 cm		Minimum Gap: 3cm	
	SPEAR: 3.0 GeV		100ma	
Number of periods	10	15	24	30
Period Length-λ (cm)	18.3	12.2	7.6	6.1
Magnet Block Size (cm)	λ/8 x λ/8 x 8	λ/8 x λ/8 x 7	λ/4 x λ/4 x 6	λ/4 x λ/4 x 7
Tuning Range* (eV)	16-417	84-622	360-1020	800-1260
K maximum (3 cm gap)	9.0	4.6	2.6	1.6
	eV, watts		eV, watts	
E ₁ · P _{tot} (max K)	11.3, 289.4	59.8, 173.2	260.7, 136.3	616.5, 82.3
E ₁ · P _{tot} (K=3.5)	65.8, 56.6	99.0, 98.5	---	---
E ₁ · P _{tot} (K=1.4)	237.5, 7.3	356.3, 16.4	570.0, 42.0	---
E ₁ · P _{tot} (K=0.5)	417.0, 0.9	621.6, 2.0	993.4, 5.0	1245.0, 8.0
E ₁ · P _{tot} (K=0.0)	467	700.8	1120.6	1401.6

* The lower limit of this tuning range is set by the beam line power limit. With suitable power filtering, the maximum K range can be reached. Note that if the storage ring energy is reduced these number scale by the square of the energy.

The Multi-undulator innovation represents a major advance in the art of permanent magnet undulator devices and solves the problem of achieving a wide range while remaining in the undulator regime. We have chosen to implement devices with N=10,15,24 and 30 periods in the available 183cm SPEAR straight section corresponding to 18.3, 12.2, 7.6, and 6.1 cm period lengths.

The undulator devices implemented use the permanent magnet arrangement described by Halbach⁵ in which there are M=4 blocks per undulator period. The relationship between the on-axis field, the magnet gap g, magnet height h, magnet period λ, and the remanent field B_r of the magnets is given by:

$$B_0 = 2 B_r \exp[-\pi g/\lambda] \frac{\sin(\pi/M) [1 - \exp(-2\pi h/\lambda)]}{\pi/M} \quad (4)$$

in the limit where the dimension of the magnets transverse to the beam is large. The magnets we have received from Vacuum Schmelztechnik achieve 0.93 Tesla for B_r. We have restricted ourselves to an out of vacuum device and thus the minimum gap for the magnets is about 3.0cm. In optimizing our devices, the 30 and 24 period devices have h = λ/4 while the 15 and 10 period devices have two square section blocks with h = λ/8 per orientation. This reduces the maximum field and thereby K and power. The length of the blocks was also made as small as feasible consistent with the magnetic field uniformity required for operation of the storage ring. One should note that reducing the volume of SmCo₅ for these latter devices represents a substantial reduction in cost. In assembling the magnets, a number of constraints were developed to sort and place the individual magnets. The sorting procedure is described in this volume⁶ and the overall construction of the Multi-undulator will be presented in a subsequent paper.⁷

The combination of periods achieves the scanning ranges for E_1 depicted in figure 3 (reproduced from reference 2) for SPEAR operating at 1.5 and 3.0 GeV and derived from equation 1 for the i th harmonic.

$$E_i(\text{eV}) = \frac{950 [E_s(\text{GeV})]^2 i}{\lambda(\text{cm}) [1 + K^2/2 + \gamma^2 \theta^2]} \quad i=1,2,3,4,\dots \quad (1)$$

The parameter K is defined as:

$$K = 0.934 B_0(\text{Tesla}) \lambda(\text{cm}). \quad (2)$$

B_0 is the on axis magnetic field, E_s is the stored electron energy, $\gamma = E_s(\text{MeV})/0.511$, and θ is the observation angle. One can think of K as a coupling constant that expresses how much the electron beam is being wiggled. Small K corresponds to the undulator regime and high K to the wiggler regime. In optimizing the undulator design for the photon range of 10 to 1000eV at an electron energy of 3.0GeV several considerations arise. For example, for the original 30 period device installed at SSRL, the fundamental cannot go below about 720eV in an out of vacuum mode. Increasing the length of the undulator's period makes this problem less severe but reduces the overall intensity in a fixed length device because of the reduction of the number of periods. With the length limitation that $N\lambda$ must be less than about 183cm one can see from equation (1) that high values of K and/or θ are required in order to get down to lower photon energies. The 15 period device covers much of the desired range, but the coverage and overlap is improved by having the 10 and 24 period devices. The 10 period device in particular makes the low energy range accessible with the first harmonic. For SPEAR at 3 GeV, pushing the fundamental below 50eV even with the 10 period device requires large values of K and thus high total power from the device.

In an earlier study⁸ some of these aspects were examined and plots were given of the magnet jaw gap size and the magnitude of K required to obtain a particular value of the first harmonic. Figure 4 presents this information with the parameters from the implemented Multi-undulator periods. Shown are the energy of the first harmonic and K as a function of undulator jaw gap for the four undulators. The gap drive system was designed with sufficient resolution that both the Multi-undulator and the monochromator can track together. This required a stepping tolerance of about 25 μm .

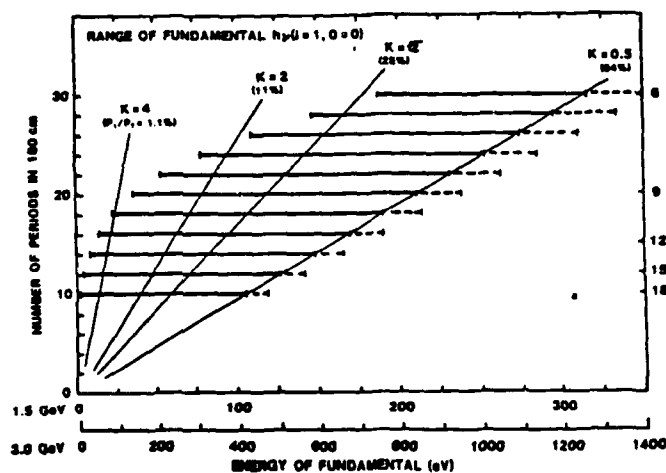


Fig. 3 Diagrammatic representation of tuning ranges for wiggler-undulators showing the consideration of parameter adjustments. The two axes are the number of periods and the energy of the fundamental for SPEAR operating at 1.5 and 3.0 GeV. At present, 10, 15, 24, and 30 period devices have been constructed and provide a set of overlapping ranges spanning 10-1000eV.

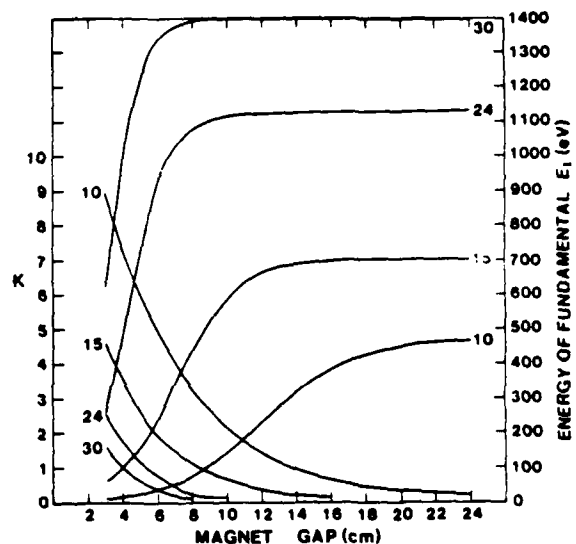


Fig. 4 Plot of K and energy of the fundamental versus magnet jaw gap for the four multi-undulator periods.

In previous papers, we have characterized our expectations for the power from these devices. Figure 5 compares the expected first harmonic flux for three of the undulators compared to bending magnet and wiggler devices. The undulator curves depict the first harmonic tuning range while the wiggler and bending magnet curves are continua. The total power radiated by the undulator per ma of electron beam current is given by².

$$P_T \text{ (W/ma)} = 0.00730 K^2 [E(\text{GeV})]^2 N / \lambda(\text{cm}) \quad (5)$$

and the power in the fundamental is given by the approximate equation

$$P_1 \approx P_T / (1 + K^2/2)^2 \quad (6)$$

This relationship is shown graphically in Figure 6. Note that to a good approximation, the first harmonic power peaks at $K = \sqrt{2}$ where it equals one quarter the total power. In general, if one can tolerate the total power loading, one can for a fixed length device usually get more power at the photon energy of interest by operating a short period device at a higher K value. Thus the design optimization criteria are fairly complicated and involve a lot of system considerations which include both spatial and spectral filtering. For the Beam Line Wunder design, the determining criteria ultimately were set by the power handling capability and the aperture of the monochromator. We thus limited the ultimate capability of elements in front of the monochromator to match and thereby limited the cost. The major design objective is to achieve as wide a range as possible while keeping the K parameter below 2 in order to stay in the undulator regime as much as possible. The undulator regime is desirable because it optimizes the flux at the desired energy to the total flux.

We show in Figure 7 selected spectra calculated for $K = 1.25, 2.25,$ and 3.5 for the 15 period undulator which, with suitable scaling of the energy and intensity scales, are typical of those for any of the devices over the same K range. The spectra are the result of integrating over all azimuthal angle ϕ and over θ up to a maximum angle of 1 mrad. The assumption that the emittance of the electron beam is zero has only a small effect when integrating over such large angles. The general trend is that as K increases, the continuum aspect increases but that there is significant modulation of the spectrum. Below $K = 1$, the spectrum is essentially dominated by the first harmonic. Note that in all the spectra, the low energy cut off energy is the same and is established by the viewing aperture.

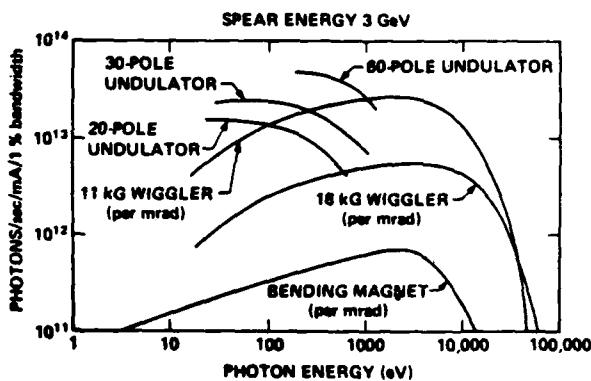


Fig. 5 Estimated first order flux into the beam line for various sources for SPEAR operating at 3GeV under dedicated conditions. The wiggler and bending magnet curves are a continuum. The undulator curves represent a tuning range with the low energy cut off determined by the minimum gap between the permanent magnets. This range also shifts with the stored energy of SPEAR beam.

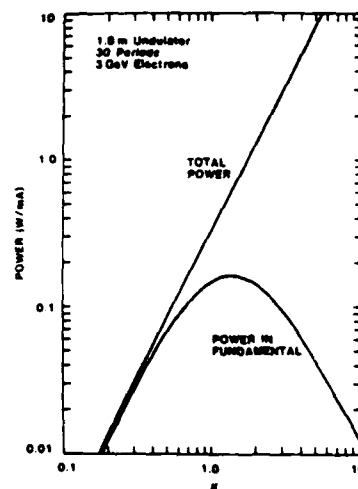
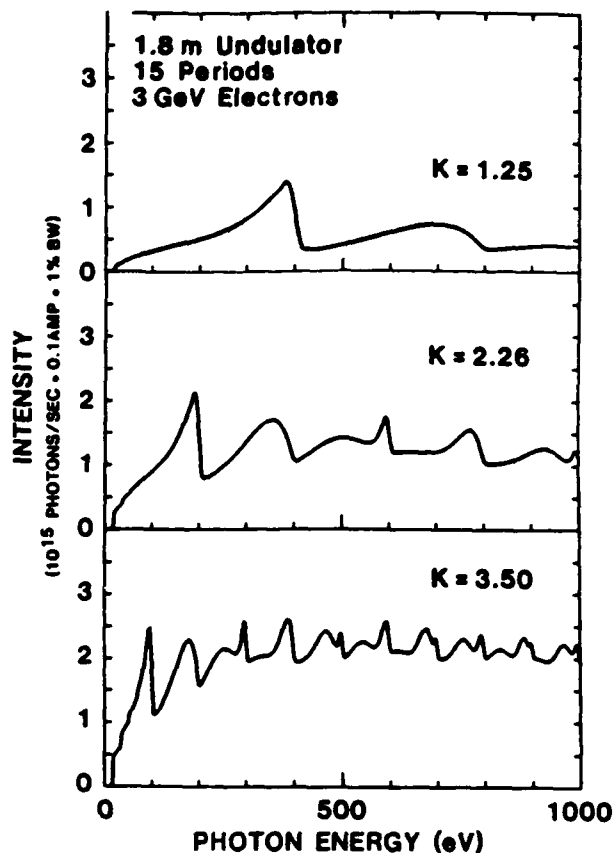


Fig 6 Comparison of total power and power in the first harmonic as a function of K showing the optimization in the vicinity of $K = 1$. One should note however that the total optical power at a desired energy can be increased by increasing K if one can handle the total power.

Fig 7 Undulator spectra for a 15 period undulator with $l = 12.2\text{cm}$ period length for SPEAR operating at an electron energy of 3 GeV. Spectra are shown for three values of the undulator parameter K , ie three different magnet jaw gap settings.



To obtain photon energies below about 60 eV with the 15 period device, it is necessary to go to large observer angles. Because the beam line elements, in particular the gratings in the monochromator, subtend a finite angle, it is important to examine the effect of an angular restriction on the spectra. In the spectrum for $K = 3.5$ the angular cutoff is seen clearly as the step like structure at low energies. It is clear that the constraints for Beam line V at SSRL require that relatively large acceptance angles be available in order to get to low photon energies with the 15 period device. One can extend the range however by working in the tail of the first harmonic. As can be seen in figure 7, the first harmonic has a considerable tail to low energy. Spatially, these lower energy components arise off axis and so if one wants to use them, one needs to collect a larger solid angle than needed for the first harmonic energy. Ideally one would extend to 3 milliradians in the horizontal, but for a number of reasons we limited this implementation to 1.5 milliradians. We propose to obtain the wider range if necessary with the power filter described below.

Examination of the spectra for the 15 period undulator in figure 7 shows that it is easy to cover the range from ~20 to 1000eV with one setting (e.g. $K = 3.5$) if one does not require the fundamental to be scanned. It is clear that careful monitoring of the incident photon flux and good higher order rejection would be necessary for spectroscopic experiments in this case because of the intrinsic modulation of the input beam. To scan the fundamental over a similar range requires the full complement of devices.

Table 1 summarizes the parameters characterizing the Multi-undulator for SPEAR operating at 3GeV, a typical dedicated operating condition. For each device the range of the fundamental will have a low energy cutoff set by the requirement that the magnets have a remanent field of 0.93 Tesla and a minimum gap of 3.0cm, and an absolute high energy cutoff set by $K = 0$ in equation (1). Table one shows the tuning ranges achievable with the Multi-undulator based upon power criteria and also characterizes the photon energy and radiated power at K values of 3.5, 1.4, and 0.5 corresponding to the half power and maximum of the fundamental.

In the principal operating mode, the SPEAR control room will enable the Beam Line V computer to control the variation of the magnet jaw gap within appropriate limits. The dual control system also allows the Multi-undulator to be operated from the SPEAR control room when appropriate. Some of these aspects are discussed further in section VI.

III. BEAM TRANSPORT SYSTEM

The beam transport system is the backbone of the beam line and incorporates a number of essential elements for beam forming, control, and diagnostics. A previous paper outlined the functional elements required in detail². Initially we had hoped to utilize a rather small diameter pipe, but more detailed examination of the spatial characteristics of the beam and issues of radiation safety led us to a design that was more typical of bending magnet transport systems. Avoiding transitions in flange sizes is also advantageous, so that we propagated a given pipe size until a transition was necessary for other reasons.

A series of masks, stoppers, valves, shutters, and apertures constitute the initial control part of the beam line. The masks serve to protect the valves from the beam power loading and also act as radiation shields. The stoppers are an absolute radiation shield and are designed to absorb the full beam should it accidentally dump down the beam line. The apertures define the useful beam and in the case of an undulator beam line, also serve to spatially filter stray radiation from upstream bending magnets. This stray source of radiation is a severe problem for position monitor design and for the control of the beam in the vicinity of the beam line takeoff. Our original design specification called for two sets of adjustable apertures, one in front of the position monitor and one after. The later set of apertures can spatially filter the undulator radiation and is useful for isolating the first harmonic and reducing extraneous higher order power. This is a particularly useful aspect with the Multi-undulator. The four periods we have available potentially allow us to drive the first harmonic over the full 10-1000 eV range.

The beam line has both horizontal and vertical steering, but only the vertical steering is maintained with a feedback system. The SPEAR beam position detector consists of a set of 1mm electrodes set 1cm apart in the fringe field of the radiation. This positioning was chosen to accommodate the spatial variation of the undulator beam over the range of operating parameters. The spatial extent of an undulator beam varies enormously, so horizontal position detection, in particular, is difficult. The SPEAR beam is currently 6mmx1mm, so that some horizontal sensing can be accomplished, but this is primarily done with intermittent use of fluorescent screens in the diagnostic sections. The position monitoring and steering is still being evaluated because of overlap of radiation from upstream bending magnets with the undulator radiation. It is hoped that apertures that have been designed but not yet installed in front of the beam position monitor will resolve this problem.

The power limits for the transport system were set by cost considerations. In order to be able to use standard water cooling we set 1200 watts/cm² as an upper limit for any element in the beam line with the understanding that the K of the undulators could be restricted to stay below this power limit. For design purposes and until operational experience is gained, we set the maximum power handling capability of the monochromator entrance slit at 40 watts or 40 watts/cm assuming that all the incident power is absorbed in some worst case alignments. This then corresponded to an input power onto the entrance mirror of about 100 watts and was consistent with the grating not absorbing more than 5 watts.

One consideration worth pointing out before proceeding further is that design of a transport for an undulator based beam line would be simpler if one were only dealing with the first harmonic of the undulator which has a relatively simple spatial characteristic. In order to best utilize the full energy and power range of the insertion devices however, one has to allow for operation both on the higher harmonics and, to reach low energies, in the spatially complicated low energy tail of the first harmonic. With all of these aspects considered, the beam line optics needs to accommodate several milliradians of horizontal collection.

In addressing this issue one also has to decide where first to horizontally focus the beam. Because of the characteristics of the undulator source, we chose not to perform any horizontal focusing prior to the monochromator. We then set the aperture of the monochromator at 1.5 mrad to allow collection of the low energy components. Note that if we were just collecting the fundamental, an aperture of 0.5 mrad would have sufficed. The horizontal demagnification on the sample is established by the refocusing optics system after the monochromator. We were also motivated in our choice by the fact that a potential SPEAR upgrade would reduce the beam size by about a factor of two. If we had used a conventional configuration with an M₀ mirror at 8 meters, the power density on the mirror in the undulator mode where the beam divergence is only about 0.5 mrad would have been about 100 times higher than our previous experience. In our current configuration, the first mirror, the elliptical cylinder entrance mirror, M₁, to the monochromator, is at about 15 meters and is made of silicon carbide.

One way to accommodate the high power present when one increases K is to place a low pass filter before the monochromator. We have considered a variety of schemes, all of which look feasible. The most promising are a vertical deflecting three mirror configuration originally proposed by Rehn⁹ and a horizontal Cassegrain configuration proposed by Pate which is both a spatial filter, beam compressor and reflective filter. The latter filter removes the inner 1.5 mrad and compresses the outer 1.5 mrad into the central beam. Both of the schemes allow the beam to enter and exit along the same axis so that little adjustment is needed in the optics for insertion and extraction.

A diagnostics and white light section of the transport system precedes the monochromator. The intent was to accommodate experiments that wanted to use the raw power available without any reflections. It also allows for using the higher harmonics to perform x-ray experiments. This option was discussed in an earlier paper¹ where it was shown that significant flux could be achieved up to 6 or 7 KeV. The diagnostics help to monitor the input flux and beam condition.

IV. The LOCUST MONOCROMATOR

In specifying a monochromator for this beam line, we sought an instrument which would match well to the undulator and SPEAR characteristics and which would advance the state of the art. The resulting Locust monochromator implements a constant deviation Vodar geometry Rowland Circle mounting and is descended from the Grasshopper Monochromator.¹⁰ By using closed loop computer control and configurational changes, the design incorporates a number of features that would not be achievable with either the Grasshopper or the Extended Range Grasshopper, ERG,¹¹ configuration for these optics. One should note that the basic optical path¹⁰ is equivalent in all three of these designs. This descriptive presentation is a preview to a complete presentation which will be made once the instrument is operational. Reference 12 presents a general review of current soft X-ray Monochromators.

IVa. Optics Description

One of the principal objectives of the Locust^{1,2} was to optimize the working spectral range of 10-1000 eV by incorporating a selectable grazing incidence angle, α' , on the grating. This approach better optimizes the grating efficiencies over the scanable energy range. It is not possible to optimize such a wide range with a single grating in this mounting. Thus the design incorporates four gratings with different grazing angles of incidence and optimized for subranges as shown in Table 2. This approach has allowed us to satisfy the criteria for blazed gratings that the blaze angle should be small compared to the angle of incidence in order to maintain efficiency.¹³ Alternative approaches such as the recent slit-less SX-700 designed by Peterson¹⁴ for BESSY which has a small emittance and the UMO proposal by Brown and Hulbert¹⁵ would not work well on SPEAR.

The optical path for the Locust monochromator shown in Figure 8 consists of a vertically focusing silicon carbide elliptical cylinder entrance mirror, M_1 , a silicon carbide Codling mirror-slit, S_1 , one of four gratings G_i , an exit Codling mirror-slit S_2 , and a refocusing mirror. The basic scanning operation translates M_1 - S_1 - G_i relative to S_2 while G_i and S_1 rotate in a θ - $\theta/2$ relationship. The three motions are actuated independently under computer control, but are actively encoded with a laser interferometer. With respect to the exit slit S_2 , the grating is traveling along a line defined by $Y_G = X_G \tan(\alpha')$ where Y_G is the distance from the line between slits which is collinear with the input beam axis and X_G is the distance from the exit slit to the center of the grating. At zero order, $X_G = S_{1G} \cos(\alpha')$ where $S_{1G} = D \sin(\alpha')$ is the entrance slit to grating distance and D is the Rowland Circle Diameter. (Note that D is also the grating radius of curvature.) By making the exit slit of the Codling mirror type, we were able to keep the refocusing optics fixed for all the different grating angles of incidence. Although we examined a number of schemes to eliminate this reflection, they did not seem advantageous or advisable at this time. Note that the total number of reflections is the same as on current Grasshopper or ERG beam lines because we do not have an M_0 collection mirror.

The equation of motions for this optics can be derived from the diffraction equation and the properties of the Rowland Circle. These are:

$$\lambda = d \cos(\alpha') \{ 1 - X_{sa} / D \cot(\alpha') - [1 - (X_{sa} / D)^2]^{1/2} \} \quad (7)$$

$$X_{sa} = D \{ \sin(\alpha) [\cos(\alpha') - \lambda / d] + \cos(\alpha') [1 - (\cos(\alpha') - \lambda / d)^2]^{1/2} \} \quad (8)$$

Where X_{sa} is the S_1 - S_2 distance and d is the ruling period of the grating or $1/d$ is the density in grooves/mm.

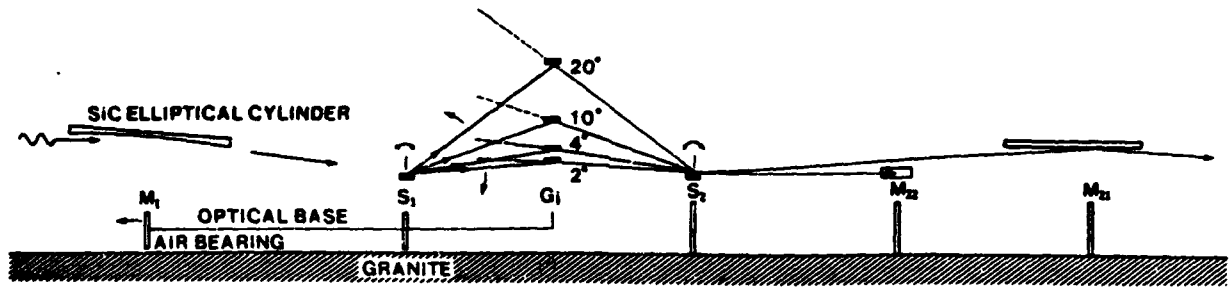


Fig. 8 Schematic of the Locust optics showing the placement of the elements for a zero order setting. The elements M_1 - S_1 - G_1 translate on the air bearing relative to S_2 . The motions are coordinated so that as G_1 rotates and translates, the grating travels along the lines emanating from S_2 and the Rowland circle to which the gratings are tangnt pass through the two slits S_1 and S_2 .

The basic design approach in the Locust was to make use of the relation for S_{1G} so that the gratings could be mounted on a common circle and their interchange accomplished by a rotation that is an extension of the primary scanning motion. Our nominal optical design parameters were the set (α', D) equal to $(2^\circ, 10m)$, $(4^\circ, 5m)$, $(10^\circ, 2m)$, and $(20^\circ, 1m)$ which established $S_{1G} \approx 350cm$ and allows all gratings to reach zero order. As discussed below, in the practical implementation, we modified these somewhat and the actual parameters are presented in Table 2. One advantage of this approach is that it allows one to more easily adjust for manufacturing tolerances in the grating radius of curvature which some suppliers quote as loose as $\pm 5\%$.

S_{1G} establishes the intrinsic scale of the instrument which is a 10 meter diameter Rowland circle as compared to 2 meters in the Grasshopper and 5 meters in the ERG. This increase in scale enabled us to achieve the desired range using a mechanism encompassed by a vacuum tank with the beam traversing out through a large bellows. One should note that in the ERG or Grasshopper design, the grating mechanism projects into the translation bellows which limits its angular excursion. This feature was a major constraint on the evolution of that configuration. Although the ERG incorporates more than one grating, only one of them can reach zero order. SSRL Grasshopper II has two gratings, but interchange requires subsequent realignment.

A second category of objectives for this implementation was to have all the major aspects of the monochromator under computer control to facilitate experimental use. This includes scanning, slit adjustment, and grating interchange. Grating interchange in other soft X-ray instruments requires manual re-alignment and our approach should avoid that. This feature should facilitate spectroscopic use of the instrument and avoid misconfigurations.

A third category of objectives was to enhance the alignment capability through incorporating appropriate fixtures into the design. Alignment consists of establishing the required spatial relationships of the optical elements to the typically *micron* tolerances required. This includes making the slit to slit axis colinear with the beam axis, centering the entrance slit on the axis of rotation, establishing the slit to grating distance, and placing the grating on the Rowland circle, etc. The tools and facilities built into the Locust design should greatly facilitate the alignment process and go far beyond the capability of the Grasshopper and ERG. The alignment is also facilitated by the incorporation of a three axis interferometer so that the absolute position and rotations are actively directly determined. Alignment systems add complexity to the design, but are appropriate to a second generation instrument such as this.

A fourth category of objectives was to incorporate water cooling of the optical elements necessitated by the high input power delivered by the undulator source. The water cooling also needed to have a minimum of loading and vibration effect on the optics and needed to meet construction criteria established by SLAC, namely that there be no water to vacuum welds and that pipes have minimal deflections. One secondary benefit of the water cooling is that it will help thermally stabilize the instrument which is necessary for the ultimate performance.

We presented in a previous paper the results of modeling studies which showed the effect of power loading on the optical elements and presented strategies for minimizing the optical distortion.² These are reproduced here as examples of the thermal loading studies. A difficult issue is what design rule to use to estimate the absorbed power for normal and exceptional cases. Particularly in the case of the grating, the problem is likely to be dominated by defects and irregularities. Thermal effects have several aspects which relate to energy, power, and power densities and the capacity of the paths to the sink where it is dumped. In most of our cases, we do not have so much energy that the sink is overwhelmed. We describe the results for two elements: the Codling mirror and the grating.

The Codling slit which is currently implemented in Grasshopper monochromators with SiC because of its better surface roughness capability.^{16,17} We needed to estimate the power handling capability of this element for two situations: singly focused vertically to fill the slit and doubly focused horizontally to meet other optical objectives. Thermal calculations are quite difficult for general geometries so Nelson Hower performed model calculations based on some ideal geometries. The present objective is to be able to handle one hundred watts into the monochromator which would give an absorbed power of about 40 watts into the Codling slit in worst case situations. We found that double focused optics which produces power densities of 10^6 - 10^7 watts/cm² would damage the entrance slit. We have therefore restricted our considerations to singly focused situations for this monochromator.

Figure 9 presents a schematic representation of the response of the Codling mirror to the focused input power. The table shows parameters for three materials and the distortion response for a back cooled geometry in terms of a slope error. The input parameters were 40 W absorbed or 7000 W/cm² considering the demagnification. With conservative estimates for the mirror reflectivity, this result should correspond to a total power capacity of 100W for our geometry. Whereas quartz would fail catastrophically, SiC seems to be satisfactory to these power densities.

Figure 10 shows the results derived by Hower and Tatchyn for two different strategies for extracting heat deposited in the grating. The results are shown for quartz and then the optimal quartz design is shown with a SiC implementation. For the purposes of this discussion, the variable f_p represents either the resolving power or the throughput of the monochromator. We do not present the purely radiatively cooled case because the grating temperature would rise to above 500°C which we considered unacceptable. The back cooled case is very sensitive to the input power because the radius of curvature changes. In fact the optimal solution is to extract the power from the side near the input surface. By keeping the aspect ratio approximately 3:1, this approach uses the cool back to stiffen the structure. The significant improvements are readily seen in the curves. The substitution of SiC for quartz produces the expectation of dramatic improvements in power handling capability. This is principally because of the much better thermal conductivity to thermal expansion ratio (K/α) of SiC. Copper or molybdenum do almost as well, but for all of these, the technology of forming gratings has not been established. We are proceeding with quartz gratings in the current implementation, but SiC gratings have recently been reported by Astron.¹⁸

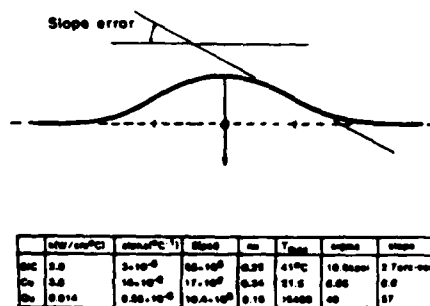


Fig 9 Schematic representation of the response of the codling mirror to the focused input power. The table shows parameters for three materials and the distortion response for a back cooled geometry in terms of a slope error. The input parameters were 40 W/cm or 7000 W/cm². Whereas quartz would fail catastrophically, SiC seems to be satisfactory to these power densities. (reproduced from ref 2)

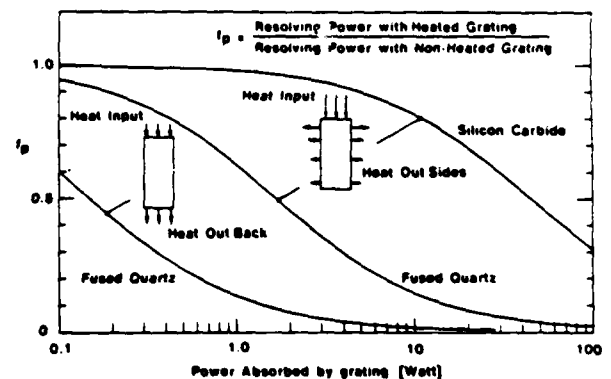


Fig 10 Estimation of throughput degradation from a combined sensitivity analysis of the Rowland Circle optics and thermal calculations. The dominant effect is the change in radius of curvature of the grating with power loading. Three cases are selected for a geometry that is considered near optimal. The two quartz cases compare back and side cooling for quartz. Quartz and SiC are compared for the side cooled case. (reproduced from ref 2)

IVb Configurational Description

Figure 11 shows the primary configurational elements in the monochromator: the entrance separation chamber; the entrance bellows; the moving chamber; the exit chamber; the air bearing system; the laser interferometer; and the granite reference surface. Figure 12a shows the vacuum chamber while Fig 12b shows the optical mechanism, and the lower half of the vacuum chamber mounted on the granite base. The moving component of the instrument weighs approximately 1300 Kg, but the drive shaft and stepping motor seen in the lower right of figure 12b is capable of driving the the mechanism through a single resolution step in less than 50 msec and attain a maximum velocity of about 10 mm/sec. Thus the system can scan its full range in about 1.5 minutes.

The synchrotron radiation enters from the lower right and impinges on mirror, M_1 , a silicon carbide elliptical cylinder being fabricated by TRW¹⁹. The use of an asphere was motivated by the poor focusing characteristics of the spherical M_1 mirrors used on the original Grasshopper Monochromators. Comparison of spherical, cylindrical, parabolic cylinders and elliptical cylinders using the ray trace program SHADOW developed by Lai and Cerina²⁰ found that the elliptical cylinder performed best ($\sigma \leq 20 \mu\text{m}$) with our approximately 2 meter undulator extended source. (A similar conclusion for the ERG was found by Hulbert and Brown¹¹.) The water cooling pipes are visible on the right. The water pipes were kept as large as possible to minimize vibration that might be induced by turbulent flow. This aspect of mechanical engineering is not well developed, so many of the decisions were based on intuition or other constraints. For example, the gratings are heat sunk well to copper pads which are then connected to the cooling system through flexible braid. The vacuum base and the inner optical base ride on independent air bearings. On the left side are visible the grating angular actuator, part of the laser interferometer optics and the laser beam ports, and then the slit actuator. The Codling slit actuator is on the right side along with the water piping to the slit and gratings. The Codling slit assembly sits within the shaft and the Codling mirror can be removed through the aperture. The grating carriages are mounted between the two arms and have levered adjustment. The grating is mounted in a carrier that is prepared externally. Provision is made for inserting alignment aids during setup. All the connections to the optics come through the base so that the top can be completely removed.

Figure 12a shows the upper part of the vacuum envelope which mates to the flat bottom with a Helicoflex seal. The vacuum chamber is supported independently from the optical mechanism so that any flexing as the system is put under vacuum will not disturb the optics. The ion pumps and Ti sublimation are integrally built into the chamber. The primary ports on the two ends are for the 6" ID entrance and exit bellows. An array of ports allow for monitoring the internal parts, replacement of gratings and alignment without removing the top.

IVc The control system and static and dynamic alignment

A key aspect of the design is the the control system and incorporation of alignment fixtures. The alignment needs have been principally specified based upon our experience with the SSRL Grasshopper monochromators. The performance objectives of these subsystems was determined by analysis of the sensitivities of the expected performance to tolerance variation and control of the various mechanical parameters. We have gone further in this aspect than previous high vacuum designs in the hope of significantly improving the operational functionality of the instrument. One by-product of our design and the inclusion of alignment and metrology is that this will be the first soft X-ray optical system capable of creating absolute wavelength standards above 100 eV and below the range accessible to crystal instruments.

There are two alignment regimes, static and dynamic. The static regime is established in the initial positioning and phasing of the elements. The dynamic regime consists of maintaining the optical elements in the required spatial positions as they are moved for a scanning operation. The control system needs to move the three axes in a coordinated way such that the elements remain in dynamic alignment.

LOCUST MONOCHROMATOR

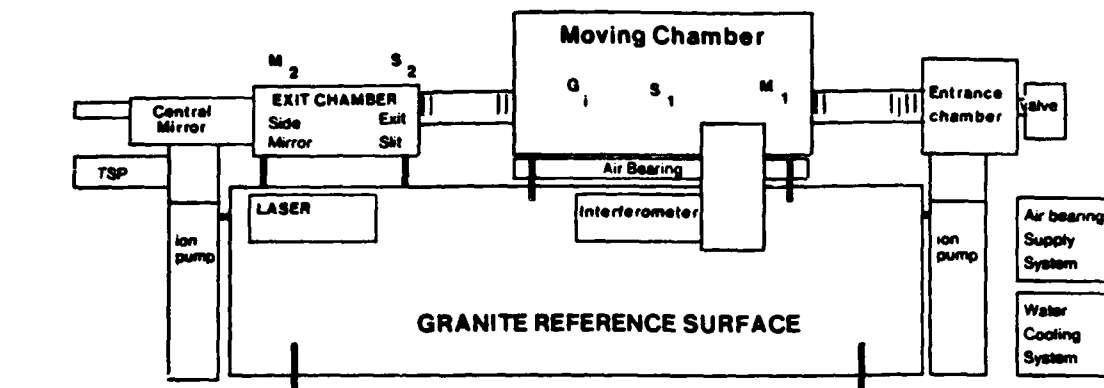


Fig. 11 Schematic side view of the Locust Monochromator showing the major assemblies. The details are given in the text. A perspective view of the Moving Chamber is shown in figure 12. The exit chamber contains the exit slit and the refocusing mirrors.

TABLE 2

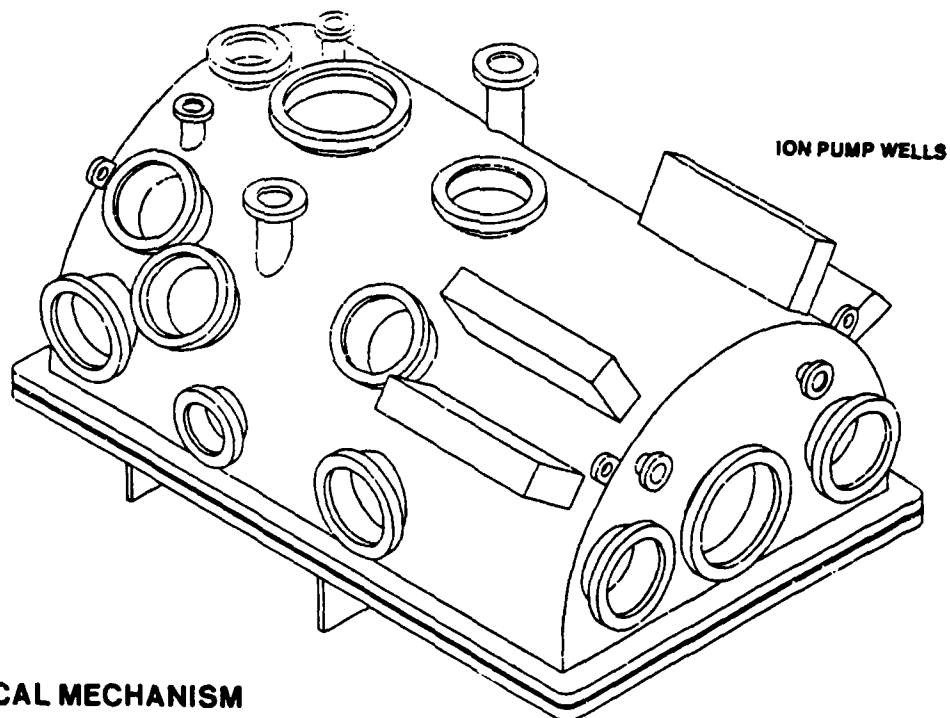
Locust Monochromator Parameters

Operating Range: 10-1000 eV
 100 Watts Input Power
 Silicon Carbide Optics
 Water Cooled Optics
 Laser Interferometer Encoding
 Fully Computer Controlled

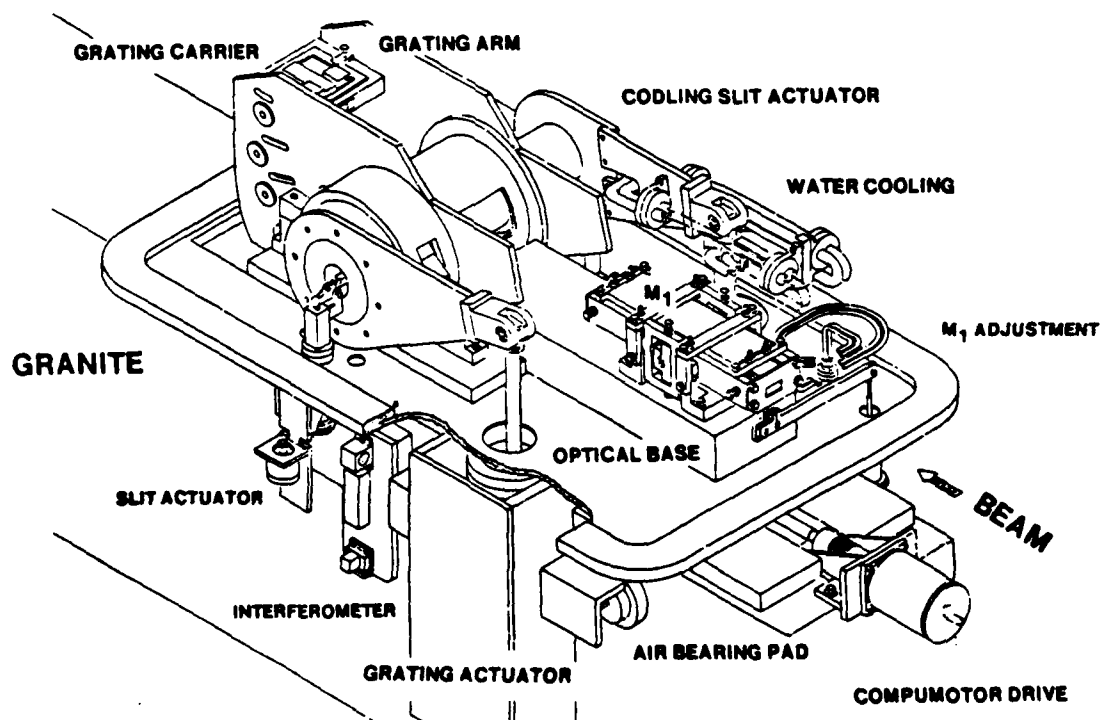
Grating Angle	2°	4°	10°	20°
Grating Radius (mm)	9355	4817	1986	1037
Grating Blank (l.w.d.-mm)	100,40,30	80,40,30	60,40,30	60,40,30
grooves/mm	1200	1200	600	600
Resolution (Å)	0.0126	0.0242	0.0593	0.1136
S ₁ G (mm)	3265	3360	3448	3547
Linear Travel (mm)	820	800	400	150
Angular Travel	5°	12°	18°	13°
Blaze angle	1.3°	2.0°	..*	..*
Blaze Energy (eV)	600	210	70*	20*
Resolution at Blaze (eV)	0.37	0.086	0.023	0.0036
Optimized Range (eV)	1500 - 250	450 - 90	150 - 30	50 - 10
Mechanical Range (eV)	zero order - 220	zero order - 60	zero order - 27	zero order - 10

* These are laminar cylindrical gratings which are not blazed

MOVING VACUUM CHAMBER



OPTICAL MECHANISM



Sensitivity and tolerance studies have been employed to understand critical operational requirements such as grating angle tracking, Codling slit rotation axis centering, granite reference slab flatness, etc.^{21,22} Our design is consistent with the requirement that the effect of any one of these isolated errors will contribute an uncertainty of no greater than an energy resolution element ($10\mu\text{m}$ slits) to the energy calibration of the instrument over its entire scanning range.

In the alignment process, the principal optical axis of the monochromator is determined by the synchrotron beam, the granite reference surface and the S_1 - S_2 axis must be made to coincide with this so as S_1 scans over the $\approx 800\text{mm}$ travel, the deviation from the spatial axis is a minimum. The M_1 mirror needs to be adjusted for optimal focus onto the entrance slit and the slit coordinated with the grating. The grating is statically aligned to place it on the Rowland circle. Once alignment is established, tracking is followed with a Hewlett-Packard three axis interferometer. This primary system is backed up by a set of optical encoders.

IVd Ranges and expected performance

Achieving the desired ranges shown in Table 2 was a process of considerable trade off. As the design evolved and configurational implications became clear, we were continually revising the needed and achievable parameters. A major constraint was established by the decision to use a 6" ID bellows for the beam extraction. This limited both the achievable angular range and set the maximal translation limit of 870mm. We thus came up with the ranges presented in Table 2. We describe these ranges as optimized range predicated by the choice of grating blaze which is included between the accessible range. This categorization is useful because all the gratings can go to zero order. Figure 12 shows the resolution versus photon energy over the ranges for each of the gratings. These are accompanied with some flux numbers based upon a theoretical estimate of the monochromator throughput with 100ma in the ring. Note the high resolution over the wide operating range if realized will be significantly greater than that available with most currently operating instruments and competitive with the best ever achieved. The beam spot size on the sample with the optics described below should be about 0.6mm half width at focus.

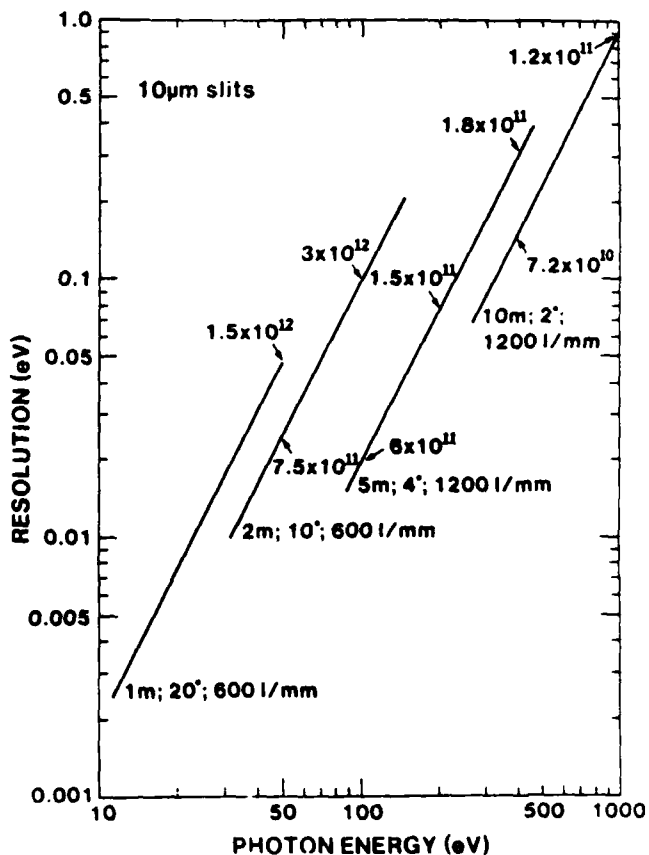


Fig 13 Estimated energy resolution versus photon energy for each of the gratings. The inset numbers give estimated fluxes at the sample for SPEAR running 100 ma at 3 GeV.

V. EXPERIMENTAL AREA and REFOCUSING

The Beam Line comprises two basic experimental areas. The first is an approximately one meter long white beam station between the diagnostic section and the monochromator. Although we would have preferred to bring the white beam through the monochromator, no tractable means except setting the monochromator at zero order could be found. The remaining experimental areas come after the monochromator and are created by a filtering and refocusing system built into the monochromator. The exit Codling mirror deflects the beam vertically and then the refocusing system creates the end station and the two horizontally deflected side stations. Before entering the refocusing system, the beam can be filtered either with one or two transmission filters mounted on concentric wheels or with a transmission grating. Since the transmission grating further deflects the beam, this is compensated by adjusting the exit Codling mirror.

The refocusing system thereby creates three work areas by providing two beams deflected horizontally at 14 degrees from mirrors 0.5 meters from the exit slit and one vertically at four degrees with a mirror 1.0 meter from the exit slit. The side stations are at 2.25 meters and the end station 3.5 meters from their respective mirrors. Determining the parameters for these stations was a complicated trade off of a number of parameters since the only optimal solution would have entailed having only one work area. We did consider a number of schemes where chambers were moved around a single port, but they were deemed difficult to implement. Although we would have liked to have moved experimental stations further back, the focusing aberrations substantially increased the size of the beam so that the apertures of typical electron spectrometers would have been overfilled.

The current design plan is based on toroidal optics with evolution to conically formed optics planned in the future. The two side stations have a more limited energy range than the end station, but this is offset by the participating research groups being able to maintain experimental chambers in place permanently. The end station port is for general use and has no permanently installed chamber. Provision has been developed, however, for rapidly changing and positioning chambers including the SSRL facility chambers available for general users.

VI. COMPUTER CONTROL SYSTEM

The computer system is an integral part of the beam line formulation. Because of the use of closed loop control for coordinating the monochromator, the computer control system is an integral part of the design. All the basic functions of the monochromator are controllable by the computer. In one of the primary scanning modes, the monochromator and the Multi-undulator are scanned simultaneously by the computer.

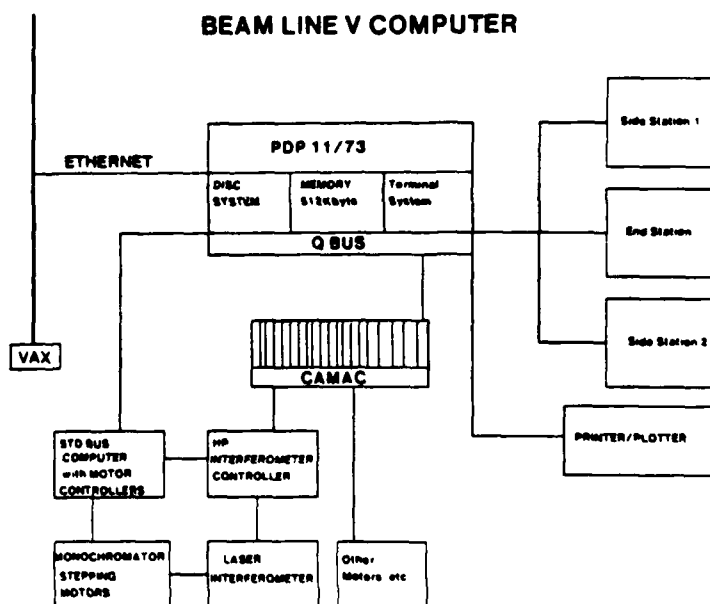


Fig 14 Schematic of the computer system that will control the monochromator and multi-undulator and will support the three experimental stations. Each experimental station has a terminal and CAMAC crate.

The primary computer is an evolution of our previous PDP11 CAMAC systems using the RSX11M operating system²³ and the XC CAMAC device driver.²⁴ In the specific implementation, we have used a PDP 11/73 with 512Kbytes of memory, 2 RL02 disks, and an RD52 30 Mbyte winchester. An ethernet system utilizing DECNET connects the beam line computer to the SPEAR control room for operation of the Multi-undulator. We have created three operating stations consisting of terminals and CAMAC crates, one for each of the experimental areas. In order to achieve the control response time desired, a secondary slave microprocessor was implemented for the control of the monochromator stepping motors operated in a feedback loop with a laser interferometer. It interacts directly with the interferometer encoder and the motors during a move operation. The other beam line motor actuators are driven directly from CAMAC.

The CAMAC system also provides a general data acquisition system. A specialized monochromator/undulator task using the XC driver is being developed which will work in coordination with any of the data acquisition and control program in use at SSRL, eg PRG, EXP, and SPECTRA.

ACKNOWLEDGEMENT: We are indebted to Ingolf Lindau, Art Bienenstock, Bill Spicer and Stig Hagstrom for their efforts on behalf of establishing and their continuing support of the Beam Line V project. A number of people provided key support which enabled us to establish this project in 1981: George Pake and Chuck Hebel of Xerox, Fred Betz, Adrian DeGraaf, and Bill Oosterhuis of the NSF, and Richard DeLauer and Richard Reynolds of DARPA. Nelson Hower and Lars Erik Swartz have made important contributions to the designs. We thank Herman Winick for his interest and for discussion of the Multi-undulator. We thank Brad Youngman for his management of the SSRL BLV Engineering effort and his important contribution to the construction of the Multi-undulator. Jim Montgomery, Richard Boyce, Carl Cork, John Yang, and Harry Morales of SSRL have also made important contributions to the beam line.

This work was supported by NSF/UIC Grant DMR 81-08343, DARPA, the DOE, and Xerox and was performed at the Stanford Synchrotron Radiation Laboratory and SLAC which are supported by the DOE.

REFERENCES:

1. R.Z. Bachrach, L.E. Swartz, S.B. Hagstrom, I. Lindau, M.H. Hecht, and W.E. Spicer, Nucl. Inst. and Meth., 208, 105, (1983).
2. R.Z. Bachrach, R.D. Bringans, N. Hower, I. Lindau, B.B. Pate, P. Pianetta, L.E. Swartz, R. Tatchyn, Nuclear Instruments and Methods, 222, 70-79 (1984); also R.Z. Bachrach, R.D. Bringans, N. Hower, I. Lindau, B.B. Pate, P. Pianetta, L.E. Swartz, R. Tatchyn, Science with Soft X-rays, SPIE Proceeding Series 10 (1984).
3. H. Winick, G. Brown, K. Halbach, and J. Harris, Physics Today, 34, 50, May, 1981. and K. Halbach, J. Chin, E. Hoyer, H. Winick, R. Cronin, J. Yang, and Y. Zambre, IEEE Trans. Nucl. Sci. NS28, (1981).
4. G. Brown, K. Halbach, J. Harris, and H. Winick, Nucl. Inst. and Meth., 208, 65, (1983).
5. K. Halbach, Nucl. Inst. and Meth., 187, 109, (1981).
6. T. Cox and B. Youngman, this proceedings.
7. R.D. Bringans et al, to be published.
8. M.H. Hecht, R.D. Bringans, I. Lindau, and R.Z. Bachrach, Nucl. Inst. and Meth., 208, 113, (1983).
9. V. Rehn, AIP Conf. Proc #75, D.T. Attwood and B.L. Hinks eds, p162, (1981).
10. F.C. Brown, R.Z. Bachrach, and N. Lien, Nucl. Inst. and Meth., 152, 73, (1978).
11. F.C. Brown, S.L. Hulbert, and N.C. Lien, 6th Int Conf on VUV Physics (1980), unpublished; S.L. Hulbert, J.P. Stott, F.C. Brown, and N.C. Lien, Nucl. Inst. and Meth., 208, 43, (1983).
12. R.L. Johnson, Proc Int Conf on X-ray and VUV Synchrotron Rad Inst. 1985, Nucl. Inst. and Meth. in press (1986).
13. A. Franks and M. Stedman, Nucl. Inst. and Meth., 172, 249, (1980).
14. H. Petersen, Optics Comm, 40, 402, (1982).
15. F.C. Brown and S.L. Hulbert, Nucl. Inst. and Meth., 222, 42, (1984).
16. V. Rehn, J.L. Stanford, A.D. Baer, V.O. Jones, W.J. Choyke, Appl Optics, 16, 1111, (1977).
17. M.R. Howells, editor, Reflecting Optics for Synchrotron Radiation, SPIE Proceedings 315, (1981).
18. M. Lewis, Proc Int Conf on X-ray and VUV Synchrotron Rad Inst. 1985, Nucl. Inst. and Meth. in press (1986).

19. For information contact: H.Y. Chmait, TRW Space and Technology Group, Optics Dept 01/1141, One Space Park, Redondo Beach, Ca 90278. (213) 536-4278.
20. B. Lai and F. Cerrina, Proc Int Conf on X-ray and VUV Synchrotron Rad Inst. 1985, Nucl. Inst. and Meth. in press (1986).
21. R. Tatchyn and I. Lindau, Nucl. Inst. and Meth., Proc Int Conf on X-ray and VUV Synchrotron Rad Inst. 1985, Nucl. Inst. and Meth. in press (1986).
22. B.B. Pate, to be published
23. J. Cerino, J. Stohr, N. Hower, and R.Z. Bachrach, Nucl. Inst and Meth., 172, 227, (1980); G.V. Hansson, B. Goldberg and R.Z. Bachrach, Rev. Sci. Instr. 52, 517, (1981).
24. J. Gallup and R.Z. Bachrach, SSRL Report.

International Conference on Insertion Devices for
Synchrotron Sources, SPIE, Vol. 582 (eds. R. Tatchyn
and I. Lindau); Proceeding of a confernce held at
Stanford, October 27-30, 1985: Table of Contents.

Proceedings of SPIE—The International Society for Optical Engineering

Volume 582

International Conference on Insertion Devices for Synchrotron Sources

Roman Tatchyn, Ingolf Lindau
Chairmen/Editors

Cosponsored by
The Stanford Synchrotron Radiation Laboratory

27-30 October 1985
Stanford, California

Published by
SPIE—The International Society for Optical Engineering
P.O. Box 10, Bellingham, Washington 98227-0010 USA
Telephone 206/676-3290 (Pacific Time) • Telex 46-7053

SPIE (The Society of Photo-Optical Instrumentation Engineers) is a nonprofit society dedicated to advancing engineering and scientific applications of optical, electro-optical, and optoelectronic instrumentation, systems, and technology

The papers appearing in this book comprise the proceedings of the meeting mentioned on the cover and title page. They reflect the authors' opinions and are published as presented and without change, in the interests of timely dissemination. Their inclusion in this publication does not necessarily constitute endorsement by the editors or by SPIE.

Please use the following format to cite material from this book:

Author(s), "Title of Paper," *International Conference on Insertion Devices for Synchrotron Sources*, Roman Tatchyn, Ingolf Lindau, Editors, Proc. SPIE 582, page numbers (1986).

Library of Congress Catalog Card No. 85-063542
ISBN 0-89252-617-3

Copyright © 1986, The Society of Photo-Optical Instrumentation Engineers. Individual readers of this book and nonprofit libraries acting for them are freely permitted to make fair use of the material in it, such as to copy an article for use in teaching or research. Permission is granted to quote excerpts from articles in this book in scientific or technical works with acknowledgment of the source, including the author's name, the book name, SPIE volume number, page, and year. Reproduction of figures and tables is likewise permitted in other articles and books, provided that the same acknowledgment-of-the-source information is printed with them and notification given to SPIE. Reproduction or systematic or multiple reproduction of any material in this book (including abstracts) is prohibited except with the permission of SPIE and one of the authors. In the case of authors who are employees of the United States government, its contractors or grantees, SPIE recognizes the right of the United States government to retain a nonexclusive, royalty-free license to use the author's copyrighted article for United States government purposes. Address inquiries and notices to Director of Publications, SPIE, P.O. Box 10, Bellingham, WA 98227-0010 USA.

Printed in the United States of America.

INTERNATIONAL CONFERENCE ON INSERTION DEVICES FOR SYNCHROTRON SOURCES

Volume 582

Contents

Conference Committee	v
Introduction	vi
SESSION 1. RADIATION CHARACTERISTICS OF INSERTION DEVICES.	1
582-01 A new formulation of synchrotron radiation optics using the Wigner distribution, K.-J. Kim, Lawrence Berkeley Lab. (Invited Paper).	2
582-03 Undulators as a primary source of coherent x-rays, D. T. Attwood, K.-J. Kim, K. Halbach, M. R. Howells, Lawrence Berkeley Lab. (Invited Paper).	10
582-04 Coherent and incoherent radiation from charged particle beams, R. Coisson, Univ. di Parma (Italy).	20
582-05 Phase space distribution of brilliance of undulator sources, R. Coisson, Univ. di Parma (Italy); R. P. Walker, SERC, Daresbury Lab. (UK).	24
SESSION 2. MODELING OF SPECTRAL PROPERTIES OF INSERTION DEVICES.	31
582-07 An overview of programs for calculation of undulator radiation spectra, S. Bartalucci, Istituto Nazionale di Fisica Nucleare/Lab. Nazionali di Frascati (Italy).	32
582-08 Properties of undulator radiation, B. W. Veal, Argonne National Lab.	38
582-09 Undulator spectra: computer simulations and modeling, R. Tatchyn, A. D. Cox, SSRL/Stanford Univ.; S. Qadri, U.S. Naval Research Lab.	47
SESSION 3. HARDWARE PROPERTIES OF INSERTION DEVICES.	67
582-10 Some new ideas about undulators, K. Halbach, Lawrence Berkeley Lab. (Invited Paper).	68
582-11 Random errors in undulators and their effects on the radiation spectrum, B. M. Kincaid, AT&T Bell Labs. (Invited Paper).	72
582-12 REC and NdFe magnetic moment irreversibility from temperature cycling, E. Hoyer, J. W. G. Chin, D. Shuman, Lawrence Berkeley Lab.	84
582-13 Systematic selection of undulator magnets using the techniques of simulated annealing, A. D. Cox, B. P. Youngman, SSRL.	91
582-14 Optimization of pole parameters for a REC multipole wiggler magnet, J. Pflüger, BESSY (West Germany); W. Gudat, Institut für Festkörperforschung der KFA Jülich GmbH (West Germany).	98
582-15 A permanent-magnet field source for the production of circularly polarized radiation via helical free-electron lasers, H. A. Leupold, A. B. C. Morcos, U.S. Army Electronics Technology and Devices Lab.	100
SESSION 4. MACHINE/INSERTION DEVICE INTERACTIONS.	109
582-16 Design potential of insertion device storage rings, H. Wiedemann, SSRL (Invited Paper).	110
582-17 Properties of the BESSY low emittance beam, G. Mülhaupt, H.-G. Hoberg, W.-D. Klotz, H. Lehr, R. Maier, E. Wehreter, BESSY (West Germany); P. Kuske, Institut für Atom- und Festkörperphysik der Freien Univ. Berlin (West Germany) (Invited Paper).	118
582-18 FEL undulator technology and synchrotron radiation source requirements, K. Robinson, D. Quimby, J. Slater, T. Churchill, A. Pindroh, A. Valls, Spectra Technology, Inc.	123
582-19 Optimization of the parameters of a storage ring for a high power XUV free electron laser, A. Jackson, J. Bisognano, S. Chattopadhyay, M. Cornacchia, A. Garren, K. Halbach, K.-J. Kim, H. Lancaster, J. Peterson, M. S. Zisman, Lawrence Berkeley Lab.; C. Pellegrini, G. Vignola, Brookhaven National Lab.	131
582-20 Aperture-dependent electron beam lifetime for the BESSY storage ring, P. Kuske, Institut für Atom- und Festkörperphysik der Freien Univ. Berlin (West Germany); A. Gaupp, W.-D. Klotz, R. Maier, G. Mülhaupt, W. B. Peatman, J. Pflüger, E. Wehreter, BESSY (West Germany); W. Gudat, Institut für Festkörperforschung der KFA Jülich GmbH (West Germany).	143
SESSION 5. INSERTION DEVICE/INSERTION DEVICE SYSTEM STUDIES.	147
582-21 The Orsay undulators, C. Bazin, M. Bergher, LURE (France); M. Billardon, Ecole Supérieure de Physique et Chimie (France); P. Elleaume, Y. Lapiere, J. Marilleau, CEA (France); J. M. Ortega, Ecole Supérieure de Physique et Chimie (France); Y. Petroff, LURE (France); M. Velghe, Univ. de Paris-Sud (France) (Invited Paper).	148
582-22 Options for the development of FEL oscillators from 200 to 1000 angstroms, J. E. La Sala, Stanford Univ.; D. A. G. Deacon, Deacon Research; J. M. J. Maday, Stanford Univ. (Invited Paper).	158
582-46 High quality hybrid wiggler for infrared FEL and coherent harmonic generation, G. Stolovy, W. Wadensweiler, J. M. J. Maday, S. Benson, Stanford Univ.; M. Velghe, LURE (France).	163

582-24	The variable gap permanent magnet linear undulator for the ENEA FEL experiment, F. Ciocci, E. Fiorentino, A. Renieri, E. Sabia, Centro Ricerche Energie Frascati (Italy)	169
582-25	Development of a NdFe-steel hybrid wiggler for SSRL, K. G. Tinsell, T. C. Brown, P. J. Ebert, W. C. Dickinson, E. M. Lent, Lawrence Livermore National Lab.; E. Hoyer, K. Halbach, S. Marks, D. Plate, D. Shuman, Lawrence Berkeley Lab.; R. Tatchyn, SSRL	177
582-26	Performance of insertion devices in the ESRF, R. P. Walker, SERC, Daresbury Lab. (UK); R. Coisson, Univ. di Parma (Italy)	185
582-27	Short period undulators—design and performance, T. Meinander, Technical Research Ctr. of Finland (Finland)	193
582-28	Predictions on the performance of the soft x-ray undulators, C. Jacobsen, SUNY/Stony Brook; H. Rarback, Brookhaven National Lab.	201
582-29	Design of a 3.0 Tesla wiggler for European Synchrotron Radiation Facility, M. Castiglioni, Commission of the European Communities, Joint Research Ctr. (Italy); E. Baravalle, CRITA (Italy)	213
582-30	Electron optical properties and electron trajectories of the multipole magnet for BESSY, J. Pflüger, W.-D. Klotz, BESSY (West Germany); W. Gudat, Institut für Festkörperforschung der KFA Jülich GmbH (West Germany)	223
582-31	Exploratory heat transfer studies on critical elements of a proposed 6 GeV synchrotron, T. M. Kuzay, G. S. Knapp, Argonne National Lab.	227
	SESSION 6. BEAM LINES AND BEAM LINE OPTICS BASED ON INSERTION DEVICES.	237
582-32	Optics for insertion-device beam lines, V. Rehn, Michelson Lab. (Invited Paper)	238
582-35	The SSRL insertion device beam line 'Wunder', R. Z. Bachrach, R. D. Bringans, Xerox Palo Alto Research Ctr.; B. B. Pate, R. G. Carr, SSRL	251
582-34	Mirror degradation and performance requirements in free electron lasers, D. A. G. Deacon, Deacon Research (Invited Paper)	268
582-36	Predicting thermal distortion of synchrotron radiation mirrors with finite element analysis, R. DiGennaro, W. R. Edwards, E. Hoyer, Lawrence Berkeley Lab.	273
582-37	Finite element analysis of the distortion of a crystal monochromator from synchrotron radiation thermal loading, W. R. Edwards, E. H. Hoyer, A. C. Thompson, Lawrence Berkeley Lab.	281
582-39	Surface heating in a lacquer-coated mirror irradiated with undulator light, R. Tatchyn, SSRL, P. L. Csonka, Univ. of Oregon; E. Källne, JET Joint Undertaking (UK); A. Toor, C. Gillespie, Lawrence Livermore National Lab.; I. Lindau, A. Fuller, SSRL	291
	SESSION 7. NOVEL DEVICES, THEORIES AND LIMITATIONS.	297
582-40	Insertion devices, future developments, limitations, P. L. Csonka, Univ. of Oregon (Invited Paper)	298
582-41	Quantum theory of the free-electron laser, W. Becker, J. Ges-Banacloche, J. K. McIver, M. O. Scully, Univ. of New Mexico (Invited Paper)	318
582-42	Novel radiation sources for infrared to gamma rays, R. H. Pantell, Stanford Univ. (Invited Paper)	330
582-43	Experimental results of microwave undulator, T. Shintake, National Lab. for High Energy Physics (Japan)	336
582-45	Variational theory of insertion devices, R. Tatchyn, SSRL	344
582-44	Three-dimensional simulations of an XUV free-electron laser, J. C. Goldstein, B. D. McVey, B. E. Newnam, Los Alamos National Lab.	350
582-49	The evolution of the radiation-beam system in long undulators, K.-J. Kim, Lawrence Berkeley Lab.	361
	Addendum	366
	Author Index	367

INTERNATIONAL CONFERENCE ON INSERTION DEVICES FOR SYNCHROTRON SOURCES

Volume 582

Conference Committee

Chairmen: Roman Tatchyn, Stanford Synchrotron Radiation Laboratory/Stanford Linear Accelerator Center; Ingolf Lindau, Stanford Synchrotron Radiation Laboratory/Stanford Linear Accelerator Center

Program Committee:

Roberto Coisson, Università di Parma, Italy; Paul Csonka, Institute of Theoretical Science/University of Oregon; Klaus Halbach, Lawrence Berkeley Laboratory; Albert Hofmann, Stanford Synchrotron Radiation Laboratory/Stanford Linear Accelerator Center; H. Kitamura, National Laboratory for High Energy Physics, Japan; G. Kulipanov, Nuclear Physics Institute, USSR; John Madey, Hansen Laboratories/Stanford University; Claudio Pellegrini, Brookhaven National Laboratory; Victor Rehn, Michelson Laboratory/U.S. Naval Weapons Center; R. P. Walker, SERC, Daresbury Laboratory, UK; Helmut Wiedemann, Stanford Synchrotron Radiation Laboratory/Stanford Linear Accelerator Center; Herman Winick, Stanford Synchrotron Radiation Laboratory/Stanford Linear Accelerator Center

Session Chairmen

- Session 1—Radiation Characteristics of Insertion Devices, Roman Tatchyn, Stanford Synchrotron Radiation Laboratory/Stanford Linear Accelerator Center
- Session 2—Modeling of Spectral Properties of Insertion Devices, Roberto Coisson, Università di Parma, Italy
- Session 3—Hardware Properties of Insertion Devices, Ingolf Lindau, Stanford Synchrotron Radiation Laboratory/Stanford Linear Accelerator Center
- Session 4—Machine/Insertion Device Interactions, George S. Brown, Stanford Synchrotron Radiation Laboratory
- Session 5—Insertion Device/Insertion Device System Studies, Helmut Wiedemann, Stanford Synchrotron Radiation Laboratory/Stanford Linear Accelerator Center
- Session 6—Beam Lines and Beam Line Optics Based on Insertion Devices, Ross D. Bringans, Xerox Palo Alto Research Center
- Session 7—Novel Devices, Theories and Limitations, Claudio Pellegrini, Brookhaven National Laboratory

INTRODUCTION

The field of insertion devices is one of the newest and most rapidly growing areas of applied photon science. Devices such as the undulator, optical klystron, and the free electron laser (FEL), which are well-suited for insertion into synchrotron storage rings, have been studied extensively in recent years. Studies of these devices have traditionally encompassed a broad range of disciplines, ranging from accelerator physics and engineering, through mathematics, to classical and quantum optics, leading to a rich diversity of viewpoints and areas of expertise in this field.

The unprecedented coherence and power promised by various insertion devices have in recent years brought about the launching of major projects and capital commitments around the world to install them in synchrotron rings (indeed, even to build rings dedicated to such devices). In view of that, this conference was called to bring together the world's leading authorities on various aspects of insertion device theory and technology, so that a rational look could be taken at the problems and prospects associated with the latest developments in this area of photon research. In addition to covering several traditional subject areas which we felt to be of major importance, the conference also featured a session on novel devices, theories, and limitations, in which a number of exciting novel concepts were presented; we enthusiastically refer our readers to the papers in that session.

As may be expected from any conference which is the first in its series, there were also, in our estimation, some noticeable gaps in the represented subject areas. For example, one particular subject of the potentially major importance for which no contributions could be elicited was the question of global stability of synchrotron rings containing large numbers of insertion devices. Other novel topics, such as, e.g., laser-driven accelerators, were also missing from the presentations. Yet another limitation, also to be expected in a newly developing field, was the use of non-standard terminology for some of the physical quantities under discussion, a problem that could generate bothersome obstacles to effective future communication. It is hoped that these and other gaps and limitations will have been remedied by the time of the next conference.

For now, it is our hope that these proceedings will be found useful by those of our colleagues who are concerned with the efficient implementation and utilization of insertion devices in synchrotron storage rings, as well as those who are interested in entering this exciting and dynamic field for the first time.

Roman Tatchyn and Ingolf Lindau
Stanford Synchrotron Radiation Laboratory /
Stanford Linear Accelerator Center

Article: "New Experiments Using a Soft X-Ray
Undulator" by W. Eberhardt et al, Nucl.
Inst. Meth A 246, 825-834 (1986).

NEW EXPERIMENTS USING A SOFT X-RAY UNDULATOR

W. EBERHARDT

Exxon Research and Engineering Co., Route 22 E, Annandale NJ 08801, USA

E.W. PLUMMER and C.T. CHEN

University of Pennsylvania, Department of Physics, Philadelphia PA 19104, USA

R. CARR

SSRL, PO Box 4349 Bin 69, Stanford CA 94305, USA

W.K. FORD

Montana State University, Physics Department, Bozeman MT 59717, USA

We discuss some of the exciting new experimental possibilities offered by soft X-ray undulators as a radiation source. In addition to the general discussion we present two specific experiments on isolated molecules for which the undulator source is extremely important. The first one of these experiments is a coincidence experiment between Auger electrons and ions generated in the events following the absorption of a soft X-ray photon by an isolated molecule. This gives a detailed picture of the involvement of individual valence electrons into the molecular bond. The second experiment is a study of the electronic decay of a resonant core electron excitation into a bound molecular orbital. The decay of these states yields new information about the localization of the molecular valence orbitals around the atom where the core hole was created.

1. Introduction

Soft X-ray undulators offer some exciting new possibilities for research in the VUV and soft X-ray spectral range in the near future. Currently several beamlines are under construction worldwide, but only three of them actually deliver photons to various experiments [1-3]. Since these beamlines open new dimensions for experiments, we would like to give our perspective of these new possibilities as an introduction to this report. In the second part we are going to discuss a specific experiment, a coincidence study between Auger electrons and ions generated in the events following the absorption of a soft X-ray photon by an isolated molecule. This absorption event leads to the production of a core hole in either a neutral or ionic configuration depending on the photon energy. In low Z atoms, which have a low fluorescence yield, the core hole decays predominantly via an Auger type process depleting the valence electronic states involved in the molecular bond. As a result of the removal of bonding electrons the molecule becomes unstable and falls apart into ionic fragments. Making use of the increased intensity out of the SSRL beam line V 36 pole undulator we were able to separate individual final state configurations of the Auger decay and measure the energy and charge distribution of the fragments associated with each of these specific chan-

nels by a coincidence experiment. In the third part of this paper we finally introduce a new experimental technique, Deexcitation Electron Spectroscopy (DES), which yields information about the localization of valence electron wavefunctions around individually selectable atomic centers within larger molecules. This information is obtained by studying the electronic decay of core electron excitations into unoccupied molecular orbitals. Making use of the chemical shift in chemically nonequivalent atoms or the difference in core electron binding energies in general, we can selectively create core holes in individual atoms within a molecule by tuning the photon energy. The subsequent electronic decay of this core to bound excitation has a highly localized character because of the small extent of the core hole wavefunction. This technique has been explored for molecules containing carbon or nitrogen atoms, but we were unsuccessful in the study of oxygen atoms within these molecules because of photon flux limitations on the SSRL grasshopper bending magnet beamlines.

2. Undulator experiments in the VUV and soft X-ray energy range

Insertion devices producing hard X-rays have been installed and operated for several years at SSRL and

other synchrotron radiation sources throughout the world. Many successful experiments have been carried out on these beamlines and the use of these facilities is a common feature of state of the art X-ray synchrotron radiation experiments. In the soft X-ray and VUV spectral ranges, on the other hand, insertion devices are not in use and the implementation of these next generation sources lags several years behind. To an outside observer it might even appear as if there is no interest in undulator sources for these spectral ranges. Therefore we want to start this report with a discussion of some experiments which would greatly benefit from an undulator source or even are impossible to do without one. Obviously this list is incomplete and biased by our own experimental background, but the intent is to communicate some of the excitement we feel about these fantastic new sources of VUV and soft X-ray synchrotron radiation.

The potential benefits from an undulator beamline compared to a bending magnet beamline are twofold. First there is generally an increase in overall flux because of the increased magnetic pathlength visible to the experiment and because of stimulated emission which causes the peaks in the undulator spectrum. Second there is the dramatic increase in brilliance of the source. This latter factor, the increased brilliance, is usually quoted in figures that compare undulators, wigglers, and bending magnet sources. However only a few experiments can really make use of the increase in brilliance rather than just flux at the sample. The monochromator plays a crucial role in delivering all the advances made in the source to the sample. At high photon energies near the carbon, nitrogen or oxygen K-edges it is rather difficult to design a monochromator that has a resolution better than the natural linewidth of these atoms, which is approximately 100 meV. Toroidal grating monochromators (TGMs) can in theory achieve a resolution of a few tenths of meVs, if the horizontal acceptance is limited to about 1 mrad. This makes a TGM a good match for an undulator source since it takes advantage of the narrow horizontal beam coming from this source. However at low photon energies (less than 50 eV) it is fairly easy to construct a TGM monochromator with a resolution of 100 to 200 meV that accepts 40 mrad of radiation from a bending magnet. Therefore any experiment that only requires this resolution and energy range is very well served by a bending magnet line and the gain in moving to an undulator beamline would be minimal.

Obviously, in improving an individual experiment, one has to consider the whole experimental setup. A multichannel parallel detector, for example, also will increase the detection efficiencies and count rates. The same would be true for better monochromators having a higher resolution and transmission. The whole design of the storage ring and its beam current and emittance are

of the same importance. The undulator consequently has to be regarded as only one component of the whole experiment. The current demand for undulators however arises, because at the present time undulators seem to be the components where the largest gains can be realized for a given investment in time and resources.

When making up a list of experiments that greatly benefit from a soft X-ray undulator source, it is easy to start with experiments where the better source performance is translated into *higher resolution*. Core level studies on atoms, molecules, solids, and surfaces with the possibility of resolving vibrational substructure seem to be a very exciting prospect. Accurate linewidth and lineshape studies will give new insight into lifetimes and dynamical screening processes of electronically excited states.

Because of the increase in flux it will also be much easier to study *dilute samples* like gas phase molecules or impurities in solids and on surfaces with photoemission or other techniques. A special category of these experiments would be the study of cluster beams with a selectable cluster size. At present neither the geometry nor the electronic structure of these clusters are known. It will be very interesting to study how the individual atoms arrange themselves in the formation of small particles.

Using low yield detection techniques like *soft X-ray fluorescence* of C- N- or O-atoms one can perform absorption fine structure studies on chemisorbed molecules in a high pressure environment or on impurities deep inside a solid. This opens a new territory because the X-rays emitted in these processes have a much larger penetration depth than the electrons conventionally used in these techniques.

Time, spin, or spatially resolved photoemission experiments will truly open up new dimensions. Using some of the photoemission detectors currently under development it will be possible to study the dynamics and intermediates in chemical reactions on surfaces or a spin resolved bandstructure. It also seems feasible to build a photoemission microscope by focusing the beam after the monochromator exit slit with a zone plate and scanning the sample through the focal spot. The latter application really takes advantage of the high brightness of an undulator source and clearly would be impossible without it.

Two photon experiments or a double excitation experiment where a laser is used as the additional source also will become possible. This will mean an extension of the wavelength range of two photon spectroscopy into the core level excitation region which is not possible with today's laser sources because of the limitation in laser energy. Excited state lifetime measurements, where the laser is used either to prepare or to probe the excited state will also be possible.

Another class of experiments waiting for an undula-

tor source are *coincidence studies* between two electrons, a photoelectron and an Auger electron for example, or electron-ion or ion-ion coincidences. One example of these types of experiments will be discussed later in more detail. Last but not least we want to include in our list *soft X-ray microscopy and holography* [4] where the spatial coherence of the undulator source plays an important role.

One important question about the undulator sources is the increase in usable photon flux at the sample for a given experiment. We want to point out however, that conceptually the undulator is only one part of the whole experiment and parallel developments of new monochromators and detectors or even storage ring improvements will also enhance the experimental capabilities. Undulators however, seem at present to offer the largest single gain. Monochromators and detectors have been developed over the past decades and order of magnitude improvements do not seem readily possible. New storage rings on the other hand are a major investment and out of reach for an individual experiment.

We have a partial answer to the question about the photon flux enhancement by an undulator in fig. 1, where we compare a nitrogen Auger spectrum taken at the beam line V undulator with the same spectrum taken at the SSRL grasshopper beamline in zero order. The undulator was set to a k -value of 1.0 which corresponds to a fundamental output energy of 1.2 keV and the spectrometer settings, as well as the gas pressure, were identical for both curves. Under these conditions we observed a gain in count rate by more than a factor of 500. We want to point out however, that this gain is specific to our experiment and cannot readily be generalized because many factors enter. Some of these are the

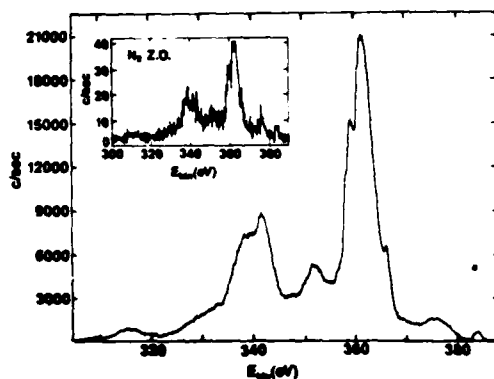


Fig. 1. Nitrogen Auger spectrum taken at the SSRL beam line V undulator. The insert shows the same spectrum taken under identical spectrometer conditions (resolution and gas pressure) at the SSRL grasshopper bending magnet line in zero order. The countrate in the spectrum taken at the undulator beamline exhibits an increase by more than a factor of 500 compared to the bending magnet configuration.

total acceptance of our experiment through the differential pumping stage [5], the difference in the cross section for photoabsorption in conjunction with the difference in the spectral output between both beam lines, and also the attenuation caused by the five reflecting elements in the grasshopper beamline.

3. Electron-ion coincidence studies on isolated molecules

In this section we are reporting an experiment conducted during the summer of 1985 on the beam line V undulator at SSRL. We started our studies of soft X-ray induced fragmentation of small molecules several years ago [6-8]. In general, any molecule that has absorbed a soft X-ray photon is going to fall apart into ionic fragments with a probability of more than 95%. The branching ratio of the fragments however changes drastically in the region of the core electron absorption threshold. The details of the fragmentation process depend on whether the core electron is excited into an antibonding molecular orbital, a diffuse Rydberg orbital or into the continuum. Our experiments showed, that the initial core electron excited state of the molecule is stable. However this excited state decays preferentially via a two electron radiationless transition into an electronic state where one or more valence electrons are missing. These are the electronic configurations that finally lead to the fragmentation. With bending magnet beamlines at SSRL we could study the fragment spectrum and even the kinetic energy distribution of the fragments as a function of the excitation energy of the core electrons. We also measured the energy distribution of the electrons emitted in the decay of the core hole excited state and found that the final electronic configurations leading to the ionic decay products are quite different for different initial core excitations. This is exactly the reason why the fragment distribution changes so drastically throughout the onset of the core electron absorption. The missing link in this experiment however, was to measure the fragment distribution not as a function of the initial core excitation, but in coincidence with specifically selected valence hole configurations after the electronic decay of the primary core excitation. We tried this experiment on the grasshopper beamline at SSRL, but the intensity was much too low. Using the quasimonochromatic beam from the beam line V undulator we were able to perform these studies for the events that follow after the ionization of the core electrons. The present magnet configuration did not allow us to tune into the core to bound state excitations. However these transitions will be accessible with a different undulator or when the ring runs at a lower energy such that the fundamental of the undulator will be near the carbon-, nitrogen-, or oxygen-K-edge.

V. RESEARCH APPLICATIONS

cally the energy needed to dissociate the molecule into neutral fragments and then ionize part of or all of these neutral fragments individually. These energies are tabulated in the literature [9]. Closing the energy cycle, we know that a specific fragmentation channel is only open if the Auger electron has carried less energy out of the system than is needed to adiabatically produce these fragments. This is graphically illustrated in fig. 2 for nitrogen and in fig. 3 for CO, the two molecules studied here. Only Auger events and consequently the associated two hole final state valence configurations to the left of the thresholds indicated in these figures can contribute to the individual fragmentation channels. Otherwise the Auger electron has removed too much energy from the system and the channel is closed. We also recognize immediately one shortcoming of the adiabatic scheme to calculate the thresholds. If both fragments are ionic, there is an additional Coulomb repulsion of the two holes involved, when the two partners are close to each other. This means that the actual thresholds for these channels have to be several eV higher. As the two ions separate, the Coulomb energy is mostly transformed into kinetic energy of the fragments. The term "Coulomb explosion" arises from the large kinetic energies observed in these fragment channels.

The experimental setup was described previously [5]. The time-of-flight mass spectrometer and the CMA electron spectrometer are oriented with their axes on opposite sides and perpendicular to the plane of the X-ray beam and the molecular gas beam. Whenever an electron is detected in the CMA it starts the ramp of a TDC which is stopped by pulses coming from the ion mass spectrometer. The time difference between the two pulses is related to the mass of the ion and its initial kinetic energy. In our previous experiments [6-8] we triggered on the unresolved Auger electron signal seen by a channeltron with a retarding grid in place of the electron spectrometer. Using instead of the channeltron an electron energy analyzer in the present experiment, we can tune into the individual lines of the Auger spectrum and only measure the ions in coincidence with this specific Auger decay, thus correlating individual two hole final state configurations with the observation of certain ionic fragments.

One experimental difficulty in any coincidence experiment is to differentiate between true and accidental coincidences. Using a pulsed source makes this problem even more severe since the accidental coincidences carry the time structure of the source. These difficulties are illustrated in fig. 4. Triggered by a pulse in the electron channel, the pulses in the ion channel are displayed as a function of the time delay between the two channels. The structure seen in the top panel of fig. 4 is essentially the spectrum of the accidental coincidences which show the modulation due to the time structure of the ring.

From theory we know that the accidental coincidences are proportional to the product of the count rates in both channels, i.e. they are proportional to the square of the incoming photon intensity. The true coincidences, however, vary linearly with the photon flux. Consequently we can increase the ratio of the true to the

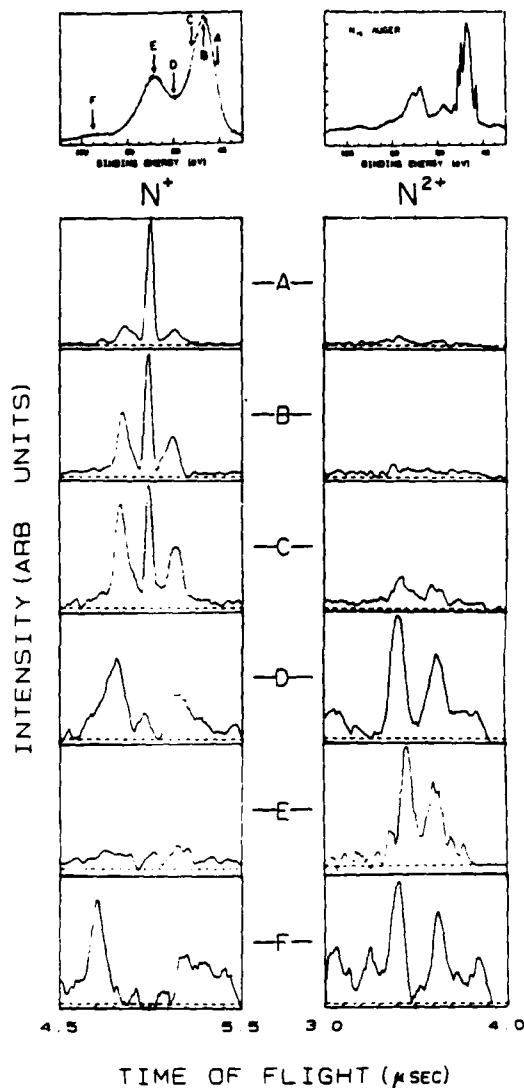


Fig. 5. TOF ion mass spectra of N_2 taken in coincidence with Auger electrons of various kinetic energies as indicated by the arrows A through F. The left column is centered at the flight time of an ion with $m/e = 14$ and the right column is for ions around $m/e = 7$. The background is subtracted as described in the text. The top panels show a comparison between the Auger spectrum taken with (left) and without (right) the ion extractor field applied across the ionization region.

V. RESEARCH APPLICATIONS

accidental coincidences by lowering the incoming photon flux. Ideally the true to accidental rate is best at zero intensity. In practice however other noise contributes to a general background and we have to keep a very delicate balance between having too high intensity and being swamped by accidental coincidences and having enough intensity such that the real signal is above the general noise level. This is accomplished in the curve shown in the second panel of fig. 4. The true coincidences clearly stand out from the machine structure background. This is verified by lowering the ion acceleration voltages which causes the truly coincident events to shift to larger flight times. In the curves we show later we have removed the timestructure background by subtracting from the measured spectrum a shifted part of the spectrum containing only accidental coincidences. This technique seems to work rather well and certainly improves the signal-to-background ratio in our curves such that we are able to discern the true coincidence features more readily.

Fig. 5 now shows a series of these Auger electron-ion coincidence spectra taken of nitrogen. The left and right hand columns show the regions of the 14 m/e and 7 m/e respectively. These are the only clear peaks observed in the coincidence spectra. The mass 28 peak, which corresponds to undissociated, singly ionized N_2 , and triply or higher charged N atoms are too weak to be observed above the background level after events following N 1s ionization as our earlier data show [7]. The two panels on top show the Auger spectrum taken with the ion extraction field applied and in the normal mode without an electric field across the interaction region. In order to take the ion TOF spectra we have to apply an electric field across the interaction region, which in turn smears out the energy distribution of the Auger electrons. The major features of the Auger spectrum however are still visible and, as our coincidence spectra show, we are even sensitive to the substructure in the major peaks.

The time-of-flight (TOF) ion mass spectra in both columns are shown in high resolution around the regions where an N^+ (left column) or a N^{2+} (right column) ion is expected to arrive. The background of the accidental coincidences was removed as described above. The TOF spectra are taken in coincidence with Auger electrons are marked by the arrows in the Auger spectrum displayed at the top of fig. 5. In coincidence with the highest kinetic energy Auger electrons we only observe a strong peak at $m/e = 14$, which can be caused by a low kinetic energy N^+ ion or by undissociated N_2^+ . The peak in the Auger spectrum at this kinetic energy corresponds to a $5\sigma^2$ final state hole configuration (we refer to the nitrogen valence orbitals in the CO notation). From our total energy schematic shown in fig. 2 we expect two channels to be open in coincidence with this Auger final state. Total charge conservation

allows us to immediately rule out the fragmentation channels where less than two charges are observed. Even though adiabatically the $N^+ + N^+$ channel is open, in practice because of the Coulomb repulsion it is still inhibited.

As we move with our Auger analyzer to point B, we pick up a strong signal of N^+ ions having approximately 3 eV of kinetic energy. These ions show up as the two side peaks in the TOF spectrum because the TOF mass analyzer preferentially detects ions flying along its axis either towards it or initially away from it and being turned around by the extraction field. Now the $N^+ + N^+$ channel has opened, but not as yet the $N^{2+} + N$ channel which is the energetically next higher one.

No drastic changes are observed at point C, the very small contribution of N^{2+} is probably due to the energy smearing in the Auger spectra taken with the extraction field applied. At point D however the N^{2+} signal is finally clear and the central peak in the N^+ region is virtually gone. At the same time the kinetic energy of the remaining N^+ ions has increased to about 6 eV. This region of the Auger spectrum is dominated by $4\sigma^2$ and $4\sigma 1\pi$ final state hole configurations. Presumably the appearance of N^{2+} is associated with the opening of the channel where the dissociation occurs into $N^{2+} + N$. The channel $N^{2+} + N^+$ is only open in the adiabatic limit at this Auger electron energy.

The next group of electronic states giving rise to the peak at position E in the Auger spectrum involves electronic configurations where one hole is located in the inner valence orbital (3σ) and the other one in the outer valence shell (4σ , 1π , or 5σ). It is remarkable that for these final state configurations N^+ ions are not observed anymore. The only open channel seems to be the dissociation into $N^{2+} + N$.

The weak structure F at the low energy end of the Auger spectrum is attributed to a $3\sigma^2$ double hole configuration. From the ion spectrum observed in coincidence with this configuration we conclude that an additional channel, the dissociation into $N^{2+} + N^+$ has opened up, because the kinetic energy of both, the kinetic energy of both the N^+ and the N^{2+} fragment has increased to about 12 eV and 5 eV respectively. Additionally the peaks have wings extending to much larger kinetic energies. The total charge in this channel is larger than the twofold ionic final state of the core hole Auger decay it is observed in coincidence with. One explanation for this discrepancy involves a secondary Auger decay of the 3σ double hole state. Another possibility is an electron shake off event in the decay process. At present the exact nature of this decay channel remains an open question.

The coincidence spectra for CO are shown in fig. 6. The results are qualitatively similar, however the ambiguity with the doubly charged parent ion does not

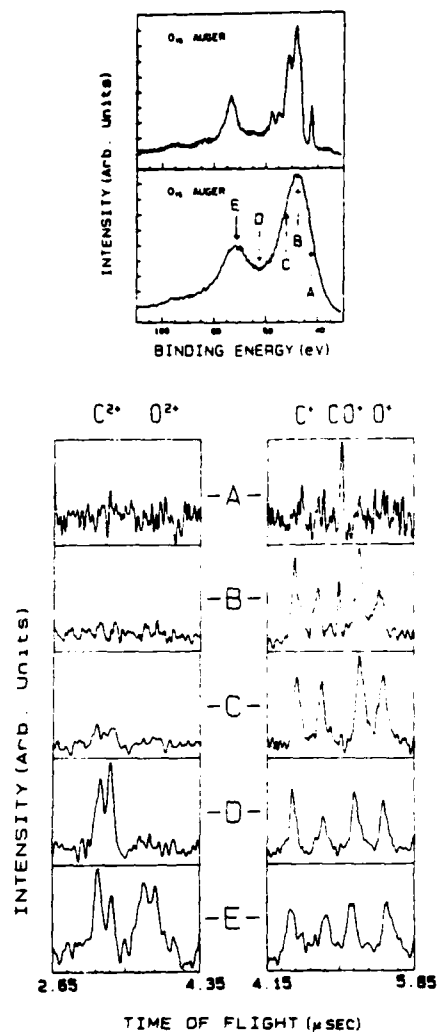


Fig. 6. Same as fig. 5 but for CO. The left column shows the region where C^{2+} and O^{2+} are expected to arrive, whereas the right column shows the region containing C^+ , CO^{2+} , and O^+ .

exist. Additionally, there are some interesting asymmetries observed in the spectra. Analyzing the coincidence spectra, it becomes very clear that CO^{2+} is only observed in coincidence with the highest kinetic energy Auger decay channel which is assigned to a $5\sigma 1\pi$ double hole state [10,11]. Note that the assignment of the lowest energy two hole configuration differs between N_2 and CO. Our series of coincidence spectra shows that this is the only stable double hole configuration in CO out of all double hole configurations present in the oxygen Auger spectrum. Any other double hole configuration in the valence orbitals causes the CO molecule to fall apart.

In coincidence with the electronic final states at

location B in the oxygen Auger spectrum of CO, we observe now a strong signal of C^+ and O^+ ions. The small amount of CO^{2+} is most likely a remnant of the previous channel due to the energy smearing of the Auger electrons in the electric field. The assigned [10,11] hole configurations in this region of the Auger spectrum are largely $1\pi^2$. From the adiabatic energy scheme shown in fig. 3 we know that at this energy there are only two channels with a total charge of 2 clearly open and we are at the threshold of a third channel. These channels are: CO^{2+} , $C^+ + O^+$, and $C^{2+} + O$ respectively. Given these alternatives, we are not surprised to see only C^+ and O^+ . The undissociated CO^{2+} would have to carry a large amount of internal energy and the $C^{2+} + O$ channel has no excess energy. Moreover, the production of a C^{2+} ion does require a fair amount of intramolecular charge transfer, because the initial core hole is produced at the oxygen end of the molecule.

In coincidence with electrons in the largest peak of the oxygen Auger spectrum, location C, the spectra develop as expected. The CO^{2+} signal is completely gone, the dominant species is C^+ and O^+ , and additionally a small amount of C^{2+} is observed. The two hole states are now not only a part of the $1\pi^2$ manifold but contain also the $4\sigma 1\pi$ double hole configuration. Presumably it is the latter one of these configurations that gives rise to the C^{2+} signal.

The previously observed trends are confirmed at location D in the Auger spectra. The C^{2+} signal is very strong and the C^+ and O^+ ions have a larger kinetic energy. The Auger two hole final states are now largely $4\sigma 1\pi$ and $4\sigma^2$. Even though the ion spectra change as expected from the adiabatic energy scheme, it nevertheless would be very interesting to understand the development in more detail. As pointed out above, the initial core hole is created at the oxygen atom and even the Auger final state two hole configurations are predominantly located at the oxygen end of the molecule. The 4σ orbital in a single particle calculation has more than 90% of its weight at the oxygen atom. It is hard to imagine that such a hole configuration develops directly into a fragmentation channel as $C^{2+} + O$. Rather a curve crossing between at least two different potential curves seems to be involved in order to rearrange the charge distribution within the molecule before it falls apart.

Finally, in coincidence with the 3σ OV (outer valence) hole configurations, at location E in the Auger spectrum, we see all four possible fragments, C^{2+} , O^{2+} , and C^+ as well as O^+ with high kinetic energy. We believe these come from the channels $C^{2+} + O$, $O^{2+} + C$, and $C^+ + O^+$ respectively. The fragmentation channels carrying a total charge of 3 have probably again a delayed onset compared to the adiabatic thresholds, because of the Coulomb repulsion when the fragments are not separated.

V. RESEARCH APPLICATIONS

Comparing our results for CO and N_2 we notice two major differences. One is that the N_2^{2+} species is not only observed in coincidence with the highest energy Auger two hole state as for CO, but persists for different final hole configurations too. Possibly these final state configurations might not be present in the oxygen Auger spectrum of CO. For example the $5\sigma^2$ configuration only shows up in the carbon Auger spectrum of CO, whereas the same final state is observed in the nitrogen Auger lines. The existence of two stable double hole configurations for N_2 , $5\sigma^2$ and $5\sigma 1\pi$, would explain why we observe N_2^{2+} over a wider range than CO^{2+} in our coincidence studies. The second difference observed between the results for CO and N_2 is that we find C^+ and O^+ in coincidences with 3σ OV final state Auger configurations but N^+ is not observed for the equivalent states of nitrogen. The answer to this question can probably be found by a calculation. At present there is no hint of an explanation for this remarkable difference between CO and N_2 .

Even though some questions remain open, we nevertheless get a rather clear and detailed picture of the mechanism leading to the production of ionic fragments following the adsorption of a soft X-ray photon. These studies also give a tremendous new insight into the involvement of individual electrons into the molecular bond.

4. Deexcitation electron spectroscopy DES

This new experimental technique involves the study of the electronic decay of a bound state core electron excitation. This decay is governed by the same type of matrix element as the Auger decay which follows core electron ionization. The final states however are different. Since it starts from a neutral configuration, even though a core hole has been created, the final state is in general a singly ionized state very much like in photoemission. This greatly simplifies the interpretation of the spectra. The main difference between DES and photoemission however is that DES contains information where the local character of the core hole in the initial state is reflected strongly in the intensities of the individual final states. These core electron bound state excitations are well defined in energy and located a few eV below the ionization limit for the core electron. They show up as rather strong absorption lines in the spectra as shown for N_2O in fig. 7. The two strong lines at 401 eV and 405 eV both correspond to bound state core electron excitations into the 3π molecular orbital. Since N_2O is an asymmetric molecule (NNO) we can resolve two core electron excitations into the same final state (3π) which is unoccupied in the ground state of the molecule. The transition at 401 eV corresponds to a creation of a core hole in the terminal nitrogen atom

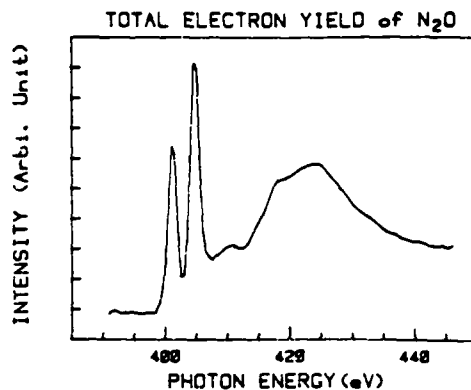


Fig. 7. Total ion yield of N_2O as a function of photon energy around the nitrogen absorption threshold. The bound state transitions for the terminal nitrogen atom (N_T) and central nitrogen atom (N_C) are observed at 401 eV and 405 eV and marked accordingly.

N_T , whereas the transition at 405 eV corresponds to a core hole at the central nitrogen atoms N_C . It is obvious from the spectra in fig. 7, that DES requires a fairly monochromatic excitation source. Therefore the spectra shown here were actually taken at the grasshopper beamline at SSRL. However this experiment would greatly benefit from an undulator. It took between 8 and 12 h to accumulate the DES spectra shown here and we were unable to collect the corresponding DES spectra at the oxygen edge, because the photon flux drops by a factor of two to three between 400 eV and 530 eV at the grasshopper beamline.

Before presenting the DES spectra of the two bound state core excitations in N_2O , we want to discuss the deexcitation process in general terms. It helps to think about the deexcitation process in two schematically separated configurations. First, if the excited core electron, which is a 3π electron in the case of N_2O , is involved in the Auger type decay of the core hole, then one additional valence electron will also participate in the decay. This Auger transition will leave the molecule without the 3π electron and with one additional hole among the valence electronic states. The end result therefore is a single valence hole configuration compared to the ground state of the molecule. The energy of this state is the single particle binding energy of the corresponding single valence hole configuration. This energy can be determined by conventional photoelectron spectroscopy. The second possible channel of deexcitation leaves the excited electron as a spectator. Consequently two valence electrons are now involved in the decay of the excitation. The end result of this process is a two hole one electron configuration, compared to the ground state of the molecule. These electronic config-

urations are observed in conventional photoemission spectroscopy too, but with much smaller intensity than the single hole states, and they are called *shake-up* states. Again, the energy of these configurations can be obtained from a standard photoemission spectrum. Based on these schematic considerations we expect to see a correspondence of peaks in a photoemission spectrum of any given molecule and its deexcitation spectra, if plotted on a common binding energy scale. This is done for N_2O in fig. 8 and indeed we see a very close correspondence among the various peaks. The intensity of the different electronic configurations giving rise to the peaks in the spectra varies between DES and photoemission, but the peaks appear at the same energies.

In the following we want to concentrate on the single particle configurations and the intensity variations observed in these states for the two DES spectra in fig. 8. The most remarkable difference we see in the single hole states between the DES spectra of the terminal nitrogen atom N_T and the central one N_C is that the 2π emission is clearly present in the N_T DES spectrum but not in the N_C DES spectrum and that the 1π exhibits essentially the opposite behaviour. This observation can be explained by the local character of DES. The 1π wavefunction is largely concentrated around the central nitrogen atom, whereas the 2π wavefunction has most of its weight at the terminal nitrogen atom. The intensity of the emission in DES reflects the local amplitude of the individual wavefunctions because of the strong localization of the core hole in the initial state. We have to add at this point that we do not yet completely understand the intensity variations in the σ -orbitals. Both the 6σ and the 7σ orbitals are extended over the whole molecule, but for example the 7σ does not show up in DES at all, whereas the 6σ seems to dominate the N_T DES spectrum. A possible explanation for this behaviour might be in the dynamic screening of the core hole excited state changing the σ -orbitals whereas the π -orbitals remain largely unchanged.

We are currently developing DES as a spectroscopic probe for the local character of wavefunctions in isolated molecules, adsorbates and complex materials. Comparing DES with Auger spectroscopy, we find that Auger spectroscopy has some local character too, but DES offers two distinct advantages. First, DES can distinguish between chemically inequivalent atoms of the same kind within a molecule. Auger spectroscopy is only sensitive to different atomic species. And second, the final states in DES are single hole configurations and their energy and assignment is readily derived from a comparison with photoemission. Auger final states on the other hand are double hole states. This not only involves a convolution of two valence electron wavefunctions for the final states, but also the energy is not readily obtainable because of the Coulomb interaction U of the two holes. This famous U can cause shifts from

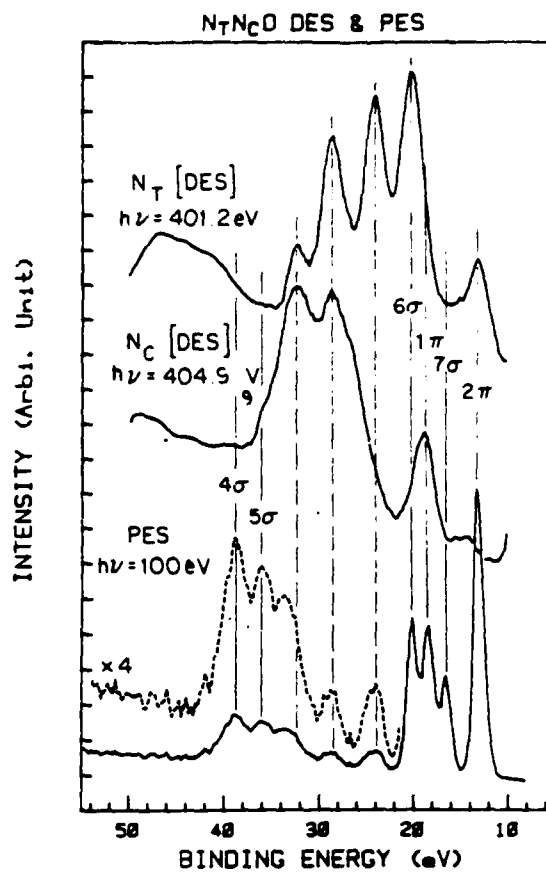


Fig. 8. DES spectra of N_2O compared to a photoemission spectrum on a common binding energy scale. The single hole configurations are marked according to their main character.

0 to 19 eV for the double hole configuration [12] compared to the sum of the single hole binding energies. Therefore a rather sophisticated theoretical machinery is needed for the assignment of the Auger final states.

A new generation beamline with a soft X-ray undulator source would greatly facilitate these studies. In combination with a high resolution monochromator we additionally might be able to resolve the vibrational substructure in the core to bound excitations. This will open new dimensions for DES as a probe for vibrational energy transfer within molecules on a very short time scale.

We would like to thank H. Winick, I. Lindau, R.Z. Bachrach and the staff of SSRL for their help and excellent support of the experiment. Special thanks are due to A. Waldhauer and S. Goldberg for helping with the computer programming and to In-Wan Lyo for help with the data evaluation. This experiment is par-

V. RESEARCH APPLICATIONS

tially supported by NSF under grant No. NSF-DMR-8120331. The SSRL beamline V is funded by NSF grant No. NSF-DMR-81-08343 and by the Office of Naval research under N00014-82-C-0772. Research at SSRL is supported by DOE.

References

- [1] F. Senf, K. Berens v. Rautenfeld, S. Cramm, C. Kunz, J. Lamp, V. Saile, J. Schmidt-May and J. Voss, these Proceedings (Synchrotron Radiation Instrumentation, Stanford, 1985) Nucl. Instr. and Meth. A246 (1986) 314.
- [2] M. Watanabe, these Proceedings (Synchrotron Radiation Instrumentation, Stanford, 1985) Nucl. Instr. and Meth. A246 (1986) 15.
- [3] R.Z. Bachrach, L.E. Swartz, S.B. Hagstrom, I. Lindau, M.H. Hecht and W.E. Spicer, Nucl. Instr. and Meth. 208 (1983) 105.
- [4] M. Howells, J. Kirz, D. Sayre and G. Schmahl, Phys. Today (August 1985) 22.
- [5] W. Eberhardt, J. Stöhr, C. Troxel Jr, J. Feldhaus, E.W. Plummer and F. Sette, Rev. Sci. Instr. 55 (1984) 354.
- [6] W. Eberhardt, T.K. Sham, R. Carr, S. Krummacher, M. Strongin, S.L. Weng and D. Wesner, Phys. Rev. Lett. 50 (1983) 1038.
- [7] W. Eberhardt, J. Stöhr, J. Feldhaus, E.W. Plummer and F. Sette, Phys. Rev. Lett. 51 (1983) 2370.
- [8] W. Eberhardt, C.T. Chen, W.K. Ford, E.W. Plummer and H.R. Moser, in: Diet II, Springer Series in Surface Science, Vol. 4 (Springer Verlag, Berlin, 1985) p. 50.
- [9] C.E. Moore, Atomic Energy Levels, NBS circular No. 467 (1958).
- [10] C.M. Liegener, Chem. Phys. Lett. 106 (1984) 201.
- [11] J.A. Kelber, D.R. Jennison and R.R. Rye, J. Chem. Phys. 75 (1981) 653.
- [12] E.W. Plummer, C.T. Chen, W.K. Ford, W. Eberhardt, R.P. Messmer and H.J. Freund, Surface Sci. 158 (1985) 58.

Article: "Focusing of Undulator Light at SPEAR with a Lacquer-coated Mirror to Power Densities of 10^9 Watts/cm²", by R. Tatchyn et al, in "Soft X-Ray Optics and Technology", eds. E.E. Koch and G. Schmahl, Proc. SPIE 733, 368-378, 1987.

Focusing of undulator light at SPEAR with a lacquer-coated mirror
to power densities of 10^9 Watts/cm²

Roman Tatchyn*

Stanford Synchrotron Radiation Laboratory
Stanford University, Stanford, CA 94305, USA
and
Department of Physics
University of Oregon, Eugene, OR 97403, USA

Paul Csonka

Institute of Theoretical Science
and
Department of Physics
University of Oregon, Eugene, OR 97403, USA

Hayrettin Kilic

Department of Physics
University of Oregon, Eugene, OR 97403, USA

Hiroshi Watanabe

Department of Physics
University of Oregon, Eugene, OR 97403, USA

Ashley Fuller

Department of Materials Science
Stanford University, Stanford, CA 94305, USA

Mark Beck

Department of Applied Physics
Stanford University, Stanford, CA 94305, USA

Arthur Toor

Lawrence Livermore National Laboratory
Livermore, CA 94550, USA

James Underwood

Center for X-Ray Optics
Lawrence Berkeley Laboratory, Berkeley, CA 94720, USA

Richard Catura

Lockheed Missiles and Space Company, Inc.
Palo Alto, CA, 94305, USA

Abstract

A lacquer-coated, diamond turned Cu ellipsoid has been used to micro-focus undulator light from Beam Line V at SPEAR down to a half-power diameter of about 13 microns. This spot was source-size limited, as has been demonstrated with ray tracings of the optical system. The symmetry of the image, as well as its size and power density, clearly make this optic ideal for many soft x-ray applications, in particular for x-ray microscopy, microprobes, and for pumping soft x-ray transitions in various media.

I. Introduction

The availability of controlled narrowband power densities of $\geq 10^9$ W/cm² over the soft x-ray/hard x-ray ranges is desirable for several reasons. Some of the more important ones include (1) pumping of soft x-ray transitions in solids, liquids, and gases;¹ (2) study of non-linear phenomena associated with outer and inner-shell processes; (3) "flash" holography and microscopy of living organisms;² (4) microprobing; and (5) study of saturation effects in surface and bulk photoemission. Apart from regions close to high-

power plasma sources or atomic explosions, however, the precisely controlled photon fluxes necessary for attaining such power densities have not been available until the fairly recent advent of undulators and wigglers (employed as x-ray sources on synchrotron storage rings). Even for these devices, unfortunately, the naturally diverging light, although highly collimated, still will not be able to attain the power densities cited above until electron beam sizes in storage rings are diminished to below the $\sim 15 \mu \times 15 \mu$ range. In view of the fact that such emittance parameters are not yet available, the most effective way, at present, to attain power densities of $\geq 10^9 \text{ W/cm}^2$ with undulator or wiggler sources is to use specially designed mirrors to "super-focus" the output light to spots with dimensions approaching the required $10 \mu \times 10 \mu$ range. It should be clear, however, that such mirrors will still remain useful even when electron beam sizes do start approaching extremely small dimensions because the possibility of refocusing will always have the advantage of allowing experiments to be placed virtually as far away from the storage ring area as the experimenter pleases.

In view of the above state of x-ray insertion device/machine technology, and having the ultimate objective of attempting to pump a Li laser in the soft x-ray range,¹ we have undertaken a design of an ellipsoidal mirror³ to focus the light from the Beam Line V undulators at SSRL⁴ down to the $< 10 \mu \times 10 \mu$ region. In this paper we will report on the mirror design and construction, and on a recent experiment at SSRL which demonstrated the attainment of $\geq 10^9 \text{ W/cm}^2$. The power reflected off the mirror was measured with a calorimeter, and the power profiles in the focal plane were recorded with PMMA and with scanning x-y knife-edge slits. The measured profiles were simulated with the ray-tracing program SHADOW,⁵ and the simulations will be presented below with some of the PMMA photographs for comparison.

II. Mirror design and construction

The basic requirement that the mirror had to fulfill was the attainment of a $\sim 10 \mu \times 10 \mu$ (FWHM) focal spot with a peak power of $\sim 5 \times 10^3$ Watts. The basic assumptions underlying the design were: (a) electron beam dimensions in SPEAR (FWHM): 3 mm x .7 mm; (b) mirror center to undulator center distance: 14.3 meters; (c) single-bunch mode of ring operation; (d) pulse length: 160 pS; (e) repetition frequency: 1.3 MHz; (f) duty cycle: 4750; and (g) first harmonic energy: 75 eV.

The total power emitted by any of the Beam Line V undulators is given by

$$P_{\text{TOT}} = 633 E^2 [\text{GeV}] B_0^2 [\text{Tesla}] L [\text{Meters}] I [\text{Amp}] \quad (1)$$

where E is the ring energy, B_0 is the peak on-axis undulator field, L is the undulator length, and I is the ring current. The first harmonic on-axis wavelength is given by

$$\lambda_{\text{OUT}} [\text{\AA}] = \frac{13.06 \lambda_u}{E^2} (1 + K^2/2) \quad (2)$$

where λ_u is the undulator period in centimeters, and

$$K = .934 \lambda_u B_0 \quad (3)$$

For the running conditions anticipated ($E = 3 \text{ GeV}$, $L = 1.83 \text{ m}$, N (number of undulator periods) = 10, $I = 100 \text{ mA}$) the computed parameters were $K = 3.23$ and $P_{\text{TOT}} = 37 \text{ Watts}$. Given the assumed source size and source-mirror distance, the required 300:1 demagnification in each dimension necessitated a focal length of 5 cm. Ray-tracing studies of different mirror surfaces⁶ showed the ellipsoid to be the most efficient focuser for the given emittance parameters and for source sizes not greatly exceeding the assumed 3 mm x .7 mm. It was found that an angle of incidence on the mirror of 6° was optimal: a greater angle would have resulted in lower reflectivity at the desired energy, and a smaller angle would have made the mirror too long for the required 5 cm focal length. A schematic layout of the assumed mirror configuration and the assumed emittance parameters is shown in Fig. 1.

Given the above design constraints, an ellipsoidal mirror was designed at SSRL and diamond-turned out of Cu At LLNL.⁷ The diamond turning was done with a special boring bar moving through a bolted-together pair of Cu monoliths. Due to symmetry, the turning process yielded two mirrors, one of which is shown in Fig. 2.

As is well known, the diamond-turning process leaves a striated surface, with a periodic

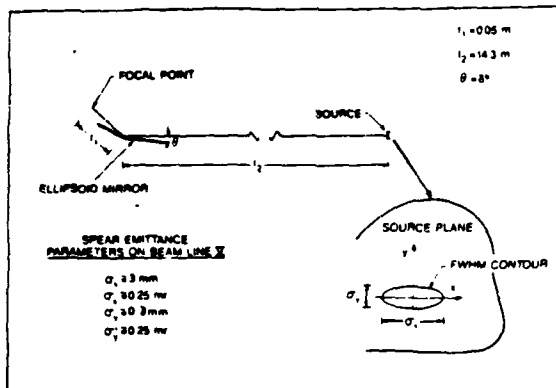


Figure 1. Schematic layout of assumed ellipsoidal mirror design parameters.

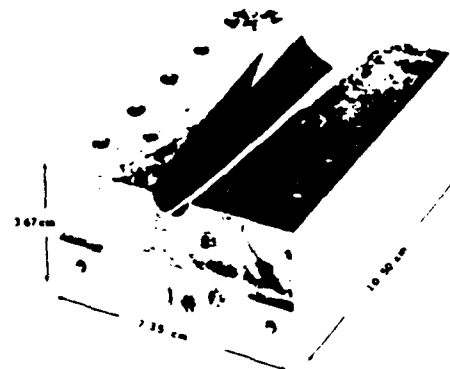


Figure 2. Photograph of metallized, lacquer-coated ellipsoidal mirror. The matrix material is predominantly Cu.

array of grooves.⁷ The groove amplitudes are typically of the order of hundreds of angstroms, and the periods are typically of the order of thousands.

As a consequence, diamond-turned surfaces of conventionally shaped optics have to be polished. For the optic under discussion, however, conventional (mechanical) polishing was impossible,⁸ primarily due to the large curvature, and large change of curvature, of the surface over its extent. In view of this, it was decided to lacquer-coat the surface, as this technique had been previously shown to be effective in smoothing surfaces due to the effect of the lacquer's surface tension "stretching" its top region out over the underlying rough topography.⁹ Following the lacquer coating, the surface was metallized with gold and platinum (see Fig. 3) to provide high smoothness and reflectivity in the desired region of the soft x-ray range. Preliminary tests of this mirror's surface were done at SSRL in the spring of 1985, and the results have been reported on elsewhere.³

III. Experimental set-up

The actual operating parameters for the present experiment differed somewhat from those assumed for the ideal mirror design. Specifically, the electron beam size in the ring was actually 1 mm (V) x 6 mm (M) FWHM, and the distance from the center of the undulator to the center of the mirror had to be 16.3 meters. These parameters, which were also used in the ray tracing simulation studies, are shown in Fig. 4.

COATED MIRROR

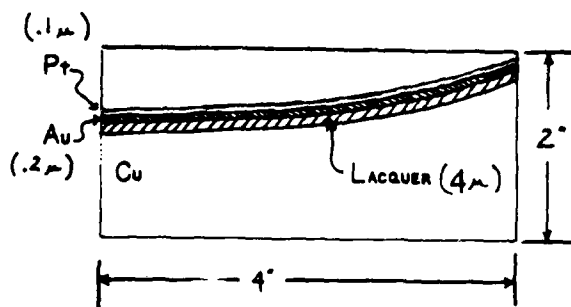


Figure 3. Lacquer-coating and metallization parameters for the Cu ellipsoid.

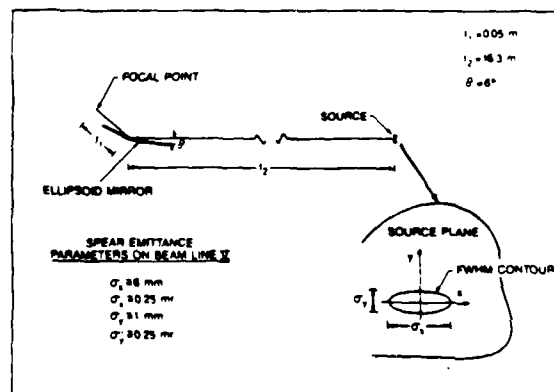


Figure 4. Schematic layout of geometrical and operating parameters for the actual testing of the ellipsoidal mirror.

The basic layout of the experimental line consisted of a 6' long differential pumping section,¹⁰ followed by the chamber containing the ellipsoidal mirror. The differential pumping section has a circular aperture with a 1 cm diameter. The experiment consisted of three distinct phases. In the first phase, PMMA was used to record the beam profiles before, in, and behind the focal plane. This was accomplished by mounting the PMMA-coated Si wafers on tilted platforms and moving them into the focused beam from the side (bottom drawing in Fig. 5). The procedure was to optimize the mirror orientation on its micrometer supports by observing the focused spot on a phosphor-coated plate, and then taking a series of exposures on the PMMA, each exposure being taken at a different distance before or behind the focal plane. No highly precise optimization was possible in this mode of data recording - the photographs were taken primarily to corroborate the contours of the simulated (ray-traced) power distributions.

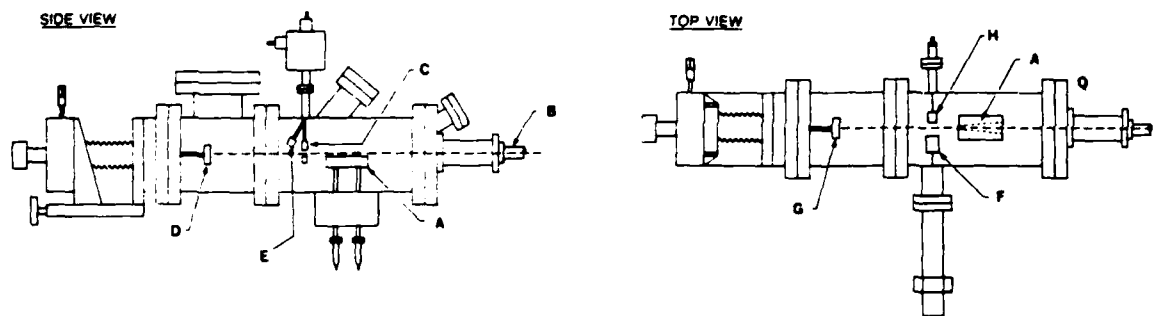


Figure 5. Schematic layout of scanning mirror characterization experiments. The "side view" picture is of the scanning x-y knife edge profiling set-up, and the bottom "top view" picture is of the set-up for PMMA photography. (A) Mirror on micrometer supports; (B) upstream differential pumping section; (C) knife-edge pinhole bracket (cf. Fig. 14); (D) beam stop; (E) calorimeter with an attached Si solar cell detector; (F) paddle with tilted platforms holding 3" PMMA-coated Si wafers and an auxiliary phosphor screen; (G) calorimeter; (H) PMMA paddle clamp.

The second phase consisted of taking power readings of the light reflected off the mirror with a calorimeter (detail E in the left-hand drawing in Fig. 5), and the third phase consisted of scanning through the light distribution in the focal plane with an x-y knife-edge slit assembly. Each of these three phases, including the associated results, are described below in more detail.

IV. PMMA photography

As outlined above, discrete photographs were taken of the reflected light's power distribution before, behind, and in the vicinity of the mirror's focal plane. Approximately twenty photographs were taken on each of approximately twenty-five 3" long PMMA-coated Si wafers. The mirror was realigned and visually reoptimized on an auxiliary phosphor screen before the exposure sequence was taken on each wafer. The platform holding the wafer was tilted by about 15° off the plane perpendicular to the light axis, thus the exposure sequences extend from about - .4" to + .4" behind and before the focal plane (or -1 cm to + 1 cm). The horizontal dimensions of the photographed exposures are, for the same reason, about 4½ longer than the actual horizontal dimensions of the light. In Fig. 6, a photograph of a light distribution very close to the focal plane is shown, together with a ray-traced profile corresponding to a perfectly-aligned mirror in the true focal plane. A detailed analysis of the exposed area in the photograph has not been done due to the availability of the knife-edge scanning measurements which were performed subsequently and which will be described below. It should be pointed out that the simulated spot's FWHM dimensions are about 20 μ(H) x 10 μ(V) (see histograms in Fig. 6), while the estimated horizontal FWHM size of the photographed distribution is about 24 μ (25 μ in the actual photograph).

For purposes of further comparison, simulated ray tracings of power distributions in planes located +1 mm, +2 mm, +3 mm -1 mm, -2 mm, and -3 mm with respect to the true focal plane are contrasted with photographs of actual power distributions located at approxi-

mately the same relative distances in Figs. 7,8,9,10,11 and 12. The minimum graph intervals in all these figures are in 40μ units. It is seen that a close geometrical correspondence exists between the two sets of data.

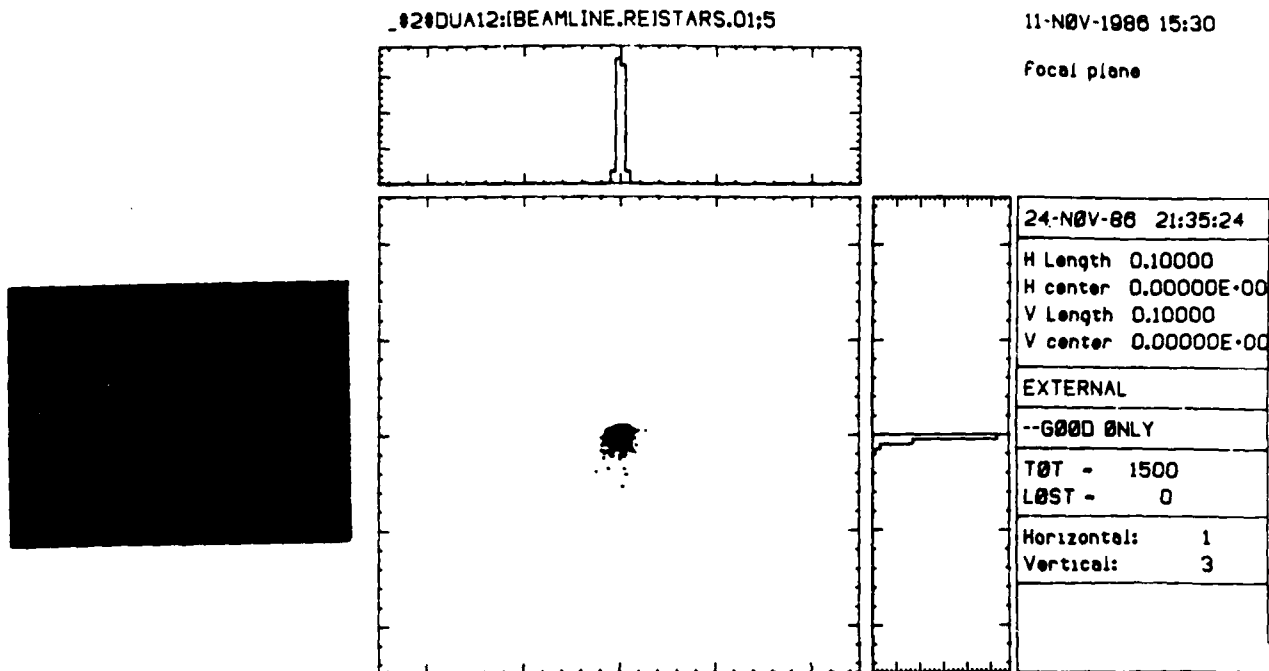


Figure 6. PMMA photograph of an optimum focal plane exposure is shown on the left, and a ray traced power distribution in the focal plane is shown on the right, together with x and y integrated power distribution histograms. Graphs intervals are in 40μ units.

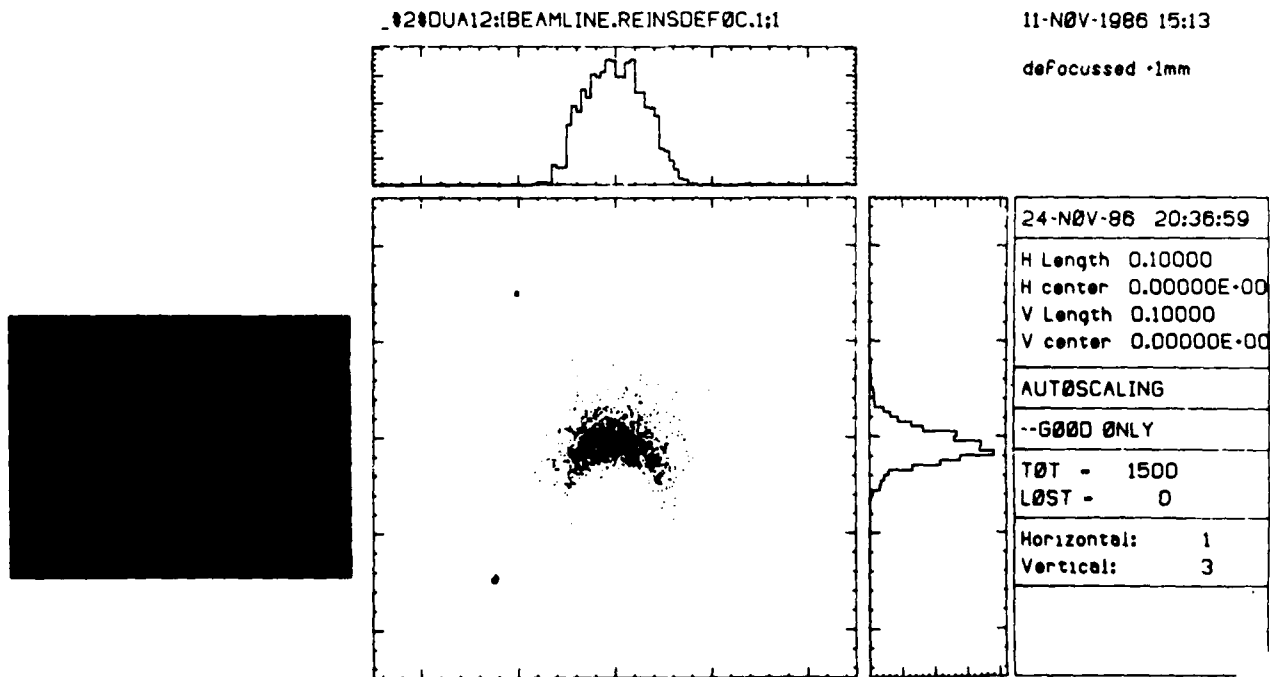


Figure 7. PMMA photograph and ray trace simulation at 1 mm downstream of focal plane.

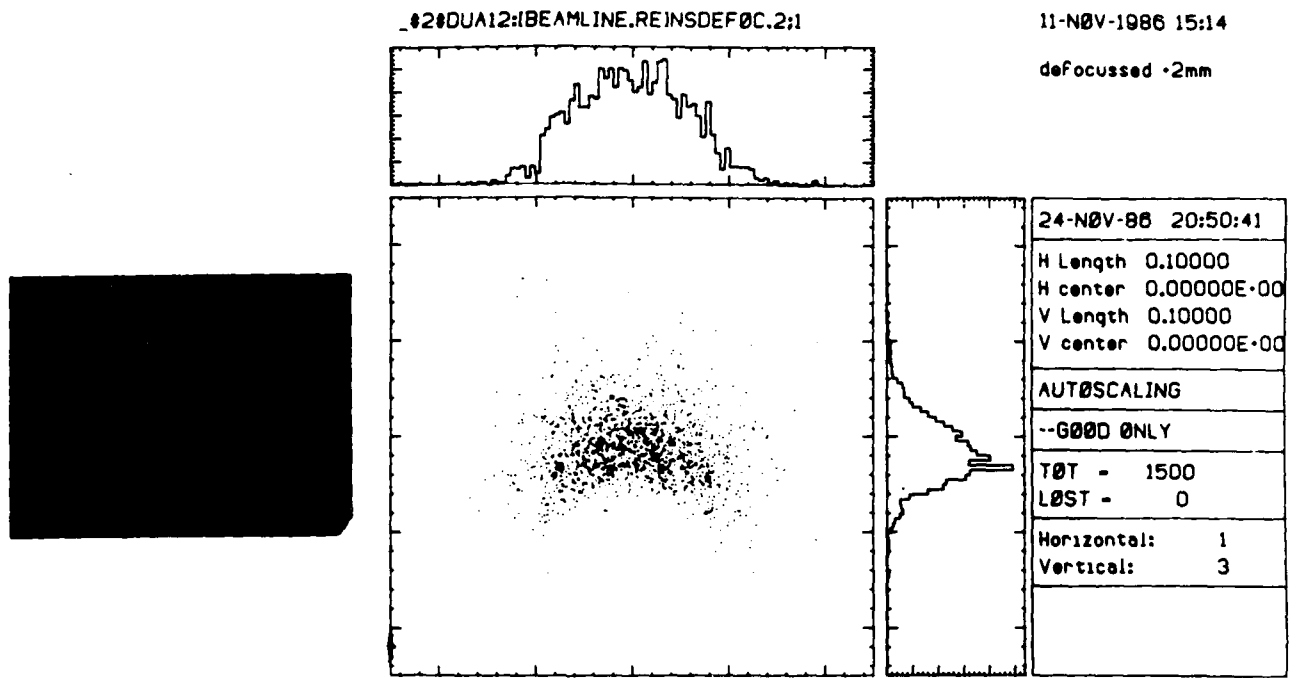


Figure 8 PMMA photograph and ray trace simulation at 2 mm downstream of focal plane.

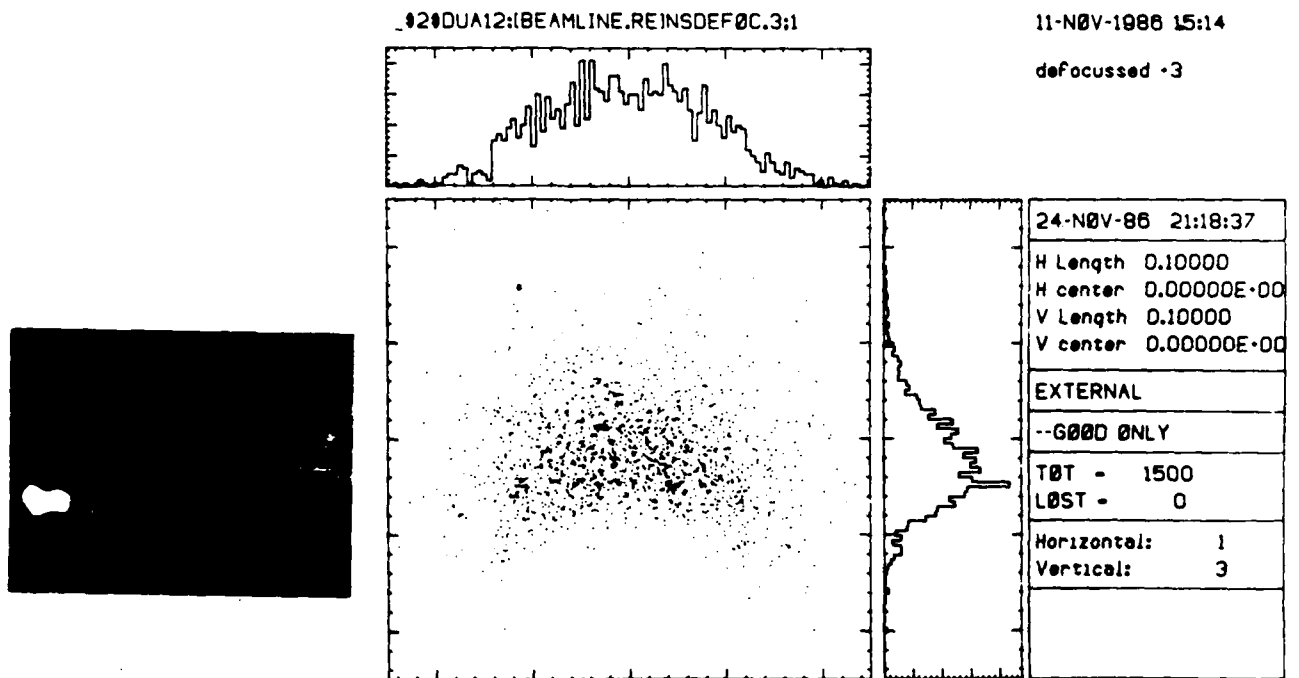


Figure 9. PMMA photograph and ray trace simulation at 3 mm downstream of focal plane.

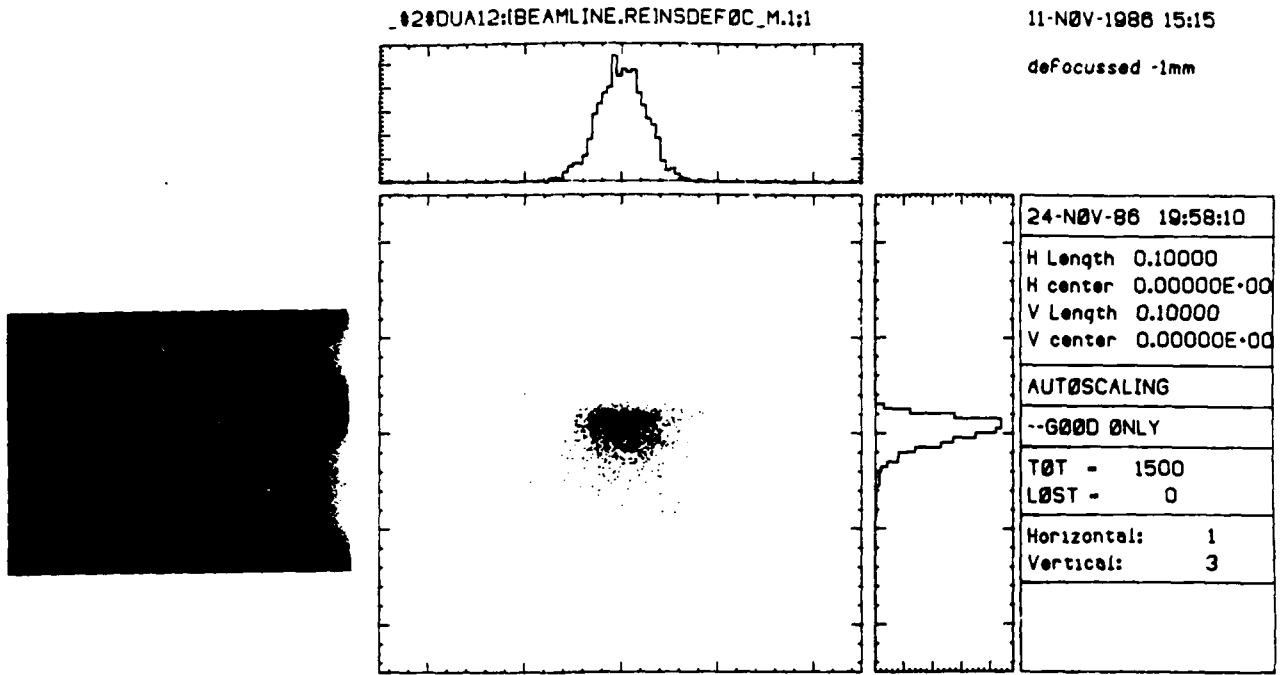


Figure 10. PMMA photograph and ray trace simulation at 1 mm upstream of focal plane.

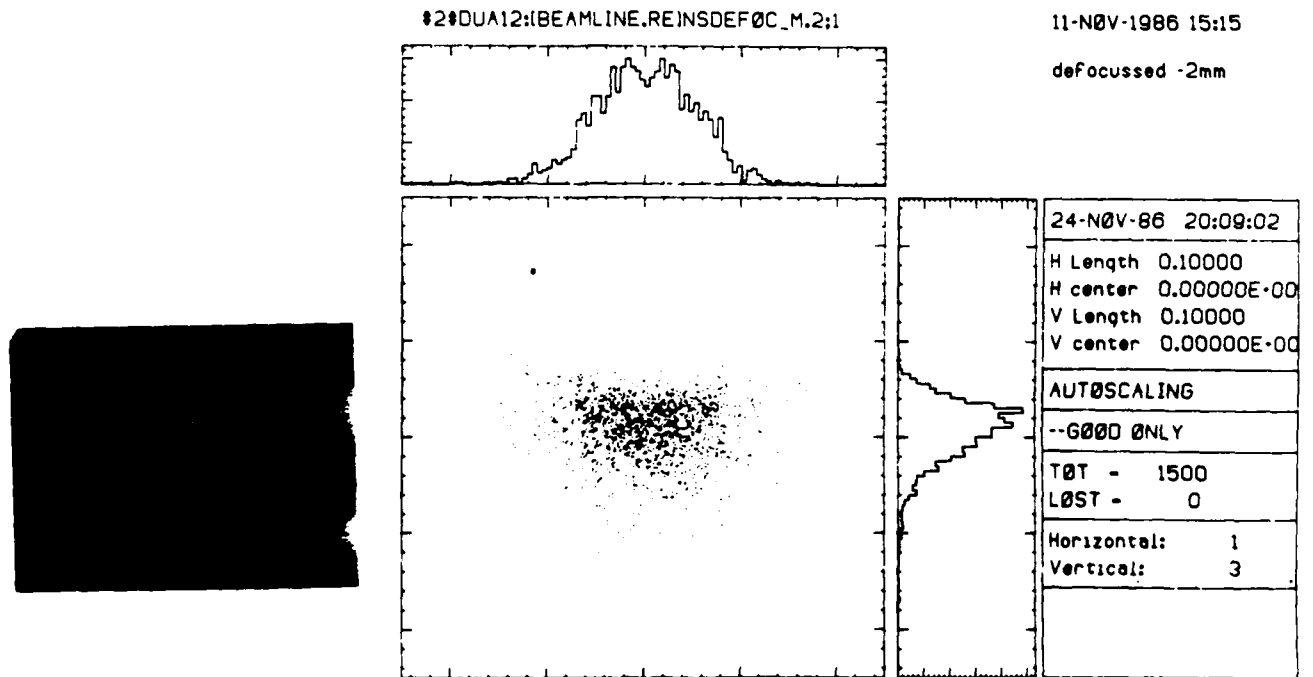


Figure 11. PMMA photograph and ray trace simulation at 2 mm upstream of focal plane.

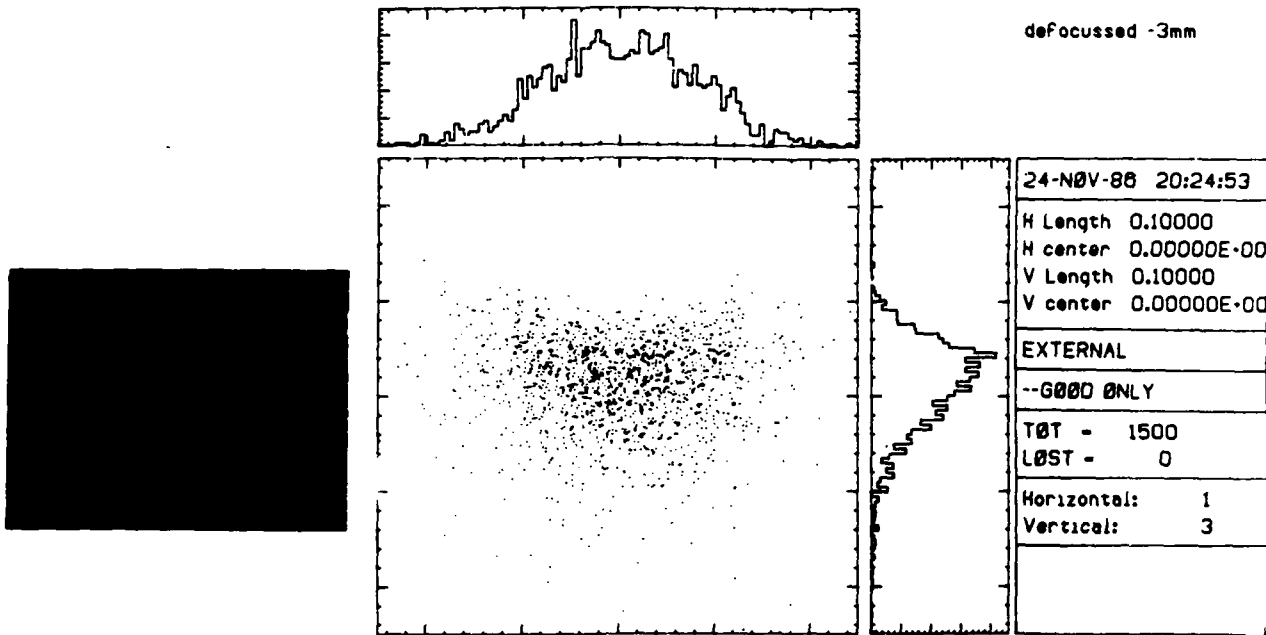


Figure 12. PMMA photograph and ray trace simulation at 3 mm upstream of focal plane.

V. Calorimetry

In this phase of the experiment, measurements were taken of the total power reflected off the mirror, so that subsequent estimates of the power density attained in the focal spot could be made. The calorimeter used in the given set-up corresponds to detail E in the left-hand drawing in Fig. 5. Due to power loading considerations on the beam line at SSRL, the 10 period undulator was operated at a gap of 11 cm ($K = 1.8$). This corresponded to a first harmonic energy of about 190 eV and a computed total output power of about 13.16 Watts (at 100 mA ring current).

The calorimeter construction and characteristics are shown in Fig. 13. Two test scans, with and without an upstream Beryllium filter are shown in the same figure. Powers of about 1 Watt were briefly established and measured off the mirror for the given undulator setting, with the ring current in the 60-70 mA range. The discrepancies between the computed and measured figures stem from the fact that the differential pumping aperture blocked a significant fraction of the undulator light, and the mirror reflectivity at 6 (and 190 eV) was in the $\leq 50\%$ range.¹¹

VI. Knife edge x-y scans

In this phase of the experiment, quantitative measurements were taken of the light distribution in the focal plane of the mirror. Scans were taken with a pinhole and with a set of knife-edges set at 90° with respect to each other. Since limited experimental time precluded use of more than one pinhole, the knife-edge data represent a somewhat more comprehensive measurement of power contours in the focal plane, and are therefore the ones presented in this paper.

The two perpendicular knife-edges were scanned through the beam at angles of 45° with respect to the (horizontal) synchrotron orbit plane. A photograph of the x-y slit/pinhole holder bracket is shown in Fig. 14 and a schematic sketch of the bracket's orientation and scanning motions is shown in the upper left hand corner of Fig. 15. The detector used for real-time signal pickup behind the slit was a standard Si solar cell, epoxied to the calorimeter case (detail E in Fig. 5). The experimental procedure consisted of repeatedly realigning the mirror visually on the phosphor coating on the knife-edges, and then

scanning in both directions. The procedure was repeated and culled for scans of maximum symmetry in both directions, and for overall minimum beam waist size.

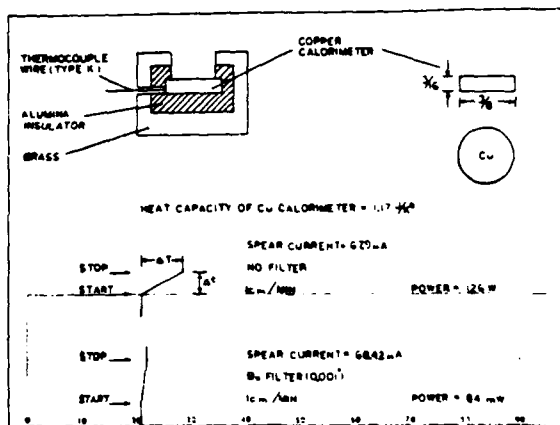


Figure 13. A schematic of calorimeter construction details and its performance parameters are shown on top, and two typical calorimeter scans are shown on the bottom.

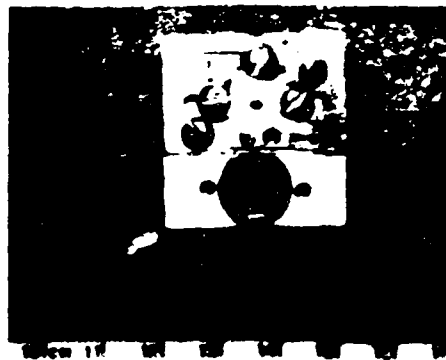


Figure 14. Bracket for holding the x-y scanning knife-edges (top) and a pinhole (bottom). The aperture formed by the knife-edges, which are coated with phosphor, measures about 1.5 mm x 1 mm.

An optimum set of scans of the solar cell detector response for the knife-edges passing through the beam in the focal plane is shown in Fig. 15. Since the solar cell output is linearly proportional to the total light flux, the scans may be interpreted as displaying the power falling on the area not covered by the knife-edge. Thus, at half-maximum, the knife-edge is blocking half the power. Points corresponding to 25%, 50%, and 75% of the maximum are marked on the leftmost scan in Fig. 15. The scan distance between the 25% and 75% points may consequently be interpreted as a "half-power" interval. For each scan shown, the "half-power" interval, calculated after subtracting background signal levels, measures approximately 13.5 microns in each scanning direction. The first-order interpretation of these measurements, therefore, is that about half the power in the focal plane was focused in a region no larger than $13.5 \mu \times 13.5 \mu$ in size.

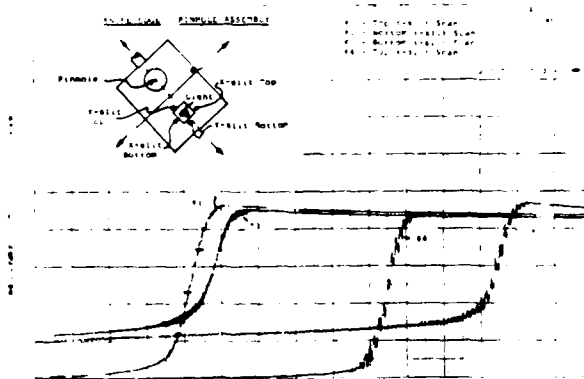


Figure 15. Schematic of knife-edge/pinhole holder bracket, together with labeled scanning parameters, is shown on the top left. Scans corresponding to each knife-edge are shown below. Distance between the heavy divisions in the horizontal direction corresponds to about 12.5 μ .

VII. Discussion

The measurements of the optimum scans described above correspond closely to both the ray-traced spot and the PMMA photograph shown in Fig. 6. The histograms in Fig. 6 describe a contour of about $18 \mu(V) \times 20 \mu(U)$ FWHM. Assuming a Gaussian distribution in the horizontal direction, it is easy to show that the central half-power interval under a Gaussian curve is about a factor of .79 smaller than its FWHM interval. This would correspond to 15.7μ . Now, scanning through a $15.7 \mu(H) \times 7.85 \mu(V)$ spot at 45° would reduce each dimension by a factor of $\sim \sqrt{2}$, resulting in a quadratic diagonal length of $\sim 12.4 \mu$. This represents a 10% agreement with the dimension actually measured.

The horizontal extent of the PMMA photograph in Fig. 6, on the other hand, shows linear dimensions of $\sim 50 \mu$. Since no interpretation of the exposed profile has been made, we can assume this area includes a significant component of scattered light in addition to a sharply focused central peak. Since the scattered light tails on the (corrected) scans in Fig. 15 show an extent of about 80μ , this can be interpreted as being consistent both with the PMMA photograph, and with an assumption of optimal focusing.

Conclusion

We have successfully focused approximately 1 Watt of undulator light spanning the $190 \text{ eV} - 10 \text{ eV}$ range (but peaked, before reflection, at about 190 eV) down to an estimated half-power spot size of approximately $15.7 \mu \times 7.85 \mu$. As this was done during single-bunch operation of SPEAR, and with an assumed 300 ps FWHM pulse length,¹² we can estimate an attained peak power density of $\sim 1.2 \times 10^9 \text{ W/cm}^2$.

This can be considered a breakthrough in the attainment of controlled narrowband power densities in the soft x-ray range, yet it is important to point out again that the actual spot size was source-size limited. For example, ray trace studies show a linear scaling of focal spot size with source size, and, in fact, the mirror under discussion was recently used in the optical region (6328 \AA) to attain a diffraction-limited focal spot size of about 2μ . Thus, the same optic could be used to attain x-ray spot sizes limited only by its surface slope errors and asperities, provided it was focusing a beam at a synchrotron beam line with significantly smaller emittance parameters. Upcoming emittance upgrades at SPEAR and PEP, specifically, should allow the same optic to attain half-power contours smaller than about 1μ in each dimension, thus controlled power densities exceeding 10^{11} W/cm^2 can now be considered to be within direct reach.

In conclusion, additional aspects of the present experiment, such as the pinhole measurements, and analysis of the scattered light distributions (see Figs. 6 and 15), are presently being studied and will be discussed in subsequent publications.

IX. Acknowledgements

The authors would like to thank James Bryan (LLNL) for leading the fabrication effort for the ellipsoidal mirror and Cal Gillespie (LLNL) and Dave Edwards (LLNL) for useful discussions. Partial support for this work was provided by the Department of Energy Grants DE-FG06-85-ER1309 and DE-AC03-82-ER13000 and by the Air Force Research Grant AFOSR-85-0326. Additional support was provided by the Stanford Synchrotron Radiation Laboratory's Beam Line V Project, which is funded by the National Science Foundation Grant NSF-DMR-81-08343, and by the U.S. Office of Naval Research under N00014-82-0C-0722. The bulk of the experimental work was performed at the Stanford Synchrotron Radiation Laboratory which is supported by the Department of Energy, Office of Basic Energy Sciences.

References

*Affiliate member, Center for X-Ray Optics, LBL, Berkeley, CA 94720, USA.

1. Csonka, P.L., "Suggested Method for Coherent X-Ray Production by Combined X-Ray and Low Energy Photon Pumping," *Phys. Rev.*, Vol. 13A, No. 1, pp. 405-410, 1976.
2. Proposed in recent years by Arthur Toor (LLNL).
3. Tatchyn, R., Csonka, P.L., Kallne, E., Toor, A., Gillespie, C., Lindau, I., and Fuller, A., "Surface Heating in a Lacquer-Coated Mirror Irradiated with Undulator Light," *SPIE Proceedings No. 582*, pp. 291-296, 1986.
4. Bachrach, R.Z., Bringans, R.D., Pate, B.B., and Carr, R.G., "The SSRL Insertion Device Beam Line 'Wunder'," *SPIE Proceedings No. 582*, pp. 251-267, 1986.
5. Lai, B., and Cerrina, F., "SHADOW: A Synchrotron Radiation Ray Tracing Program," *Nucl. Instrum. Meth.*, Vol. A246, pp. 337-341, 1986.
6. The main alternative surface considered, especially for large beam emittances, was the paraboloid. Some double mirror systems were also studied.
7. Parks, R.E., "Polishing and testing of aspheric diamond-turned surfaces," *SPIE*

Proceedings No.315, pp. 230-235, 1982.

8. Based on consultations with James Bryan, Vic Rehn, and others, it was concluded that the development time for a mechanical polishing procedure would be extremely long, and that the costs could become prohibitive.

9. Seward, F., et al., "The SCRE, a Thor-carried X-Ray Astronomy Payload," UCID 15885-1, July 1971.

10. To be described.

11. Henke, B.L., Lee, P., Tanaka, T.J., Shimabukuro, R.L., and Fujikawa, B.K., "The Atomic Scattering Factor, $f_1 + if_2$, for 94 Elements in the 100 to 2000 eV Photon Energy Range," AIP Conference Proceedings No. 75, pp. 340-388, 1981.

12. Mills, D.M. "Time Resolution Experiments Using X-Ray Synchrotron Radiation," Physics Today, No. 4, p. 22, 1984.